

**CATALYSIS AND INHIBITION OF *MYCOBACTERIUM*
TUBERCULOSIS METHIONINE AMINOPEPTIDASE**

BY

©2010
Jingping Lu

B.S., East China Normal University, 1998

Submitted to the graduate degree program in Molecular Biosciences
and the Graduate Faculty of the University of Kansas
in partial fulfillment of the requirements for the degree of
Doctor of Philosophy

Committee members: _____
Chairperson – Mark L. Richter

Chairperson - Qi-Zhuang Ye

Roberto N. De Guzman

Krzysztof Kuczero

Emily E. Scott

Date defended 5/24/2010

The Dissertation Committee for Jingping Lu certifies
that this is the approved version of the following dissertation:

**CATALYSIS AND INHIBITION OF *MYCOBACTERIUM*
TUBERCULOSIS METHIONINE AMINOPEPTIDASE**

Committee members:

Chairperson – Mark L. Richter

Chairperson - Qi-Zhuang. Ye

Roberto N. De Guzman

Krzysztof Kuczero

Emily E. Scott

Date approved:

05/25/2010

ABSTRACT

Tuberculosis, caused by *Mycobacterium tuberculosis*, is the leading cause of death due to infectious disease. Now, the prevalence of multidrug-resistant and extensively drug-resistant TB, and the emergence of co-infection of TB and HIV have highlighted the need for new antibiotics with novel mechanisms of action.

Methionine aminopeptidase (MetAP) is a ubiquitous enzyme found in both prokaryotic and eukaryotic cells and carries out an important cotranslational modification of newly synthesized proteins. The MetAPs can be divided into type I and type II based on the existence of an insert in the catalytic domain. Prokaryotic cells have only one type of MetAP, either type I or type II; encoded by a single gene. MetAP is essential for cell viability, which is demonstrated by gene deletion experiment in *E.coli* and *Salmonella typhimurium*. Therefore, MetAP is a promising target for developing novel drugs against bacterial infection, including TB-causing drug resistance bacteria.

Two genes, *mapA* and *mapB*, were found in *Mycobacterium tuberculosis* H37Rv. They encode two type I MetAP enzymes, *MtMetAP Ia* and *MtMetAP Ic*, respectively. Both *MtMetAP* proteins were over-expressed and purified in homogeneity as apoenzyme. Biochemical characterization using a fluorogenic substrate (Met-AMC) was carried out with both *MtMetAP Ia* and *MtMetAP Ic*.

Both *MtMetAPs* can be activated by divalent metals, including Ni(II), Co(II), Mn(II) and Fe(II). Ni(II) is the best activator for both *MtMetAPs*, followed by Co(II). Mn(II) and Fe(II) are the least efficient to activate *MtMetAP Ia* and *MtMetAP Ic*, respectively. Metal titration assays were used to determine the metal binding affinity to each *MtMetAP*. In both *MtMetAP Ia* and *MtMetAP Ic*, Co(II) and Fe(II) are the tightest

binding metals, as indicated by their smallest K_d values. Mn(II) gives the weakest binding in *MtMetAP* Ia and Ni(II) shows a weakest binding to *MtMetAP* Ic.

Growth complementation experiments were employed to evaluate the cellular function of *MtMetAP* in the *E. coli* that had an amber mutation in the chromosomal *EcMetAP* gene, and a pBAD plasmid, which encoded a suppressor tRNA to suppress the lethal effect of the amber mutation. The existence of glucose or arabinose in the culture medium could suppress or express the tRNA respectively, therefore result the death or survival of the *E. coli*, respectively. The plasmid-expressed *MtMetAP* Ic in the amber mutant rescued the *E. coli* from death and supported cell growth.

A set of inhibitors with selectivity for different metalated MetAPs were tested on both *MtMetAP*s. For *MtMetAP* Ib, all tested compounds retained their inhibitory activities and metal selectivity. However, in *MtMetAP* Ia, the Co(II)-, Mn(II)- and Fe(II)-selective inhibitors did not show inhibition. Only Fe(II)-selective inhibitors retained their inhibition, whereas they lost their metal selectivity.

An amino acid sequence alignment suggested some differences in the active sites between *MtMetAP* Ia and *MtMetAP* Ic. A homology model of *MtMetAP* Ia based on *MtMetAP* Ic structure was generated. A similar active site is observed in this virtual structure of *MtMetAP* Ia. Given the size of the tested compound library, the failure to find an inhibitor specific for *MtMetAP* Ia may be due to the limited number of compounds in the library. Screening of a compound library consisting of a larger number of molecules with more structural diversity will possibly identify inhibitors for *MtMetAP* Ia.

The inhibitors of *Mt*MetAP Ic were further tested for their inhibition on cellular growth. The fact that only the Fe(II)-form selective inhibitors inhibited the cellular *Mt*MetAP Ic activity and inhibited the *Mt*MetAP Ic-complemented cell growth, suggested that Fe(II) was the native metal used by *Mt*MetAP1c in an *E. coli* cellular environment.

X-ray structures of *Mt*MetAP Ic in complex with three metalloform-selective inhibitors were analyzed. The results demonstrated different binding modes and different interactions with metal ions and active site residues for these inhibitors. The *Mt*MetAP1c inhibitors with metalloform selectivity are potential leads for antitubercular drugs.

Understanding the catalytic mechanism and inhibition of the mycobacterial MetAP is an essential step towards discovering and developing effective MetAP inhibitors as therapeutics. The compounds with potent inhibition and high metal selectivity toward *Mt*MetAP may be therapeutically useful for improved TB treatment.

ACKNOWLEDGEMENTS

First and foremost, I would like to express my deepest gratitude and acknowledge my advisors, Dr. Ye and Dr. Richter, for giving me the opportunity and freedom to do research and pursue my degree.

I do not know how I can possibly express my appreciation for Dr. Ye. I am extremely fortunate to be offered the opportunity to work with him. In the past three years, Dr. Ye has given me invaluable support, encouragement, and guidance. This research would not have proceeded this far without his expertise. He has offered me the great privilege to learn and to interact with multi-disciplinary groups, which indeed made my graduate study a very precious experience.

I also would like to acknowledge Dr. Richter for his continuous support and encouragement. He has been very supportive all the time. His support helped my move to Dr. Ye's lab to continue my study. He has provided suggestions and advice for my research. He has always helped me out whenever I was required to comply with a miscellaneous policy set for international students. If not for his help, I would never be able to finish my degree.

I am very grateful to all my current and previous committee members, Dr. De Guzman, Dr. Kuczera, Dr. Scott, Dr. Picking and Dr. Lamb. I am not a good student; thank you all for your patience and commitment to my development to become a qualified Ph.D. I am very fortunate to have known you in my life when I was seeking training in Biochemistry and Biophysics. I would like to specially thank Dr. Scott for her continued kindly guidance and mentoring. She is a constant source of inspiration.

I also want to thank all the colleagues in Dr Ye's lab. They are Hai Yuan, Sergio Chai, Sarah Hudon, Xiuhua Yuan, Wenlong Wang, Hongzhen He, and Qi Zhang. I would like to thank my friends Yang Wang, Qianyi Luo, Xingxian Gu, and Daniel Zhang for their help over my graduate school career.

Last, I would like to thank my parents for their support and consideration. They have always been the source of motivation and courage for me in my life. Without their encouragement and firm belief in me, I would never have achieved this. I thank them for giving me the freedom to pursue my goal. I thank them for their unselfish love and their strong support that I can always lean on.

Table of Contents

	Page
CHAPTER 1 INTRODUCTION:METHIONINE AMINOPEPTIDASES IN ANTI-TUBERCULOSIS DRUG DISCOVERY	1
1.1 Tuberculosis (TB)	1
1.1.1 History of tuberculosis	1
1.1.2 Pathogen of tuberculosis.....	3
1.1.3 Pathogenesis and transmission of tuberculosis	5
1.1.4 Drugs used in chemotherapy of tuberculosis	6
1.1.5 The challenge encountered in anti- TB drug discovery	9
1.2 Methionine aminopeptidase	10
1.2.1 Methionine aminopeptidase family	10
1.2.2 Structure of methionine aminopeptidase	11
1.2.3 Catalysis of methionine aminopeptidase	13
1.2.4 Metal activation of methionine aminopeptidase.....	18
1.3 Methionine aminopeptidase implication in anti- TB drug discovery	21
1.3.1 Methionine aminopeptidase in <i>Mycobacterium tuberculosis</i>	21
1.3.2 <i>Mt</i> MetAPs as the potential targets for anti- TB drug	21
Reference	24
 CHAPTER 2 BIOCHEMICAL CHARACTERIAZATION OF METHIONINE AMINOPEPTIDASE Ia IN MYCOBACTERIA TUBERCULOSIS	 26
2.1 Introduction.....	26
2.2 Materials and Methods.....	28
2.2.1 Cloning of <i>Mt</i> MetAP Ia into pGEMEX-1 plasmid	28
2.2.2 Re-cloning of the <i>mapA</i> gene into pET28a plasmid	29
2.2.3 Protein solubility optimization	31
2.2.4 Over-expression and purification of His <i>Mt</i> MetAP Ia	33
2.2.5 Untagged <i>Mt</i> MetAP Ia preparation and confirmation of removal of His-tag	34
2.2.6 Metal activation of His <i>Mt</i> MetAP Ia	35
2.2.7 Kinetic measurement of different metalloform His <i>Mt</i> MetAP Ia	36
2.2.8 IC ₅₀ determination with different metalloform of His <i>Mt</i> MetAP Ia	38
2.2.9 Co-crystallization of His <i>Mt</i> MetAP Ia and <i>Mt</i> MetAP Ia with inhibitors	38
2.3 Results	40
2.3.1 constructs of <i>Mt</i> MetAP Ia	40
2.3.2 Expression and purification of His <i>Mt</i> MetAP Ia protein.....	42
2.3.3 Activation of His <i>Mt</i> MetAP Ia apoenzyme by divalent metals.....	42
2.3.4 K inetic measurement of different metalloform His <i>Mt</i> MetAP Ia	48
2.3.5 IC ₅₀ determination with different metalloform <i>Mt</i> MetAP	50
2.3.6 Co-crystallization of <i>Mt</i> MetAP Ia with inhibitors.....	52
2.4 Discussion	54
Reference	60

CHAPTER 3 BIOCHEMICAL CHARACTERIZATION OF METHIONINE AMINOPEPTIDASE Ic IN MYCOBACTERIA TUBERCULOSIS	62
3.1 Introduction	62
3.2 Materials and Methods	64
3.2.1 Cloning of <i>MtMetAP Ic</i> into pGEMEX-1 plasmid	64
3.2.2 Over-expression and purification of <i>MtMetAP Ic</i>	64
3.2.3 Metal activation of <i>MtMetAP Ic</i>	65
3.2.4 Kinetics measurement of different metalloform <i>MtMetAP Ic</i>	66
3.2.5 IC ₅₀ determination with different metalloform of <i>MtMetAP Ic</i>	67
3.2.6 Complementation of the essential function of <i>EcMetAP</i> with <i>MtMetAP Ic</i> in <i>E.coli</i>	67
3.2.7 Inhibition of cellular <i>MtMetAP Ic</i> activity	69
3.2.8 Inhibition of <i>MtMetAP Ic</i> -complemented <i>E.coli</i> growth	70
3.2.9 Crystallization and data collection	71
3.2.10 Structure solution and refinement	71
3.2.11 Identification of quaternary structure of <i>MtMetAP Ic</i> using size exclusion chromatography	72
3.3 Results	73
3.3.1 Expression and purification of <i>MtMetAP Ic</i>	73
3.3.2 Metal binding and activation of <i>MtMetAP Ic</i>	73
3.3.3 Kinetic characterization of purified <i>MtMetAP Ic</i>	77
3.3.4. Functional complementation of <i>EcMetAP I</i> in <i>E.coli</i> growth by <i>MtMetAP Ic</i>	77
3.3.5 Metalloform-selective inhibition of purified <i>MtMetAP Ic</i> and the enzyme in an <i>E.coli</i> cellular environment	81
3.3.6 Growth inhibition of <i>MtMetAP Ic</i> -complemented <i>E.coli</i> cells	83
3.3.7 Co-crystallization of <i>MtMetAP Ic</i> with inhibitors	84
3.3.8 Identification of quaternary structure of <i>MtMetAP IC</i> using size exclusion chromatography	89
3.4 Discussion	90
Reference	97
CHAPTER 4 CONCLUSIONS AND FUTURE PLANS	100
References	105

List of Figures

Figure 1-1	<i>Mycobacterium tuberculosis</i>	2
Figure 1-2	Cell wall of <i>Mycobacterium tuberculosis</i>	4
Figure 1-3	Domain architecture of Methionine Aminopeptidase	12
Figure 1-4	Crystal structures of <i>EcMetAP I</i> , <i>PfMetAP IIa</i> and <i>HsMetAP IIb</i>	12
Figure 1-5	The dinuclear metal centers and the amino acid residues in <i>EcMetAP I</i> , <i>PfMetAP IIa</i> and <i>HsMetAP IIb</i>	14
Figure 1-6	Proposed reaction mechanism of dimetalated <i>EcMetAP I</i>	16
Figure 1-7	Proposed reaction mechanism of monometalated <i>EcMetAP I</i>	17
Figure 1-8	Crystal structure of <i>MtMetAP Ic</i> (PDB ID: 1 YJ3)	22
Figure 2-1	Calculation of K_m and K_{cat} values using non linear regression curve fitting based on Michaelis-Menten equation	37
Figure 2-2	Calculation of IC_{50} using non-linear curve fitting	39
Figure 2-3A	Overexpression of His <i>MtMetAP</i> upon IPTG induction	41
Figure 2-3B	Optimization of over-expression of <i>MtMetAP Ia</i> by changing the composition of the LB medium.	41
Figure 2-4	The purification of His <i>MtMetAP Ia</i>	43
Figure 2-5	Metal activation of (A)His <i>MtMetAP Ia</i> and (B) untagged <i>MtMetAP Ia</i>	45
Figure 2-6	Calculation of the apparent K_d of different metalloforms of <i>MtMetAP Ia</i>	46
Figure 2-7	Removal of His-tag from His <i>MtMetAP Ia</i> confirmed by Western blot	47
Figure 2-8	Calculation of the K_m of different metalloforms of <i>MtMetAP Ia</i> by using no linear regression curve fitting based on Michaelis–Menten equation	49
Figure 2-9	Structure-based sequence alignment of <i>EcMetAP</i> , <i>MtMetAP Ia</i> and <i>MtMetAP</i> <i>EcMetAP I</i> , <i>MtMetAP Ic</i> and virtual <i>MtMetAP Ia</i>	57
Figure 2-10	Ribbon drawing of the ‘pita-bread’ domain fold existing in <i>EcMetAP</i> , <i>MtMetAP Ic</i> , and homology model of <i>MtMetAP Ia</i> based on <i>MtMetAP Ic</i> structure	58
Figure 3-1	Conditional control of growth of <i>E.coli</i> amer mutant	68
Figure 3-2	The purification of <i>MtMetAP Ic</i>	74
Figure 3-3	Activation of <i>MtMetAP Ic</i> apoenzyme by divalent metals	75
Figure 3-4	Calculation of the apparent K_d of different metalloforms of <i>MtMetAP Ic</i> by using a MIBS model	77
Figure 3-5	Calculation of the K_m values of different metalloforms of <i>MtMetAP Ic</i>	78
Figure 3-6	Complementation of <i>EcMetAP I</i> by <i>MtMetAP Ic</i>	80
Figure 3-7	Structure of <i>MtMetAP Ic</i> in the Mn(II)- form in complex with the Mn(II)- form selective inhibitor 4.	86
Figure 3-8	Structures of <i>MtMetAP Ic</i> in the Ni(II)- form in complex with the Co(II)- and Ni(II)- form selective inhibitors 7 and 8	88
Figure 3-9	Identification of quaternary structure of <i>MtMetAP Ic</i> using Superdex 75	91
Figure 4.1	Complementation of <i>EcMetAP</i> function by <i>MtMetAP Ia</i>	102

List of Tables

Table 1-1	First-line drugs used in TB treatment	8
Table 2-1	Primers and oligos used in cloning	30
Table 2-2	Medium recipes used in His <i>MtMetAP</i> Ia solubility optimization test	32
Table 2-3	Comparison of metal activation of His <i>MtMetAP</i> Ia and <i>MtMetAP</i> Ia	46
Table 2-4	Kinetic measurement of His <i>MtMetAP</i> Ia	49
Table 2-5	Inhibition of enzymatic activities of purified <i>MtMetAP</i> Ia	51
Table 2-6	Summary of <i>MtMetAP</i> Ia initial crystallization screens	53
Table 3-1	Activation of <i>MtMetAP</i> Ic by different metals	76
Table 3-2	Kinetic measurement of <i>MtMetAP</i> Ic	78
Table 3-3	Inhibition of enzymatic activities of purified and cellular <i>MtMetAP</i> Ic and inhibition of cell growth of <i>MtMetAP</i> Ic-complemented <i>E.coli</i> by metalloform-selective inhibitors	82
Table 3-4	X-ray data collection and refinement statistics	85
Table 4.1	Comparison of Kinetic measurement of His <i>MtMetA</i> Ia and <i>MtMetAP</i> Ic	102

Page left intentionally blank

Page left intentionally blank

CHAPTER 1

INTRODUCTION: METHIONINE AMINOPEPTIDASES IN ANTI-TUBERCULOSIS DRUG DISCOVERY

1.1 Tuberculosis (TB)

1.1.1 History of tuberculosis

Tuberculosis (TB) is a deadly pulmonary disease caused by *Mycobacterium tuberculosis* in humans. The history of TB can be backdated to ancient Egypt since the sign of TB infection was found in the fragments of spinal columns in mummies from 2400 BC. The terms of consumptions, phthisis, scrofula, Pott's disease, and the White Plague had been used to refer to tuberculosis throughout history without knowing the exact cause of the disease. In 1882, Dr. Robert Koch revealed the bacterium that caused TB, which advanced the understanding of TB. The chest X-ray enabled physicians to diagnose and track the disease. In the following years until the twentieth century, the sanatorium movement, a medical program that involved diet, rest and medical treatment, began in Europe and spread to the U.S, and greatly contributed to the decline of the incidence and fatality of TB. As the century progressed, the BCG vaccines from *Mycobacterium bovine* and new antibiotics were used for TB treatment. Particularly, the discovery of streptomycin, the first antibiotic effective against *M. tuberculosis*, was considered as the beginning of the modern era of TB treatment. Combination therapy with isoniazid and rifampicin has significantly reduced the incidence of TB.

However, the steady decline of TB incidence began to stop and even started to reverse since the middle of the 1980s. It was mainly due to the rise of multidrug-resistant (MDR) *M. tuberculosis* strains, and the emergence of co-infection with HIV. According to the data released from WHO in March 2010, in some areas of the world, one in four people with TB have MDR

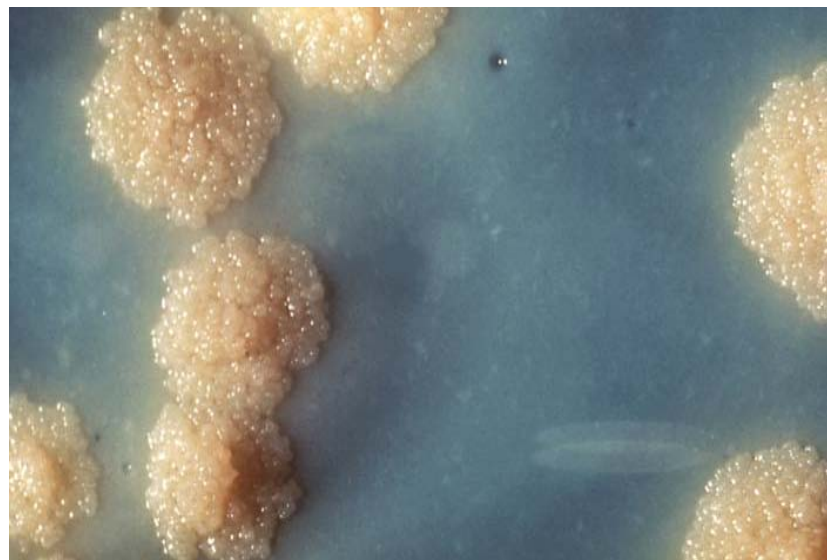
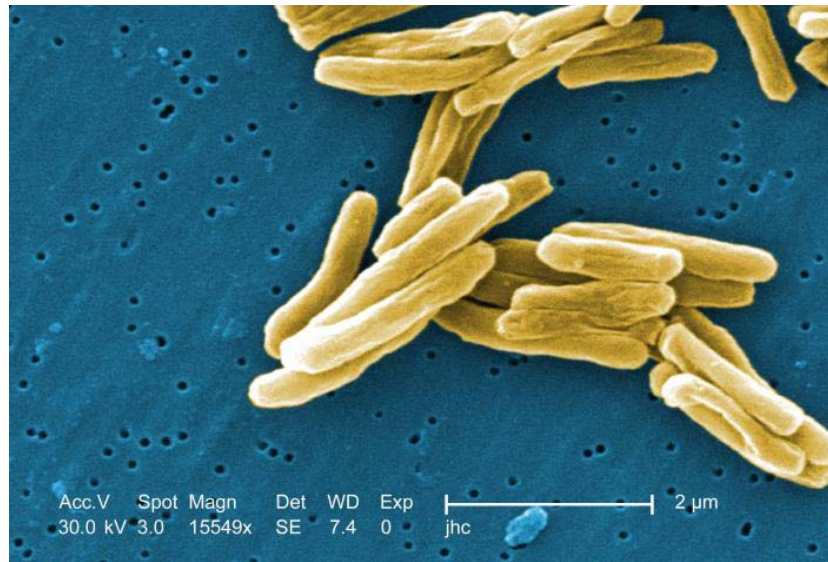


Figure 1-1 *Mycobacterium tuberculosis*

A) *Mycobacterium tuberculosis* under scanning electron microscopy. Magnification 15549 ×, *M. tuberculosis* is rod-shaped, 2-4 μm in length and 0.2-0.5 μm in width.

B) *Mycobacterium tuberculosis* colonies formed in the Middlebrook's medium.

Both pictures are from the website of Center for Disease Control

TB. This poses a tremendous challenge for TB treatment as the standard drugs currently being used show much less effect on the disease. Therefore, developing new and highly effective anti-TB medicines with novel mechanisms is essential to address the emergence of MDR TB.

1.1.2 Pathogen of tuberculosis

The etiologic agent of TB in humans is *Mycobacterium tuberculosis*. It is a Gram-resistant, non-motile, and rod-shaped bacterium. It is a relatively large bacterium as the rods are 2-4 micrometers in length and 0.2-0.5 micrometers in width. Other than in humans with TB infection, *M. tuberculosis* is usually found in water and soil, and grows under anaerobic conditions with a slow generation time of 15-17 hours. When it is cultured in a Middlebrook's medium [1], it forms visible white or light yellow colonies after 4-6 weeks (Figure 1-1). The distinctive serpentine cords can be observed in the laboratory grown colonies because of the tendency of colonies to aggregate. *M. tuberculosis* is an obligate aerobe. For this reason, the invading *M. tuberculosis* in hosts is always found in the upper bronchiole. The bacterium can also survive inside cells with slow growth rates, such as macrophages, which contributes to their virulence.

M. tuberculosis has a special cell wall with a high content of lipids. It is composed of mycolic acid/mycolate, and a peptidoglycan layer connected by polysaccharide (Figure 1-2). The extreme hydrophobic cell wall contributes to the impermeability and resistance to antimicrobial agents, the resistance of killing by acidic or alkaline agents in an intercellular or extracellular environment, and the resistance to lysosomal delivery after being taken into macrophages. Therefore, disruption of the *M. tuberculosis* cell wall, particularly interfering with the synthesis

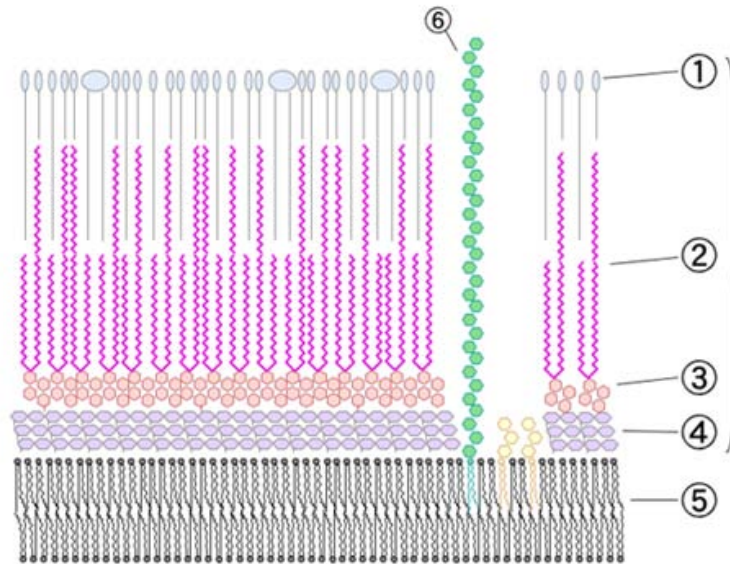


Figure 1-2 Cell wall of *Mycobacterium tuberculosis*.

M. tuberculosis has a cell wall with high lipid content above 60%. It is made of mycolic acid/ mycolate, and a peptidoglycan layer, connected by polysaccharide and arabinogalactan. ① outer lipid ② mycolic acid/ mycolate ③ polysaccharide ④ peptidoglycan ⑤ plasma membrane ⑥ lipoarabinomannan (LAM).

of virulent factors in cell membrane components, is the main strategy of the drugs currently used for TB treatment.

1.1.3 Pathogenesis and transmission of tuberculosis

Four stages are involved in pathogenesis of pulmonary tuberculosis [2]. The nuclei droplets with mycobacteria exhaled from TB patients can spread from one to another. At the first stage, the alveolar macrophages in the host can take up the inhaled droplets nonspecifically and destroy them. But this destruction of *M. tuberculosis* depends on the intrinsic capacity of host phagocytes and virulence factors of the ingested pathogen. If the macrophages cannot destroy the inhaled mycobacteria, the mycobacteria will multiply in macrophage until the macrophage burst. Upon the destruction of macrophages, which starts the second stage, blood monocytes are attracted to the place and develop into new macrophages in order to engulf *M. tuberculosis* without destroying them. Hence, the engulfed bacteria grow logarithmically inside macrophages and the macrophages accumulate within the first to the third weeks of the initial infection. No tissue damage occurs. In the third stage, when T-cell immunity develops, the lymphocytes are able to recognize the pathogen, *M. tuberculosis*, and trigger the release of interferon. The interferon leads to the activation of macrophages to kill the mycobacteria. The intracellular logarithmical growth of bacteria is halted and the extracellular growth of bacteria is inhibited because of the solid center of necrosis in the primary infection. Therefore, the bacteria become latent and may be disseminated to other organs through blood circulation.

In the last stage, which may be after months or even years later, under the circumstance of a weakening immune system, the latent pathogens could be reactivated in hosts. Because of an unknown mechanism, the centers of caseation necrosis liquefy, which provides a perfect

circumstance for extracellular multiplication of mycobacteria. Cavity formation may disrupt the nearby bronchi so that the mycobacteria will spread to other parts of the lungs and the outside environment. In summary, after entering the host, *M. tuberculosis* encounters a series of barriers from the host with different defense mechanisms. The final outcome of infection with *M. tuberculosis* depends on the balance between the outgrowth and killing of mycobacteria and the defense capability of the host's immune system.

A critical step in the pathogenesis of TB is the survival of *M. tuberculosis* in the host's macrophages. Normally, the engulfed bacteria are transferred to the lysosome and degraded. But in case of TB, mycobacterium is resistant to this transfer. A protein kinase G (PknG) from *M. tuberculosis* is suggested to relate to resistance. The PknG mediates intracellular survival of bacteria and is identified as a target for the control of mycobacteria infections [3]. More study is needed to illuminate the inactivation mechanism of macrophage and will shed light on the discovery of new agents for TB treatment.

1.1.4 Drugs used in chemotherapy of TB

The fundamental purpose of chemotherapy of TB is to kill bacteria or inhibit growth. Currently, there are five first-line drugs used for TB treatment, including streptomycin, isoniazid, rifampicin, ethambutol and pyrazinamide (Table 1-1). These drugs act in cell wall synthesis, DNA replication, RNA transcription and protein synthesis, which are essential for cell viability or logarithmic growth.

Streptomycin (SM) was the first effective antibiotic used against TB, extracted from *Streptomyces griseus*. It targets the S12 protein of the 30S subunit of the ribosome in *M. tuberculosis*, therefore interfering with the binding of formyl-methionyl-tRNA to the 30s

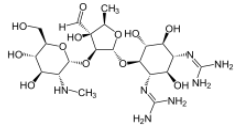
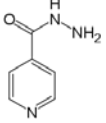
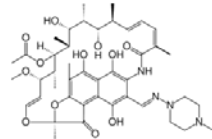
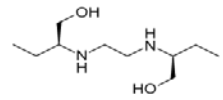
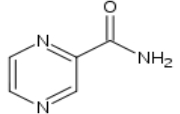
ribosome subunit [4]. This results in the failure of protein synthesis initiation and leads to cell death. This drug is given by intramuscular injection due to its poor absorbance in the gastrointestinal tract. Adverse effects include the toxicity to peripheral and central nervous systems. Drug-resistant bacteria strains exist.

Isoniazid (INH) is a pro-drug and requires the activation of catalase-peroxidase enzyme (kat G) from *M. tuberculosis* [5]. The kat G catalyzes the formation of isonicotinic acyl-NADH complex, which inhibits ketoenoylreductase (InhA) [6] and consequently blocks fatty acid synthesis. This process inhibits the synthesis of mycolic acid, a virulence factor required in cell walls. INH can be bactericidal to the *M. tuberculosis* in the log-phase, while it is bacteriostatic to the mycobacteria in the stationary-phase. The side effect includes hepatotoxicity, and the toxicity to the peripheral and central nervous systems. However, hepatotoxicity can be eliminated by the careful clinical monitoring of patients, while the toxicity to the nervous system can be avoided by the supplement of vitamin B6. The mutation in the *inhA* gene contributes to resistance to the INH in *M. smegmatis*[7].

Rifampicin (RIF) belongs to ansamycin antibiotics because its structure is similar to a basket. The aromatic moiety is the 'basket', and the long aliphatic chain that links both sides of the aromatic moiety is the 'handle'. It inhibits RNA polymerase and reduces protein synthesis in mycobacteria. The combination of isoniazid and rifampicin increases the risk of hepatotoxicity.

Ethambutol (EMB) is bacteriostatic and usually given in combination with isoniazid, rifampicin, and pyrazinamide. It disrupts arabinogalactan synthesis by inhibiting arabinosyl transferase, therefore the complex of mycolyl-arabinogalactan-peptidoglycocal in the cell wall cannot be formed, which leads to the increased permeability of the cell wall.

Tabel 1-1 First-line drugs used in TB treatment

Name	Structure	Mechanism	Gene(s) involved in resistance	Gene function	Mutation Frequency
SM		Inhibition of protein synthesis by targeting 30S subunit of ribosome	<i>rpsL</i> <i>rrs</i> <i>gidB</i>	S21 ribosomal protein 16s rRNA rRNA methyltransferase	52-59% 8-21%
INH		Inhibit fatty acid synthesis by targeting mycolate synthetase	<i>KcatG</i> <i>InhA</i>	catalase-peroxidase enoyl ACP reductase	50-95% 8-43%
RIF		Intefer with protein synthesis by targeting DNA-dependant RNA polymerase	<i>rpoB</i>	β -subunit of RNA polymerase	95%
EMB		Interfer with fatty acid synthesis by targeting arabinosyl transferase.	<i>embB</i>	Arabinosyl transferase	47-65%
PZA		to reduce the duration of treatment required	<i>pncA</i>	Nicotinamidase/pyrazinamidase	72-97%

Abbreviations: SM: streptomycin INH: isonizid RIF: rifampicin; EMB: ethambutol. PZA: pyrizinamide. Table modified from Yew *et al* 2009 [8]

Pyrazinamide (PZA) does not have significant bactericidal effects. It is used with isoniazid and rifampicin to shorten the treatment course. This pre-drug is converted to pyrazinoic acid by mycobacterial amidase. The mutation in the *pncA* gene coding pyrazinamidase confers resistance to this drug.

There are also second-line drugs for TB treatment. They are defined as such because they are unavailable in most developing countries, or they are less effective than the first-line drugs, or they have a higher toxicity or more side-effects. Aminoglycosides and fluoroquinolones are in this category and inhibit protein synthesis and membrane integrity in *M. tuberculosis*.

1.1.5 The challenge encountered in anti-TB drug discovery

All of the five first-line drugs listed above were discovered in the 1950s and have been extensively used. The high mutational frequency ($10^{-6} \sim 10^{-8}$) in the chromosome DNA is the major cause of drug resistance observed in *M. tuberculosis*. Moreover, long treatment courses as well as the misuse and mismanagement of these drugs also contribute to resistance to the drugs. Novel antibiotics to combat drug-resistant TB strains with higher potency, less adverse effects, and that facilitate a shorter treatment course, are in critical need to address this challenge. Rather than focusing on modifying current antibiotics and optimizing current treatment regimens, exploring potential targets for drug design is likely to be the most promising approach.

New antibiotics with novel mechanisms hold great promise to conquer drug-resistant TB. The completion of sequencing of the *Mycobacterium tuberculosis* H37Rv genome led to identification of essential genes for cell viability and greatly expanded the target pools for drug development. As more details of tuberculosis pathogenesis and mechanisms of drug-resistance

have been uncovered, a new paradigm targeting the virulence factor has been suggested as a better alternative for drug development [9].

1.2 Methionine aminopeptidase

1.2.1 Methionine aminopeptidase family

The methionine aminopeptidases (MetAPs) are a family of enzymes that are found in Bacteria, Archaea, and Eukarya. The enzymes cleave the N-terminal methionines from methionine-peptides in the presence of divalent metals. All protein translations begin at the N-terminus with a methionine (or N-methylmethionine), corresponding to the start codon AUG. However, 50-70% proteins have this initial methionine removed by MetAPs. This process, which variously correlates with protein stability, function and degradation, plays an essential role in almost every aspect of cellular biology.

MetAPs can be divided into two groups, type I and type II, based on the existence of the insert in the catalytic domains (Figure 1-3). Type I has no insert while type II has a 60 amino acid long insert. Eukaryotic cells have both type I and type II MetAPs, such as *Saccharomyces cerevisiae* [10] and humans [11]. In contrast, single MetAP is common in proeukaryotic cells. For instance, Eubacteria only has a type I MetAP, while Archaea only has one type II MetAP. Multiple MetAPs are rare in bacteria, but with more genomic sequences reported, two or more putative MetAP genes have been identified in a small number of bacteria [12-13].

The presence of an N-terminal extension can subdivide MetAP into three groups. MetAPa does not have the extension, while MetAP b and MetAP c have the extension. MetAP b and MetAP c are differentiated by the length of the N-terminal extension. Therefore, type Ia enzyme has neither an insert in the catalytic domain nor an N-terminal extension, and

MetAP from *E.coli* [14] is in this category. The Type Ib enzyme contains no insert in the catalytic domain, while it has an N-terminal extension, such as human MetAP Ib (*HsMetAP Ib*) and *Saccharomyces cerevisiae* MetAP Ib (*ScMetAP Ib*). Both of them have an extension of approximately 120 amino acids at the N-terminus, which includes two zinc-fingers and a linker of 50 amino acids. The proteolysis of the *ScMetAP Ib* by trypsin releases a fragment whose N-terminal sequence starts at Asp-70 with an immediately following Lys-69, indicating that *ScMetAP Ib* has an N-terminal zinc finger domain, and a C-terminal catalytic domain [15]. Metal titration experiments with wild-type *ScMetAP Ib* and the deletion mutant *ScMetAP Δ2-69* indicated that the native *ScMetAP Ib* had two zinc fingers and the zinc fingers were essential for MetAP normal function *in vivo* [16]. The type Ic MetAP has no insert in the catalytic domain and has a shorter N-terminal extension of 50 amino acid residues without a zinc finger. Type Ic MetAP was first described in *Mycobacterium tuberculosis* [17] and it was named as such in order to be differentiated from type Ib MetAP.

The alignment of MetAPs from *E.coli*, yeast and humans shows a high sequence similarity, indicating the evolutionary conservation of this type of enzyme.

1.1.2 Structure of methionine aminopeptidase

Crystal structures of *EcMetAPs* [18] reveal a pita-bread fold in the active sites. This unique fold consists of a central antiparallel β -sheet flanked by two pairs of α -helices, which have been observed in most MetAPs including *EcMetAP*, *ScMetAP*, and *HsMetAP*. Similar pita-bread folds are also found in aminopeptidase P (AMPP) and creatine amidinohydrolase (creatinase) even though these two enzymes have different activities and substrate specificities.

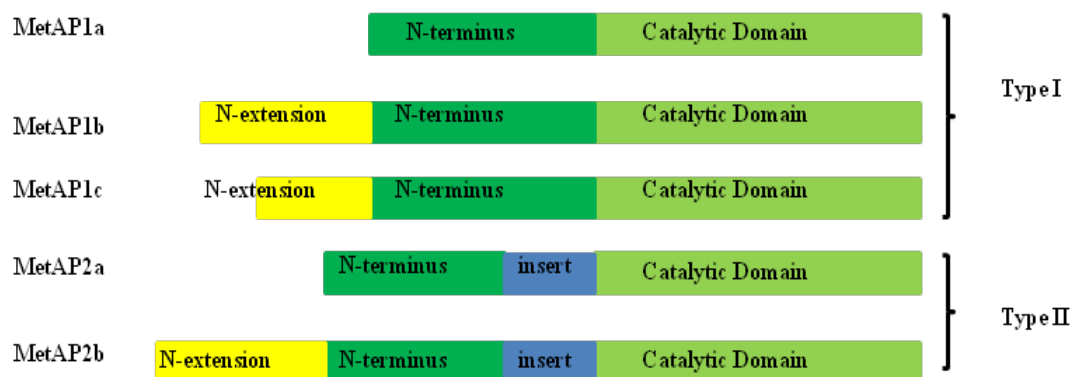


Figure 1-3 Domain architecture of methionine aminopeptidase

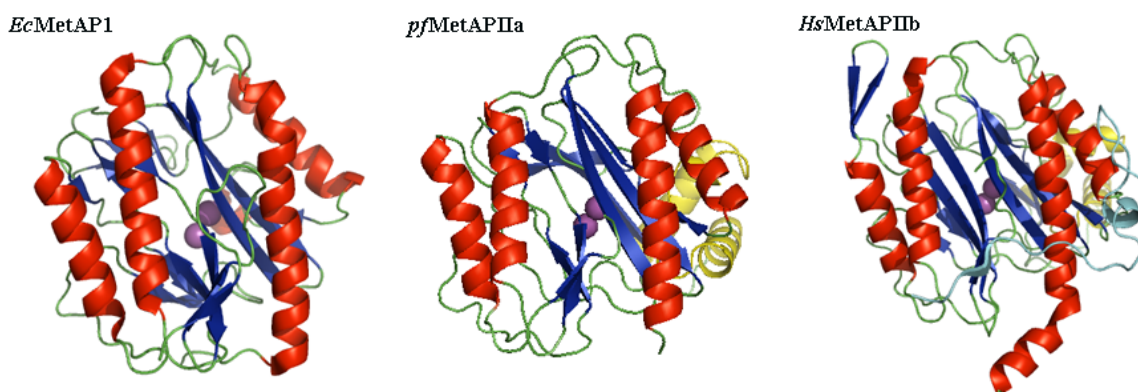


Figure 1-4 Crystal structures of *EcMetAP I*, *pfMetAP IIa* and *HsMetAP IIb*.

The pita-bread core domain is illustrated by red α -helices and blue β -sheets. The α -helical subdomain insertion in the type II enzymes is labeled in yellow. The N-terminal domain extension in *HsMetAP IIb* is indicated in blue. Metal ions are shown in magenta; Mn(II) in *EcMetAP I*, and Co (II) in *pfMetAP IIa* and *HsMetAP IIb*.

The pita-bread fold forms an internal pseudo 2-fold asymmetry. In *EcMetAP I*, which does not have the N-terminal extension or the insert in the catalytic domain, this pseudo symmetric fold can be clearly visualized. The symmetric unit consists of a β -sheet and a helix-bend-helix motif. The first half of the sequence residues from 11-116 comprises the N-terminal domain and the residues from 120-241 make another domain located at the N-terminus (*EcMetAP I* in Figure 1-4). The least squares transformation, which superimposed 64 selected α -carbon atoms from the C-terminal part on those in the N-terminal part, is equivalent to a rotation of 174° and a translation of 0.6 \AA to the axis of rotation. In addition to *EcMetAP*, chyrotrypsin-like serine proteases and the acid protease are also alike in structure within a single polypeptide. This phenomenon has been suggested as evidence of an ancestral gene duplication and fusion.

The dinuclear metal sites are located at the junction of two domains where two metal ions are clearly seen. These metals are in the center of the molecule, right between the β -sheets, and are bound through coordination with amino acids Asp-97, Asp-108, Glu-235, His-171 and Glu-204 (Figure 1-5). The metal binding coordination is very similar to that is observed in *PfMetAP IIa* and *HsMetAP IIb*. Even though the numbering of the metal coordinating residues are different in these MetAPs, the binding modes in the active sites are very comparable.

1.2.3 Catalysis of methionine aminopeptidase

By analyzing crystal structures of MetAPs with or without substrate binding (or substrate analogues), catalytic models for dimetalated and monometalated MetAP have been proposed [19-21].

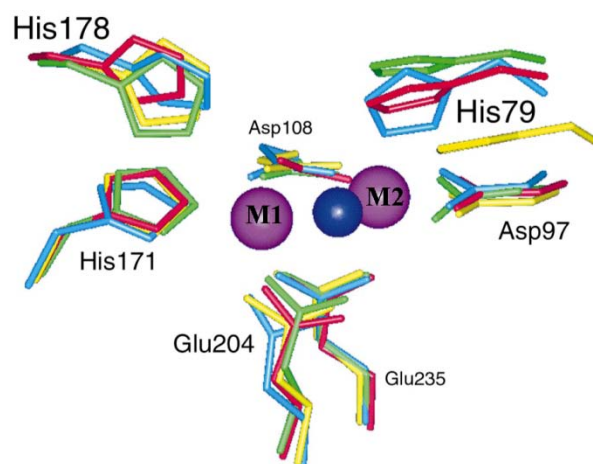


Figure 1-5 The dinuclear metal centers and the amino acid residues in *EcMetAP I*, *PfMetAP IIa* and *HsMetAP IIb*

EcMetAP is colored in yellow, *PfMetAP IIa* is colored in green, and *HsMetAP IIb* is colored in red. The blue colored enzyme is AMPP that has a similar pita-bread fold in its active site. Two metal ions are colored in magenta. The water molecule that bridges the metal ions is colored in deep blue. Only numberings in *EcMetAP* are listed. Modified from ref [22]

In dimetalated MetAP (Figure 1-6A), two metals (M1 and M2) and water molecules (A and B) are involved. The model is constructed based on following assumptions: 1) The N-terminus of the substrate binds to M2 at the cost of replacing water B; 2) A non-covalent tetrahedral *gem*-diolate intermediate is formed during catalysis; 3) The carboxyl oxygen from the scissile peptide bond interacts with Glu-204, and; 4) Water is the nucleophile during catalysis. In the resting MetAP, water A and B are clearly seen to coordinate to the metal center. Water A bridges the metal ions whereas water B behaves as the terminal ligand of M2. M1 is coordinated to Asp-108, His-171, Glu-204, Glu-235 and water A. The coordination geometry is a distorted trigonal bipyrimid. M2 is coordinated with Asp-97, Asp-108, Glu-235, water A and water B and the geometry is a distorted octahedron. Upon the substrate analog binding, water A, B and D in the active site are replaced by the O2 hydroxyl, the N-terminal nitrogen and the O1 atom of the inhibitor (Figure 1-6B). The geometry of M1 forms a distorted octahedron. The proposed reaction mechanism of dimetalated MetAP was illustrated in Figure 1-6C.

When the substrate approaches the active site, the carboxyl oxygen of the scissile bond (Oc) has been rotated so that it can interact with M1. Meanwhile, the hydroxide moiety from water A attacks the carbonyl carbon of the scissile bond. The Oc also interacts with His-178 and possibly forms a hydrogen bond to stabilize the transition state. Glu-204 is proposed to interact with the P'1 part of the substrate and shuttle a proton from the attacking hydroxide to the new N-terminus, facilitating its leaving. Mutation experiment and the binding mode adopted from substrate-alike inhibitors support this model [19].

In monometalated MetAP (Figure 1-7), only one metal (M1) and one water (A) are involved. M1 is coordinated with residues of His-171, Glu-204, Glu-235 and water A. When the

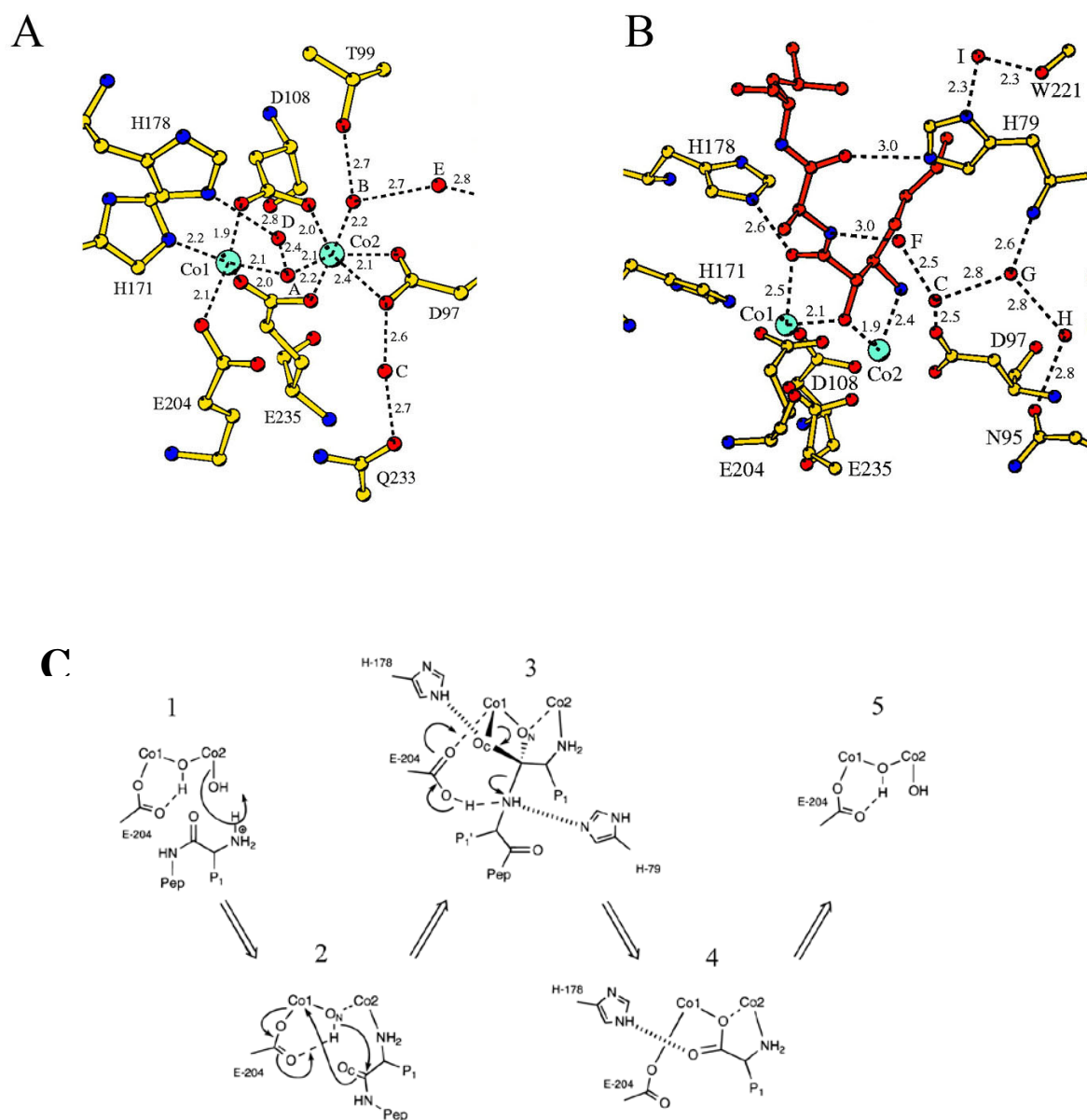


Figure 1-6 Proposed reaction mechanism of dimetalated *EcMetAP I*

A. Interactions in the metal center of *EcMetAP*.

B. Interactions in the metal center of *EcMetAP* bound with substrate-like inhibitor AHHpA. Color scheme for atoms: red, oxygen; blue, nitrogen; yellow, carbon; cyan, cobalt. Metals are labeled as Co1 and Co2; and water molecules are labeled as A to E.

C. Proposed reaction mechanism for dimetalated *EcMetAP* (Figure modified from reference [23])

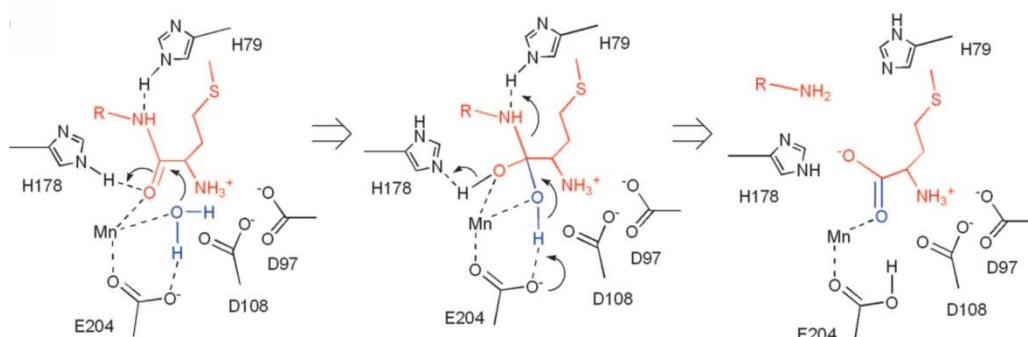


Figure 1-7 Proposed reaction mechanism of monometalated *EcMetAP I*

Substrate Met-Ala-Leu is colored red and its tetrahedral intermediate binds to the active site. The nucleophilic water molecule is colored blue. (Figure modified from ref [21])

substrate binds to the enzyme, it likely approaches M1 with the scissile bond in a *trans*-conformation. The imidazole moiety from His-79 moves toward the substrate and forms a hydrogen bond to the nitrogen of the scissile amide. Residue His-178 forms a hydrogen bond to the oxygen of the scissile carbonyl group. The metal-coordinated water A attacks the scissile carbonyl-group and a tetrahedral intermediate is formed. It shuttles a proton from the carbonyl group to the leaving group. As no M2 exists, residue Asp-97 and Asp-108 are no longer coordinated with metal. However, both residues move closer toward the positively charged moiety of the N-terminus of the peptide to develop charge-to-charge interaction, which helps to orient the peptide substrate for productive binding[21].

This catalytic mechanism of monometalated MetAP suggests the possibility of using one metal for MetAP activity and modifies the prevailing catalytic mechanisms of dimetalated MetAP.

The affinity differences were observed between two metal binding sites in a metalloenzyme. For example, the dissociation constants of Co (II) to the first and second binding sites in DNA polymerase I are 2.5 μM and 600 μM , respectively; and β -lactamase has K_d value of 0.14 μM and 2.52 mM for its tight and weak binding sites, respectively. Considering there would be no such large variation under normal physiological conditions, it is possible that only one metal binding site is occupied and used for catalysis. Therefore, caution must be exercised when structures are generated to aid in drug design.

1.1.4 Metal activation of methionine aminopeptidase

MetAP catalyzes the removal of the N-terminal methionine from nascent polypeptides. However, the loss of *Ec*MetAP activity upon EDTA treatment suggested the MetAPs were metalloenzymes, which depend on metal binding for activities [14].

Purified apo-MetAP I can be activated by divalent metals *in vitro*, usually by more than just one type of metal. MetAP from *E. coli* (*Ec*MetAP) can be activated by Co(II), Mn(II), Ni(II) and Zn(II); MetAP from *Saccharomyces cerevisiae* (*Sc*MetAP Ib) can be activated by Co(II) [24], Zn(II), Mn(II) and Ni [25]. MetAP from humans (*Hs*MetAP1b) can be activated by Co(II), Mn(II) and Zn(II). Similar metal activation was also reported for type II MetAP. *Hs*MetAP IIb shows activity in the presence of Co(II), Mn(II) and Zn(II). *Sc*MetAP IIb also showed metal activation by Co(II), Mn(II) and Zn(II). The diversity of activation by metals *in vitro* can be explained by the flexibility of the metal binding pocket. As long as the divalent metals can fit into the metal activity pocket consisting of Glu, Asp and His, it may promote nucleophilic catalysis with the hydroxide ion (-OH) via water ionization.

Even though the apoenzyme of MetAP shows activity in the presence of various metals *in vitro*, the metals used by the cellular MetAPs remain controversial. The activating metals used by metalloenzymes under physiological conditions are affected by two factors: 1) The binding affinity of a metal. An enzyme tends to bind the metals that show high affinity if the abundances of the metals are assumed to be the same. Affinities for metals tend to follow the Irving-Williams series ($\text{Mg(II)} < \text{Ca(II)} < \text{Mn(II)} < \text{Fe(II)} < \text{Co(II)} < \text{Ni(II)} < \text{Cu(II)} > \text{Zn(II)}$). For example, if all divalent metals are present and abundant, all proteins would bind Cu(II) as it has the highest binding affinity; and: 2) The available of metals for metalloprotein *in vivo*. This is determined by metal homeostasis, which is related to metal-specific importers and exporters in the membranes, and is tightly regulated by metal sensors through metal-responsive transcription [26].

Several candidates for the metals used by MetAP *in vivo* have been proposed, including Co (II) [18, 27], and Zn(II) [25], Mn(II) [28] and Fe (II) [29-30]. Co(II) is most often advocated as the metal used *in vivo*, because of its stable and repeatable activation of MetAPs [18, 24]. A low concentration of Zn(II) was observed to activate the EDTA-pretreated *ScMetAP Ib*, which was comparable to the activation by Co(II). *ScMetAP Ib* activity was further tested using high concentration of Zn(II) and Co(II) in the presence of a physiological concentration of reduced glutathione. The fact that the Zn(II)-substituted *ScMeAP Ib* retained high activity whereas the Co(II) substituted *ScMetAP Ib* lost activity suggested that Zn(II) could be the metal used under physiological circumstances [25]. *EcMetAP* substituted by Co(II) and Fe(II) in the presence of reduced glutathione gave the highest activity, indicating both metals were relevant to physiological function of MetAP. However, in the same paper, the metal content of mycobacterial extracts was measured with the extracts from two types of *E. coli* cells; one had a plasmid to express *EcMetAP* and another did not have. The mycobacterial extract from the *E.coli* with plasmid-expressed *EcMetAP* gave an increased Fe(II) content, when compared with the Fe(II) content from *E.coli* without plasmid-expressed *EcMetAP*, suggesting Fe(II) was the metal used by *E.coli in vivo* [30]. The *E.coli* growth was inhibited by the compounds that showed inhibition toward the Fe(II)-substituted *EcMetAP*, not by the compounds inhibiting Co(II) and Mn(II)-substituted *EcMetAP*. It also suggested that Fe(II) could be the metal used by *E. coli*. Chai *et al.* used metal-selective inhibitors to assign the metals used by *E.coli in vivo*. Only Fe(II)-specific inhibitors prevented the removal of N-terminal methionine in the recombinant glutathione S-transferase, which confirmed the cellular target of these compounds was MetAP and Fe(II) was likely the metal used in *E. coli* [29]. At this time, more evidence is required to clarify the metal used by MetAP *in vivo*.

1.3 Methionine aminopeptidase implication in anti-TB drug discovery

1.3.1 Methionine aminopeptidase in *Mycobacterium tuberculosis*

Mycobacterium tuberculosis has two MetAP genes (*mapA* and *mapB* in H37 Rv genome and *map_1* and *map_2* in CDC1551 genome), and both belong to type 1 MetAP with high homology to *E. coli* MetAP (*EcMetAP*). Little is known about their biochemical properties other than their DNA sequences. Addlagatta *et al.* purified *MtMetAP* 1c, which is encoded by the *mapB* gene, and crystallized it in an apoform and in a complex with methionine. The structure analysis revealed an SH3 binding motif at its N-terminus (Figure 1-8), which could potentially interact with ribosomes through the SH3 motif to facilitate removal of methionine [17]. Zhang *et al.* cloned and purified both MetAPs (*MtMetAP*1a encoded by the *mapA* gene; and *MtMetAP*1c encoded by the *mapB* gene). Both enzymes were characterized with metal activation, substrate specificity and temperature optima. Both enzymes could be activated by Co(II), Mg (II) and Zn(II). While Cu(II), Fe(II), and Ni(II) showed strong inhibitions of enzyme activity.

Transcriptional levels of two *map* genes were analyzed by real-time quantitative PCR. Gene *mapA* showed a 2-fold higher expression level in the 14-day log phase culture. In contrast, gene *mapB* gave a higher expression level in the 60-day stationary phase, which was about 1.5 fold higher than in the log phase. This result suggested that *MtMetAP* 1a and *MtMetAP* 1c could perform important functions in different growth phases of *M. tuberculosis* [31].

1.3.2 *MtMetAP*s as the potential targets for anti-TB drug

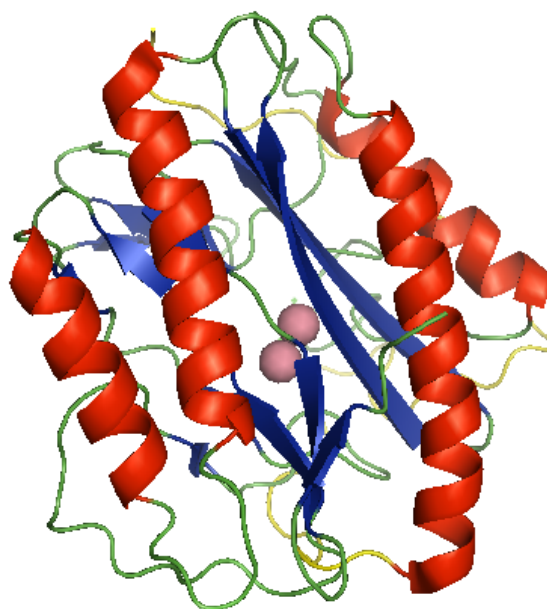


Figure 1-8 Crystal structure of *MtMetAP Ic* (PDB ID: 1YJ3)

The α -helices are colored red and β -sheets are colored blue. Two Co ions colored magenta are located in the active site. The N-terminal extension is colored yellow. PDB ID: 1YJ3

MetAPs have gained much attention as drug targets in the past few years because of their essentiality in cellular function. MetAP inhibitors targeting cancer, rheumatoid arthritis, fungal and malarial infections have been reported.

There are two putative *map* genes in *M. tuberculosis*, which share about 36.9% identity to each other. The different expression profiles of gene *mapA* and *mapB* in the log phase and the stationary phase indicate they may play different roles in *M. tuberculosis* pathogenesis [31]. The compounds that inhibit MetAP in *M. tuberculosis* hold the significant promise of effective TB therapy. However, it is important to determine if inhibition of either MetAP or both is sufficient for inhibition of mycobacterial growth.

The compounds that inhibit MetAP enzymatic activity could be used to co-crystallize with *Mt*MetAPs. Once the structure of MetAPs in the complex with the inhibitors is identified, it will provide useful information for rational design of anti-TB drugs. The inhibitors with higher potency and selectivity can be developed for TB treatment.

References:

1. Palomino, J.C., *et al.*, *Rapid culture-based methods for drug-resistance detection in Mycobacterium tuberculosis*. J Microbiol Methods, 2008. **75**(2): p. 161-6.
2. van Crevel, R., T.H. Ottenhoff, and J.W. van der Meer, *Innate immunity to Mycobacterium tuberculosis*. Clin Microbiol Rev, 2002. **15**(2): p. 294-309.
3. Walburger, A., *et al.*, *Protein kinase G from pathogenic mycobacteria promotes survival within macrophages*. Science, 2004. **304**(5678): p. 1800-4.
4. Sharma, D., *et al.*, *Mutational analysis of S12 protein and implications for the accuracy of decoding by the ribosome*. J Mol Biol, 2007. **374**(4): p. 1065-76.
5. Zhang, Y., *et al.*, *The catalase-peroxidase gene and isoniazid resistance of Mycobacterium tuberculosis*. Nature, 1992. **358**(6387): p. 591-3.
6. Suarez, J., *et al.*, *Antibiotic resistance in Mycobacterium tuberculosis: peroxidase intermediate bypass causes poor isoniazid activation by the S315G mutant of M. tuberculosis catalase-peroxidase (KatG)*. J Biol Chem, 2009. **284**(24): p. 16146-55.
7. Ahmed Kamal, S.A., M. Shaheer Malik, Ahmad Ali Shaik, Maddamsetty V. Rao, *Efforts Towards the Development of New Antitubercular Agents: Potential for Thiolaactomycin Based Compounds*. J Pharm Pharmaceut Sci, 2008. **11**(2): p. 56s-80s.
8. Zhang, Y. and W.W. Yew, *Mechanisms of drug resistance in Mycobacterium tuberculosis*. Int J Tuberc Lung Dis, 2009. **13**(11): p. 1320-30.
9. Clatworthy, A.E., E. Pierson, and D.T. Hung, *Targeting virulence: a new paradigm for antimicrobial therapy*. Nat Chem Biol, 2007. **3**(9): p. 541-8.
10. Li, X. and Y.H. Chang, *Amino-terminal protein processing in Saccharomyces cerevisiae is an essential function that requires two distinct methionine aminopeptidases*. Proc Natl Acad Sci U S A, 1995. **92**(26): p. 12357-61.
11. Arfin, S.M., *et al.*, *Eukaryotic methionyl aminopeptidases: two classes of cobalt-dependent enzymes*. Proc Natl Acad Sci U S A, 1995. **92**(17): p. 7714-8.
12. You, C., *et al.*, *The two authentic methionine aminopeptidase genes are differentially expressed in Bacillus subtilis*. BMC Microbiol, 2005. **5**: p. 57.
13. Chen, X., *et al.*, *Inhibitors of Plasmodium falciparum methionine aminopeptidase 1b possess antimalarial activity*. Proc Natl Acad Sci U S A, 2006. **103**(39): p. 14548-53.
14. Ben-Bassat, A., *et al.*, *Processing of the initiation methionine from proteins: properties of the Escherichia coli methionine aminopeptidase and its gene structure*. J Bacteriol, 1987. **169**(2): p. 751-7.
15. Zuo, S., *et al.*, *Evidence that two zinc fingers in the methionine aminopeptidase from Saccharomyces cerevisiae are important for normal growth*. Mol Gen Genet, 1995. **246**(2): p. 247-53.
16. Vetro, J.A. and Y.H. Chang, *Yeast methionine aminopeptidase type I is ribosome-associated and requires its N-terminal zinc finger domain for normal function in vivo*. J Cell Biochem, 2002. **85**(4): p. 678-88.
17. Addlagatta, A., *et al.*, *Identification of an SH3-binding motif in a new class of methionine aminopeptidases from Mycobacterium tuberculosis suggests a mode of interaction with the ribosome*. Biochemistry, 2005. **44**(19): p. 7166-74.
18. Roderick, S.L. and B.W. Matthews, *Structure of the cobalt-dependent methionine aminopeptidase from Escherichia coli: a new type of proteolytic enzyme*. Biochemistry, 1993. **32**(15): p. 3907-12.

19. Lowther, W.T., *et al.*, *Escherichia coli* methionine aminopeptidase: implications of crystallographic analyses of the native, mutant, and inhibited enzymes for the mechanism of catalysis. *Biochemistry*, 1999. **38**(24): p. 7678-88.
20. Lowther, W.T., *et al.*, *Insights into the mechanism of Escherichia coli* methionine aminopeptidase from the structural analysis of reaction products and phosphorus-based transition-state analogues. *Biochemistry*, 1999. **38**(45): p. 14810-9.
21. Ye, Q.Z., *et al.*, *Structural basis of catalysis by monometalated methionine aminopeptidase*. *Proc Natl Acad Sci U S A*, 2006. **103**(25): p. 9470-5.
22. Lowther, W.T. and B.W. Matthews, *Structure and function of the methionine aminopeptidases*. *Biochim Biophys Acta*, 2000. **1477**(1-2): p. 157-67.
23. Lowther WT, Z.Y., Sampson PB, Honek JF, Matthews BW., *Insights into the mechanism of Escherichia coli* methionine aminopeptidase from the structural analysis of reaction products and phosphorus-based transition-state analogues. *Biochemistry*, 1999. **38**(45): p. 14810-9.
24. Chang, Y.H., U. Teichert, and J.A. Smith, *Purification and characterization of a methionine aminopeptidase from Saccharomyces cerevisiae*. *J Biol Chem*, 1990. **265**(32): p. 19892-7.
25. Walker, K.W. and R.A. Bradshaw, *Yeast methionine aminopeptidase I can utilize either Zn²⁺ or Co²⁺ as a cofactor: a case of mistaken identity?* *Protein Sci*, 1998. **7**(12): p. 2684-7.
26. Waldron, K.J. and N.J. Robinson, *How do bacterial cells ensure that metalloproteins get the correct metal?* *Nat Rev Microbiol*, 2009. **7**(1): p. 25-35.
27. Ghosh, M., *et al.*, *Characterization of native and recombinant forms of an unusual cobalt-dependent proline dipeptidase (prolidase) from the hyperthermophilic archaeon Pyrococcus furiosus*. *J Bacteriol*, 1998. **180**(18): p. 4781-9.
28. Li, J.Y., *et al.*, *Mutations at the S1 sites of methionine aminopeptidases from Escherichia coli and Homo sapiens reveal the residues critical for substrate specificity*. *J Biol Chem*, 2004. **279**(20): p. 21128-34.
29. Chai, S.C., W.L. Wang, and Q.Z. Ye, *FE(II) is the native cofactor for Escherichia coli methionine aminopeptidase*. *J Biol Chem*, 2008. **283**(40): p. 26879-85.
30. D'Souza V, M. and R.C. Holz, *The methionyl aminopeptidase from Escherichia coli can function as an iron(II) enzyme*. *Biochemistry*, 1999. **38**(34): p. 11079-85.
31. Zhang, X., *et al.*, *Expression and characterization of two functional methionine aminopeptidases from Mycobacterium tuberculosis H37Rv*. *Curr Microbiol*, 2009. **59**(5): p. 520-5.

CHAPTER 2

BIOCHEMICAL CHARACTERIZATION OF METHIONINE AMINOPEPTIDASE 1A IN MYCOBACTERIA TUBERCULOSIS

The work described in this chapter was published in Bioorganic & Medicinal Chemistry Letters, entitled “Expression and characterization of *Mycobacterium tuberculosis* methionine aminopeptidase type 1a”.

2.1 Introduction

Mycobacterium tuberculosis, the etiological factor of tuberculosis (TB), is one of the toughest microbe that humans have ever fought against [1]. According to the data released by WHO in 2010, about one third of the world's population are infected with TB Bacillus [2]. The emergence of multidrug-resistant *M. tuberculosis* strains and the co-infection of TB with HIV complicate the disease; and the long duration of the required treatment reduces the efficiency of the therapy. New antibiotics with novel mechanisms are urgently needed to solve the problem.

Methionine aminopeptidase (MetAP) is a promising target for anti-bacterial drug development, including anti-TB agents. It is widely distributed in prokaryotic and eukaryotic cells, catalyzing the removal of the N-terminal methionine in the nascent peptides [3]. The essentiality of the enzyme was demonstrated in deletion mutants in *Escherichia coli* [4], *Salmonella typhimurium* [5], and *Saccharomyces cerevisiae* [6], which were lethal, suggesting it as a potential drug target for antibiotic development.

A critical step in discovering anti-TB agents is to characterize the MetAP of *M. tuberculosis*, and to find inhibitors targeting MetAP with strong potency and high selectivity. Determining the activation metal ions of MetAP is particularly important as MetAP is a

metalloenzyme, for which divalent metal ions play a key role in the hydrolysis. It shows metal-dependant activities in the presence of a series of divalent metals *in vitro*, such as Co (II) [7], Mn (II) [8], Fe(II) [9], and Zn(II) [10]. However, which metal is utilized by MetAP *in vivo* has remained contentious. Fe (II) [9, 11], Mn(II) [12], and Zn(II) [13] have all been suggested to be the metal used under physiological conditions. The fact that compounds showed potent inhibition of MetAP from *in vitro* screening, but failed to inhibit the enzyme *in vivo* indicated the a discrepancy between the metals used *in vitro* and *in vivo* [14-15]. Therefore, in order to develop anti-TB drugs based on MetAP, the covalent metals used by MetAP *in vivo* should be taken into consideration. Thus, determining which metal is responsible for the activation of MetAP is a necessary step in anti-TB drug development.

There are two putative MetAP genes (*mapA* and *mapB*) found in the *M. tuberculosis* H37Rv strain [16] and both of them are type I MetAPs with high homology to *E. coli* MetAP (*EcMetAP*). Little is known about the biochemical properties of these putative MetAPs other than the DNA sequences. Recently, two MetAP proteins from *M. tuberculosis* were purified, and characterized for metal binding and activation [17]. However, the metal activation results from their experiment were not convincing. The MetAPs tested in their experiments showed activity in the absence of metal ions, indicating the enzymes were not apo form enzymes. Their result, therefore, be misleading.

In order to characterize MetAP in *M. tuberculosis*, particularly its metal activation, both *MtMetAP* genes were cloned and the enzymes were purified and characterized in our laboratory. In this chapter, characterization of *MtMetAP* Ia is described, including metal activation, kinetic measurements, metal-selective inhibition, and crystallization. The results offer further insight into discovering and developing *MtMetAP* Ia inhibitors for anti-TB treatment.

2.2 Materials and Methods

2.2.1 Cloning of *MtMetAP Ia* into pGEMEX-1 plasmid

The DNA encoding *MtMetAP Ia* (*mapA*, locus_tag Rv0734) from the genomic DNA of *Mycobacterium tuberculosis* H37Rv (a generous gift from Professor Scott G. Franzblau at the University of Illinois at Chicago) was amplified by PCR. The PCR fragments were digested by *EcoRI* and *NheI* (New England Biolabs, Ipswich, MA) and cloned into plasmid pGEMEX-1 (Promega, Madison, Wisconsin). The primers for PCR were synthesized by Enrofins MWG Operon (Enrofins MWG Operon Biotech, Huntsville, Alabama). All the sequences are listed in Table 2-1.

The construct pGEMEX1-*MtMetAP Ia*-1 was checked by DNA sequencing analysis. It showed that a shorter *mapA* gene was cloned into the pGEMEX-1 plasmid instead of the complete *mapA* gene. It was due to an *EcoRI* restriction site (G-AATTC) in the *mapA* gene. The DNA sequence at the end of the *mapA* gene is shown below. The missing nucleotides are framed and the *EcoRI* restriction sites are underlined.

Construct	CGACCGCCGATGGGTCACGTGCGGCACACTGGGAACACACCGTGGCGGTAACCGACGACG	
<i>mapA</i>	CGACCGCCGATGGGTCACGTGCGGCACACTGGGAACACACCGTGGCGGTAACCGACGACG	
Construct	GGCCCC <u>GAATTC</u> GTCTGAC-CTCGAG	854
<i>mapA</i>	GGCCCC <u>CTTAA</u> G -T-GACGCTCGGG	143192

To fix this problem, two DNA oligonucleotides were designed to change the *EcoRI* restriction site from GAATTC to GTATAC. Two *ApaI* digestion sites (G-GGCCC) and one *AvrII* digestion site (C-CTAGG) were introduced for easy confirmation of the new construct. Both DNA oligonucleotides had the same sequences and were reverse-complement to one another. As shown below, the *ApaI* restriction sites are framed, and the *AvrII* restriction site is underlined.

Oligonucleotides RF: TGCGACGAC **GGGCCC** CGTATACTGAC CCTAGG TTAGAATTC **GGGCCC** TCTAGATGC
 Oligonucleotides RR: GCATCTAGA **GGGCCC** GAATTCTAA CCTAGG GTCAGTATACG **GGGCCC** GTCGTCGCA

These two oligonucleotides (100 µM) were mixed together in the annealing buffer (1 mM EDTA, 10 mM Tris-HCl pH 8.0, and 50 mM NaCl) in a 1.5 mL centrifuge tube and heated both in a boiling water bath for 5 minutes. The mixture was left in the water and allowed to cool down to room temperature. The annealed oligonucleotides were kept at -20 °C, ready for use.

Both the annealed oligonucleotides and pGEMEX1-*MtMetAP Ia* were digested by *ApaI* at 37 °C for 2 hours, followed by treatment with calf intestinal alkaline phosphatases (CIP) to remove the 5'- phosphates and prevent recircularization of the vector. The digested DNA oligonucleotides and pGEMEX1-*MtMetAP Ia*-1 were joined by T4 ligase. The fixed *EcoRI* restriction site in the resulting pGEMEX1-*MtMetAP Ia*-2 was confirmed by DNA sequencing.

2.2.2 Re-cloning of the *mapA* gene into pET28a plasmid

The *mapA* gene was cut from plasmid pGEMEX1-*MtMetAP Ia* by *NheI* and *EcoRI* and cloned into pET28a (EMD Biosciences, Gibbstown, NJ) to put a hexahistidine tag at its N-

Table 2-1: Primers and oligonucleotides used in cloning

Protein	Primer sequence	Restriction Enzyme	Plasmid
<i>MtMetAP</i> Ia	forward 5'-GGATCA CCA <u>GCTAGCAT</u> GCGCCCACTGGCA CGG-3'	NheI	pGEMEX-1
	Reverse 5'-AGCA CTC <u>GAATTCTA</u> ACCGA GCGTCA GAAT-3'	EcoRI	
Oligonucleotides to fix <i>MtMetAP</i> Ia-Mutant	Oligonucleotide RF: 5'-TGC GACGA CGGGCCC CGTATACTGAC <u>CCCTAGG</u> TTAGAATT CGGGCCC TCTAGATGC-3'	<u>AvrII</u>	pGEMEX-1
	Oligonucleotide RR: 5'-GCA TCTAGA GGGCCC GAATTCTAA <u>CCTAGG</u> GTCA GTATAC GGGGCCC GTCGTCGCA -3'	ApaI	

terminus. The sequence of the plasmid pET28a-*MtMetAP Ia* was confirmed by DNA sequencing analysis.

2.2.3 Protein solubility optimization

Due to the poor solubility of His*MtMetAP Ia*, an optimization test was carried out based on Kim's publication [18] to improve the solubility. Kim et. al indicated that protein solubility can be improved by changing the constitution of the LB medium. Adding salt, sorbitol, or betaine as well as exposing bacteria to a heat shock can increase the cellular concentration of osmolytes or of chaperones, thereby helping to express soluble target proteins. The medium recipes investigated in optimization tests are listed in Table 2-2.

Solubility optimization tests were carried out in 10 mL culture tubes. Cells were grown in 5 mL LB with ampicillin at 37 °C until an OD₆₀₀ of 0.6 ~ 0.8. Isopropyl-β-D-thiogalactopyranoside (IPTG) was added at a final concentration of 0.3 mM to induce protein expression. All of the heat-shock tubes were incubated in a 47 °C water bath for 10 minutes before they were put in a shaker and incubated at 20 °C for 20 hours.

The cells were harvested and cell densities were adjusted to the same level. One milliliter samples of cell culture grown in the different mediums were taken from each sample and centrifuged (5000 × g, 5 minute, 4°C), The pellets were resuspended with 100 μL 50 mM Tris-HCl, pH 8.0 and 150 mM NaCl and sonicated for 10 x 10 sec (with 10 second rest between each sonication) at full power in an ice bath to avoid overheating of the samples. The cellular debris was removed by centrifugation at 16,873 × g for 10 min at 4 °C. The whole cell sample, as well as the supernatant, was collected after centrifugation. All the samples were examined by SDS-PAGE gel to check the expression level of soluble protein.

Table 2-2 Medium used in His*Mt*MetAP Ia solubility optimization test

Medium ID	Ingredient
LB	LB
LBS	LB + 0.5 M sorbitol
LBSB	LB + 0.5 M sorbitol + 1 mM betaine
LBSG	LB + 0.5 M sorbitol + 0.2% glucose
LBSBG:	LB + 0.5 M Sorbitol+ 1 mM betaine + 0.2% glucose
LBG	LB + 0.2% glucose
LBN	LB + 0.5 M NaCl
LBNB	LB + 0.5 M NaCl + 1 mM betaine
LBNG	LB + 0.5 M NaCl + 0.2%glucose

2.2.4 Over-expression and purification of His*Mt*MetAP Ia

The pET28a-*Mt*MetAP Ia plasmid was introduced into *E.coli* BL21(DE3) (Invitrogen, Carlsbad, CA) for protein expression. A single colony freshly transformed was cultured in LB medium with 50 ng/mL kanamycin at 37 °C overnight. The pre-culture was inoculated into 1 liter LB with kanamycin (50 ng/mL) and kept growing at 37 °C until the optical cell density reached 0.6 - 0.8 at 600 nm. Protein production was induced by adding 0.4 mM IPTG and the temperature was reduced to 16 °C. After 20 hours, the cells were harvested by centrifugation at $4400 \times g$ for 10 minutes and the pellets were resuspended with suspension buffer (50mM Tris-HCl, pH 8, and 150 mM NaCl). The pelleted cells were stored at -20 °C until purification.

Frozen cells were disrupted by passing through French Press three times consecutively and the cellular debris was removed by centrifugation at $47,810 \times g$ for 45 minutes at 4 °C. Sodium chloride and imidazole were added to the supernatant to make their concentrations in the supernatant to be the same as in the elution buffer (50 mM Tris-HCl, pH 8, 500 mM NaCl, 5 mM imidazole). The supernatant was loaded onto a HiTrap FF His column (GE Healthcare Life Science, Piscataway, NJ) equilibrated with the elution buffer. A linear gradient of imidazole, from 10 mM to 200 mM, was applied and the His*Mt*MetAP Ia was eluted at the approximately 150 mM imidazole. Fractions containing the His-tagged *Mt*MetAP Ia were examined by SDS-PAGE before being pooled and concentrated with an Amicon stirred cell through a YM-10 membrane (Millipore, Billerica, MA). The concentrated protein was treated with 1,10-phenanthroline to remove the divalent metals. The treated protein, about 4 -5 mL, was loaded to a 5 mL HiTrap desalting column (GE Healthcare Life Science, Piscataway, NJ) to change the buffer to 50 mM MOPS-NaOH, pH 7.5, and 150 mM NaCl, which was pretreated with Chelex-

100 resin (BioRad, Hercules, CA). The apoenzyme was aliquoted into 0.2 mL fractions and kept at -20°C.

2.2.5 Untagged *MtMetAP Ia* preparation and confirmation of removal of His-tag

A small amount of untagged *MtMetAP Ia* was prepared to compare the kinetic characteristic with His-tagged *MtMetAP Ia*. The purified His*MtMetAP Ia* was treated with thrombin (1000 units /mg protein) (EMD, San Diego CA) at 4 °C for 48 hours in a buffer containing 50 mM Tris-HCl pH 8.0, and 1.5 mM CaCl₂. The thrombin treated sample was loaded onto a HiTrap FF His tag column and the untagged *MtMetAP Ia* was recovered in the flow-through. All fractions including the flow-through fractions and the eluted fractions were collected for Western blotting test.

Western blotting was carried out to check the removal of the His-tag from His*MtMetAP Ia* by thrombin treatment. A horseradish peroxidase (HRP) conjugated His•Tag® antibody (EMD, San Diego, CA) was used to check for the existence of the consecutive His- tag in combination of luminescence detection. All the fractions mentioned above and the pre-treated fractions were adjusted to appropriate concentrations to make one microgram of each sample for SDS-PAGE. After electrophoresis, the separated protein bands in the polyacrylamide gel were transferred to a PVDF membrane (Pall Corp. Pensacola, FL) using Bio-Rad Semi-dry Transfer Cell (BioRad, Hercules, CA). The transfer was performed at 400 mA for 30 minutes. The PVDF membrane was washed with 1 × TBS (150 mM NaCl, 10 mM Tris-HCl, pH 7.5) twice, 10 minutes for each wash and incubated with 5% non-fat milk at 4 °C overnight. The blocked membrane was washed with 1 × TBSTT (500 mM NaCl, 20 mM Tris-HCl, 0.2% v/v Triton X-100, 0.05 % v/v Tween-20, pH 7.5) twice, 10 minutes for each time, and with 1 × TBS for 10 minutes. Thereafter, it was

incubated with HRP conjugated His-tag antibody (1:2000) at 4 °C for 1 hour, followed by membrane washing with 1 × TBSTT twice, and with 1 × TBS once, 10 minutes for each wash. The substrate for detection was made immediately prior to use by combining equal parts of 2 × Luminol/Enhancer Solution and 2 × WestPico Stable Peroxide Solution (ThermoFisher Scientific, Rockford, IL). They were mixed briefly and added to the membrane. The PVDF Membrane was ready for luminescent signal detection after being soaked in the substrate mix for 1 minute. Excess substrate was drained from the membrane by touching the membrane edge to a paper towel. The membrane was placed on a fresh sheet of plastic wrap. Bubbles between plastic and membrane were removed by folding plastic over the membrane. The liquid was gently removed from the exterior of the plastic and a gLOCATOR™ Luminescent Label was put into the plastic folder to record blot-identifying data for future reference. The image was taken in the chamber of the imaging system from UltraLum, (Claremont, CA).

2.2.6 Metal activation of His*Mt*MetAP Ia

Kinetic analysis with His*Mt*MetAP Ia was carried out with a fluorescence based assay, using the fluorogenic substrate methionine-7-amido-4-methyl-coumarin (Met-AMC) (Bacham, Bioscience, King of Prussia, PA), which was hydrolyzed by MetAP in the presence of covalent metal. The released AMC emits fluorescence that can be detected at 460 nm with λ_{ex} 360 nm as an enzymatic activity monitor. All kinetic experiments were carried out in 384-well plates in a SpectraMax Gemini XPS plate reader (Molecular Devices, Sunnyvale, CA), at room temperature as described [8, 19].

For metal activation, each well contained 50 mM MOPS-NAOH, pH 7.5, 100 μ M Met-AMC, 50 nM apoenzyme and increasing amounts of metal ions (NiCl_2 , CoCl_2 , MnCl_2 , or FeCl_2

with twice the concentration of ascorbic acid). The total volume was 80 μ L. The initial velocity values were converted to specific activity values and plotted against increasing concentrations of the metal.

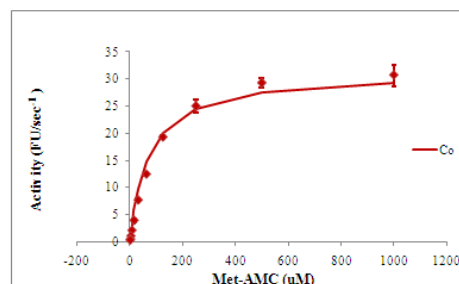
In order to describe metal activation of *Mt*MetAP Ia, we determined the metal concentration that gave 50% activity of the enzymes, and defined it as apparent K_d as it suggested the binding affinity. For determination for binding of the divalent metals to His*Mt*MetAP Ia, the titration curves were generated using different amounts of His*Mt*MetAP Ia (12.5 nM apoenzyme for Ni(II), 25 nM apoenzyme for Co(II) and Fe(II), and 50 nM apoenzyme for Mn(II)) in 50 mM MOPS-NAOH-NAOH, pH 7.5, 100 μ M Met-AMC and increasing concentrations of either CoCl_2 , MnCl_2 , NiCl_2 or FeCl_2 . In the case of FeCl_2 , ascorbic acid was added at a two-fold concentration of FeCl_2 .

The metal activation was also carried out with untagged *Mt*MetAP Ia for comparison with that of His*Mt*MetAP Ia.

2.2.7 Kinetic measurement of different metalloform His*Mt*MetAP Ia

For determination of Michaelis-Menten kinetic parameters, enzyme activities were measured in the 80 μ L assay mixture containing 50 mM MOPS-NAOH, pH 7.5, His*Mt*MetAP Ia (25 nM Co(II)- or Fe(II)- substituted enzyme, 50 nM Mn(II)-substituted enzyme, or 12.5 nM Ni(II)-substituted enzyme), covalent metals (10 μ M FeCl_2 with 20 μ M ascorbic acid, 20 μ M CoCl_2 , 200 μ M MnCl_2 , or 20 μ M NiCl_2), and substrate Met-AMC in a 2-fold dilution up to 2 mM at room temperature. The initial rates were plotted with the corresponding substrate concentrations, and the curve was fitted to the Michaelis-Menten equation to obtain K_m and k_{cat} values (Figure 2-1).

Co					
[Substrate]	Va	Vc	(Va-Vc) ²	STD	
2000	30.591	30	80294	2	Km 70.5
1000	30.678	29	2887	2	Vmax 31.4
500	29.242	27	380	1	Sum(Va-Vc) ² 45
250	24.964	24	331	1	
125	19.253	20	465	0	
62.5	12.420	15	78	0	
31.25	7.655	10	391	0	
15.625	3.919	6	65	0	
7.8125	2.071	3	32	0	
3.90625	1.034	2	5	0	
1.953125	0.471	1	15	0	
0.9765625	0.282	0	23	0	



Mn					
[Substrate]	Va	Vc	(Va-Vc) ²	STD	
2000	13.805	14	0	0	Km 169.9
1000	12.939	13	0	0	Vmax 15.0
500	11.092	11	0	0	Sum(Va-Vc) ² 0
250	9.124	9	0	1	
125	6.664	6	0	1	
62.5	4.365	4	0	0	
31.25	2.556	2	0	1	
15.625	1.395	1	0	0	
7.8125	0.530	1	0	0	
3.90625	0.353	0	0	0	
1.953125	0.162	0	0	0	
0.9765625	0.225	0	0	1	

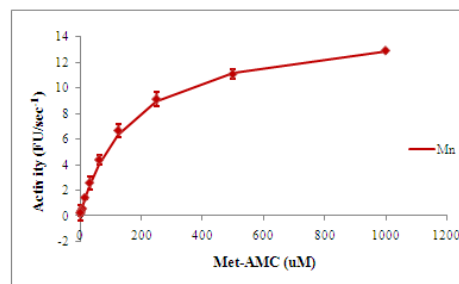


Figure 2-1 Calculation of K_m and K_{cat} values using non linear regression curve fitting based on Michaelis-Menten equation. Va represents the measured enzyme activities. Vc represents the calculated activities based on Michaelis-Menten equation ($V = V_{max} * [S] / (K_m + [S])$).

2.2.8 IC₅₀ determination with different metalloform His*Mt*MetAP Ia

The IC₅₀ is the compound concentration at which 50% of the enzyme activity is inhibited. For IC₅₀ determination, enzyme activities were monitored in the presence of inhibitors at different concentrations and converted into percent inhibitions. The IC₅₀ value was obtained from the non-linear curve fitting of percent inhibition (% inhibition) vs. inhibitor concentration [I] using the equation,

$$\%inhibition = \frac{100}{1 + \left(\frac{IC_{50}}{[Inhibitor]} \right)^k}$$

where k is the Hill coefficient, the [inhibitor] is the inhibitor concentration, and the % inhibition is the percent of activity in the presence of inhibitor at the corresponding concentration.

The inhibitors were serially diluted with eight concentrations in total, and the maximal concentration of inhibitor was 1 mM. The 80 μ L assay mix included 50 mM MOPS-NAOH, pH 7.5, 100 μ M Met-AMC, His*Mt*MetAP Ia (50 nM Co(II)- or Fe(II)- substituted enzyme, 200 nM Mn(II)-substituted enzyme, or 12.5 nM Ni(II)-substituted enzyme), and metal ions at the optimal concentrations for the activity of *Mt*MetAP Ia (10 μ M FeCl₂ with 20 μ M ascorbic acid, 20 μ M CoCl₂, 200 μ M MnCl₂, or 20 μ M NiCl₂ for the optimal enzymatic activities). The percentages of inhibition converted from the activities were applied to calculate IC₅₀ (Figure 2-2).

2.2.9 Co-crystallization of His*Mt*MetAP Ia and *Mt*MetAP Ia with inhibitors

Concentrated His*Mt*MetAP Ia samples were combined with 2 mM covalent metals before mixing with inhibitors at a ratio of 1:5 or 1:10 (Table 2-5). The enzyme-compound complex was mixed up with well solution at a 1:1 ratio and used to set up crystal trays using a hanging drop vapor-diffusion method at room temperature. The screening kits from Hampton

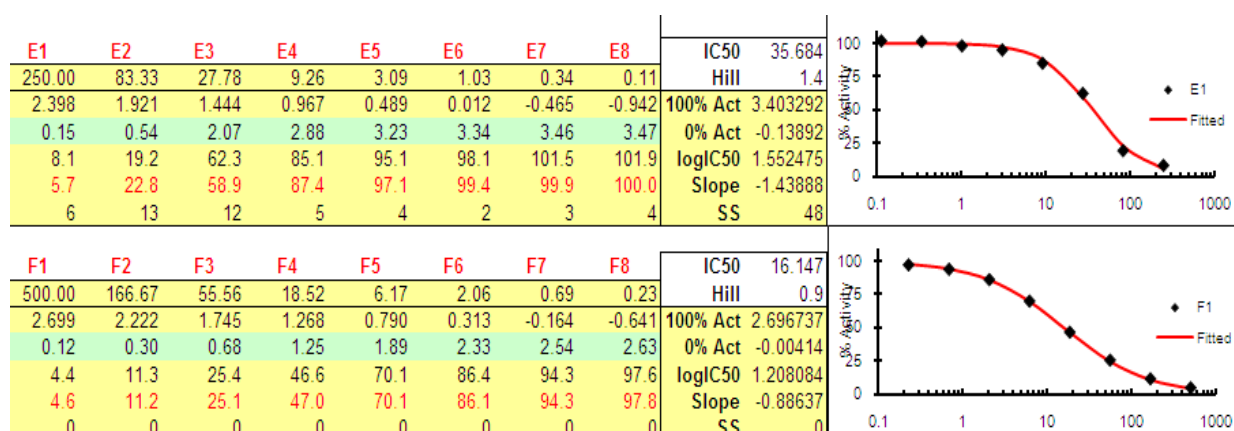


Figure 2-2 Calculation of IC₅₀ using non-linear curve fitting. The percentage of inhibition (% inhibition) was plotted against inhibitor concentration using the equation described in Method 2.2.8.

Research (Aliso Viejo, CA) were tested, including Crystal Screening TM, Crystal Screening 2TM, Index TM, and PEG/ION TM. A small amount of untagged *MtMetAP Ia* was also prepared and concentrated to 2.5 mg/mL to test using the PEG/ION.

2.3 Results

2.3.1 Constructs of *MtMetAP Ia*

The gene *mapA* was first cloned into the pGEMEX1 plasmid. The DNA sequence showed that the last 12 nucleotides at the end of the *mapA* gene were missing in the constructed plasmid of pGEMEX1-*MtMetAP Ia*-1 due to an *EcoRI* restriction site (G-AATTC) in the *mapA* gene. Two DNA oligos (Table 2-1), oligonucleotide RF and oligonucleotide RR, were designed to mutate the *EcoRI* restriction site in the *mapA* gene. Meanwhile, a restriction site of *AvrII* was introduced to identify the mutant. The modified plasmid pGEMEX1-*MtMetAP Ia*-2 was confirmed with a corrected DNA insert and transformed into *E.coli* BL21(DE3) competent cells for protein expression.

MtMetAP Ia protein was overexpressed upon IPTG induction (Figure 2-3A), which was indicated by a single band observed in the post-induction sample but not in pre-induction sample. The observed molecular weight of *MtMetAP Ia* was around 37 Kd, which was larger than its theoretical molecular weight of 29.7 Kd. It might be due to the hydrodynamic radius of the protein which in turn affected the protein mobility on SDS-PAGE.

Due to the poor solubility of *MtMetAP Ia*, an expression optimization test was carried out by changing the components of the culture medium [18]. The *MtMetAP Ia* proteins expressed in different kinds of media were examined by SDS-PAGE (Figure 2-3B). The *MtMetAP Ia* protein was expressed as it was observed in the whole cell lysate of IPTG-induced samples on the gel

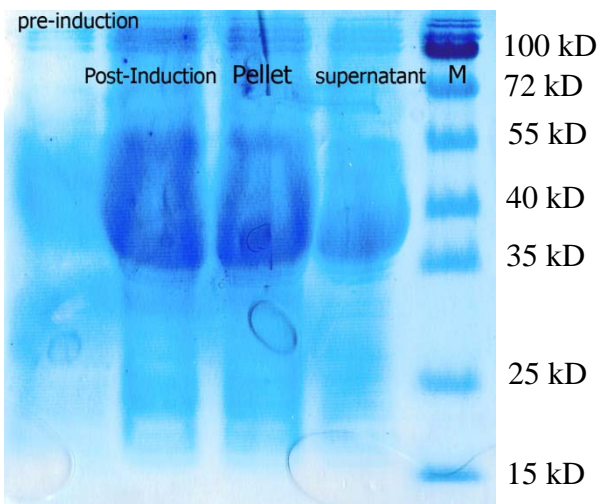


Figure 2-3A Overexpression of HisMtMetAP upon IPTG induction.

From left to right are whole cell lysate from pre-induction sample, whole cell lysate from post-induction sample, the pellet and the supernatant of post-induction sample separated by centrifugation at $16,873 \times g$ for 10 minutes. M is the prestained protein ladder from Fermentas. The expressed MtMetAP Ia showed a Mw of 37 Kd, which was larger than its theoretical Mw of 29.7 Kd.

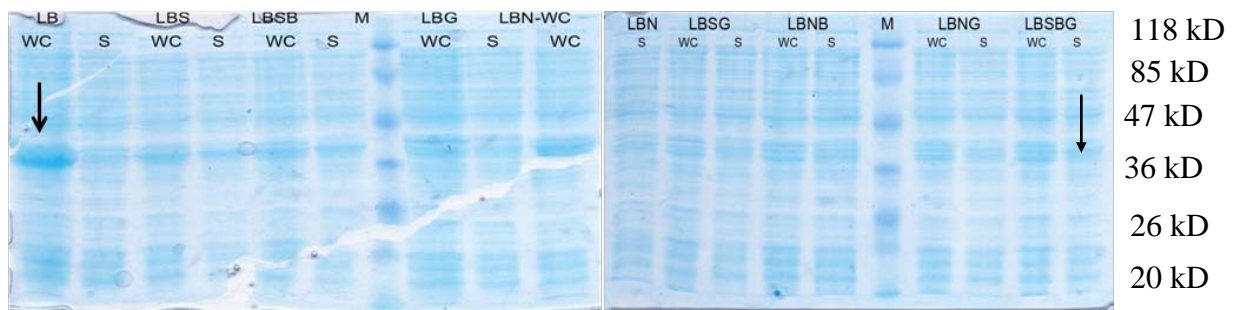
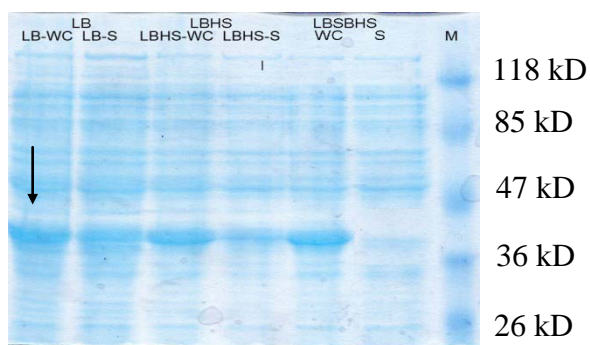


Figure 2-3B Optimization of overexpression of MtMetAP Ia by changing the composition of the LB medium.

The medium IDs are written in capital letters. WC represents the whole-cell lysate fractions and S represents the supernatant fractions. M represents Fisher BioReagents* EZ-Run* Prestained Protein Marker. The observed Mw of HisMtMetAP Ia is 37 Kd.



and it was not seen in the pre-induction samples. However, the molecular weight of the expressed protein was around 37 KD, which was larger than the theoretical molecular weight of *MtMetAP Ia*, 29.7 KD. However, it could barely be seen in the supernatant, indicating very little soluble proteins was expressed. The culture medium and the heat shock treatment seemed not to improve the solubility of *MtMetAP Ia*. Therefore, LB medium was subsequently used to grow *E.coli* cells for *MtMetAP Ia* expression.

2.3.2 Expression and purification of His*MtMetAP Ia* protein.

MtMetAP Ia was first cloned into plasmid pGEMEX-1 as an untagged protein, because of the possible interference between the His-tag and divalent metals. However, the untagged *MtMetAP Ia* showed poor solubility and it was extremely hard to trace the enzyme during purification. Therefore, the gene *mapA* was cloned into pET28a to introduce a His-tag at the N-terminus. Even though His*MtMetAPa* did not have a better solubility, the small amount of soluble protein with a His-tag was easily purified by metal-affinity chromatography (Figure 2-4). Purified His*MtMetAP Ia* was treated with 1,10-phenanthroline to remove metal ions, and the purified apoenzyme showed no activity in hydrolyzing the fluorogenic substrate Met-AMC unless metal was added in the assay mixture. The yield of His*MtMetAP Ia* was around 2 mg per liter of *E.coli* cell culture.

2.3.3. Activation of His*MtMetAP Ia* apoenzyme by divalent metals.

Activity of *MtMetAP Ia* was monitored by detecting an increase of fluorescence of 7-amido-4-methylcoumarin released from the hydrolysis of the non-fluorogenic substrate Met-AMC. The metal activation was immediate, and the fluorescence increased linearly for at least 30 min once the apoenzyme was mixed with the metals (10 minutes for Fe (II) with 2-fold

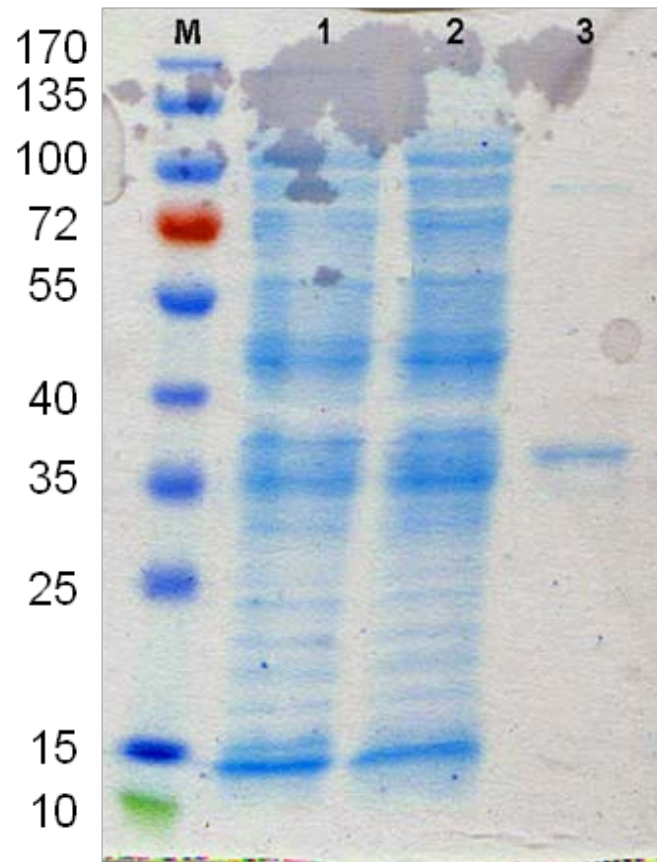


Figure 2-4 The purification of HisMtMetAP Ia

M: protein ladder from Fermantas

Lane1: flow-through

Lane2: supernatant

Lane3: eluted His-tagged MtMetAP Ia

concentration of ascorbic acid). The apoenzyme concentration was held constant at 50 nM and increasing concentrations of metal were added for activation. Ni(II) was the most efficient metal to activate *MtMetAP Ia*, followed by Co(II), Mn(II) and Fe(II) (Figure. 2-5). These were very similar to the observations in other MetAPs [8] [20] [21], but were significantly different from those reported by Zhang et al. [17], in which Co(II) was an activator, Mn(II) had no effect, and Ni(II) and Fe(II) showed inhibition instead of activation. The discrepancies likely resulted from the proteins used in the assays. The *MtMetAP Ia* characterized in our assay was in the apoform, while Zhang and colleagues used proteins with metal ions likely already incorporated. It is clear from the activation curves that high concentration of a metal ion often inhibited the enzyme activity; therefore inhibition could be observed for an activator when a metalated MetAP is used.

Since the His-tag could potentially affect metal binding, a small amount of untagged *MtMetAP Ia* was purified and tested to compare with that of *HisMtMetAP Ia*. After being treated by thrombin, the *HisMtMetAP Ia* was loaded onto a HiTrap His tag column to separate the untagged *MtMetAP Ia* (Figure 2-7A). Three peaks in total appeared during elution; peak 1 and peak 2 were eluted at low imidazole concentration while peak 3 was eluted at high imidazole concentration. All three fractions were identified by Western blotting using HRP-conjugated anti-His antibody. Only fractions in peak 2 were untagged *MtMetAP Ia* (Figure 2-7B).

This untagged *MtMetAP Ia* was used for metal activation and measurement of binding affinity indicated as an apparent K_d in comparison with *HisMtMetAP Ia* (Table 2-2). The result showed comparable metal activation curves. Fe(II) showed the tightest binding to both the tagged and untagged enzymes with smallest apparent K_d values, followed by Co(II), and Ni(II). The apparent K_d of Mn (II) indicated the weakest binding to the protein.

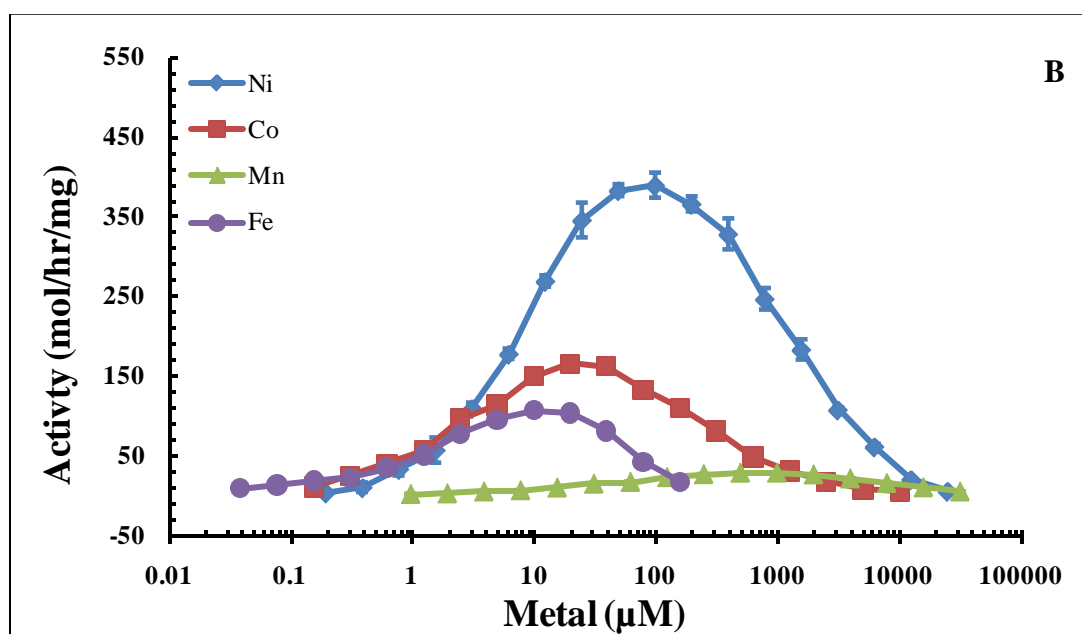
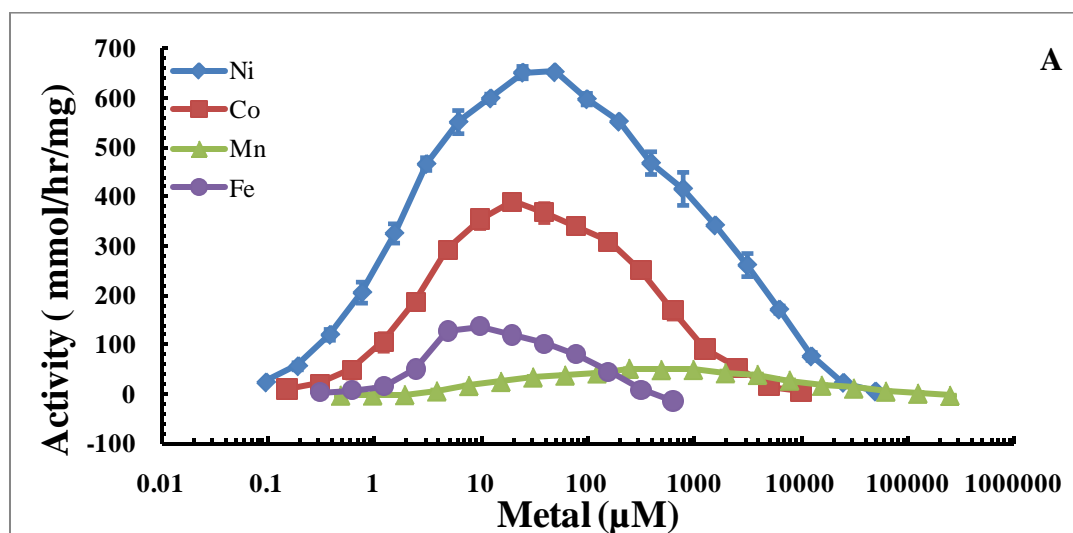


Figure 2-5 Metal activation of (A) HisMtMetAP Ia and (B) untagged MtMetAP Ia

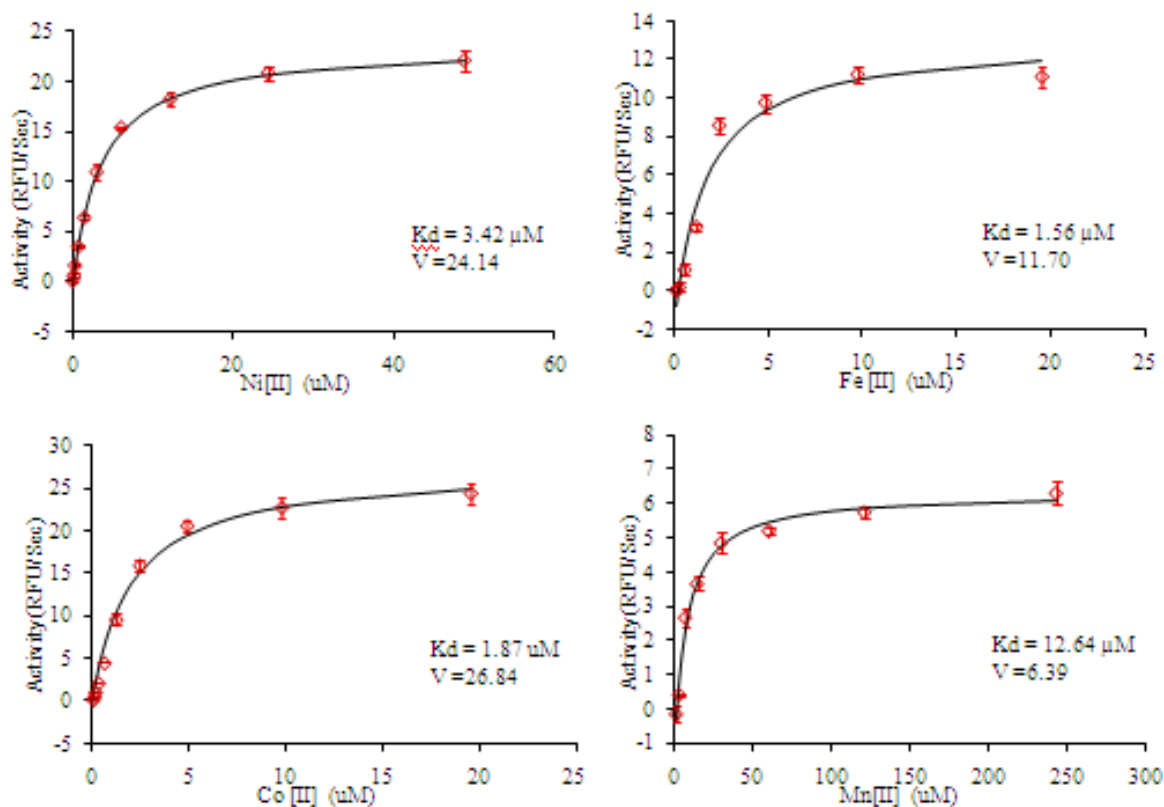


Figure 2-6 Calculation of the apparent K_d of different metalloforms of *MtMetAP Ia*. Details were described in Method 2.3.3.

Table 2-3 Comparison of metal activation of His*MtMetAP Ia* and *MtMetAP Ia*

His <i>MtMetAPa</i>	Fe(II)	Ni(II)	Co(II)	Mn(II)
<i>App K_d</i> , μM	1.56 ± 0.03	2.31 ± 0.11	1.87 ± 0.10	12.64 ± 0.71
<i>V_{max}</i> (RFU/Sec)	11.70 ± 2.16	24.14 ± 2.55	26.84 ± 1.27	6.39 ± 0.83

<i>MtMetAP1a</i>	Fe(II)	Ni(II)	Co(II)	Mn(II)
<i>App K_d</i> , μM	1.59 ± 0.11	6.29 ± 0.5	2.33 ± 0.37	33.76 ± 2.30
<i>V_{max}</i> (RFU/ Sec)	8.43 ± 0.38	14.57 ± 0.51	12.87 ± 0.19	4.04 ± 0.23

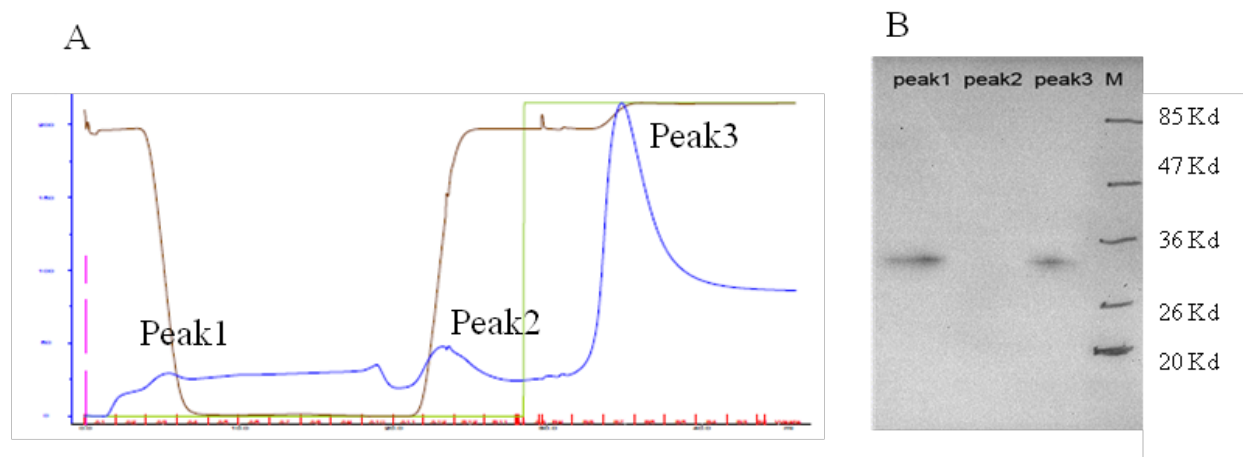


Figure 2-7 Removal of His-tag from HisMtMetAP Ia confirmed by Western blot

A: The *HisMtMetAP Ia* was loaded onto 5 mL HiTrap His column after thrombin treatment. There were three peaks during the elution: peaks 1-3.

B: Fractions from peaks 1-3 were identified by Western blotting using HRP-conjugated anti-His antibody.

When the metal activation of His*MtMetAP* Ia to the untagged *MtMetAP* Ia were compared, no significant difference in binding affinity among the metals was observed (Table 2-2, Figure 2-7). The apparent K_d of Co(II) to His*MtMetAP* Ia and untagged *MtMetAP* Ia were 1.87 μM and 2.33 μM , respectively; and the apparent K_d for Fe(II) binding to His*MtMetAP* Ia and untagged *MtMetAP* Ia were 1.56 μM and 1.59 μM , respectively. The similar binding affinity of Co(II) and Fe(II) to *MtMetAP* Ia regardless of the His-tag was also coincident with the metal titration curves (Figure 2-5).

In the cases of Ni (II) and Mn (II), a smaller K_d with untagged *MtMetAP* Ia than His*MtMetAP* Ia was observed. The K_d value of His*MtMetAP* Ia and *MtMetAP* Ia for Ni (II) were 2.31 μM and 6.29 μM , respectively. The K_d values for Mn-substituted His*MtMetAP* Ia and *MtMetAP* Ia were 12.64 μM and 33.76 μM , respectively (Figure 2-6). Theoretically, the apparent K_d measured from His-tagged protein should be bigger than the apparent K_d measured from untagged protein if there is any interaction between the His-tag and the metal. The reason for the reverse observation could possibly be the loss of the enzyme activities (Table 2-3), so that the binding was not reflected by the AMC production.

In summary, the activation of all the metals showed similar order in both His-tagged and untagged *MtMetAP* Ia, which was Fe(II) > Co(II) > Ni(II) > Mn(II), with the binding affinity from high to low. The metal concentration for optimal enzyme activity were used for the following kinetic characterization.

2.3.4. Kinetic measurement of different metalloform His*MtMetAP* Ia:

For K_m measurements, it is usual that the substrate concentration is significantly higher than the enzyme concentration. In the His*MtMetAP* Ia case, the enzyme concentration was

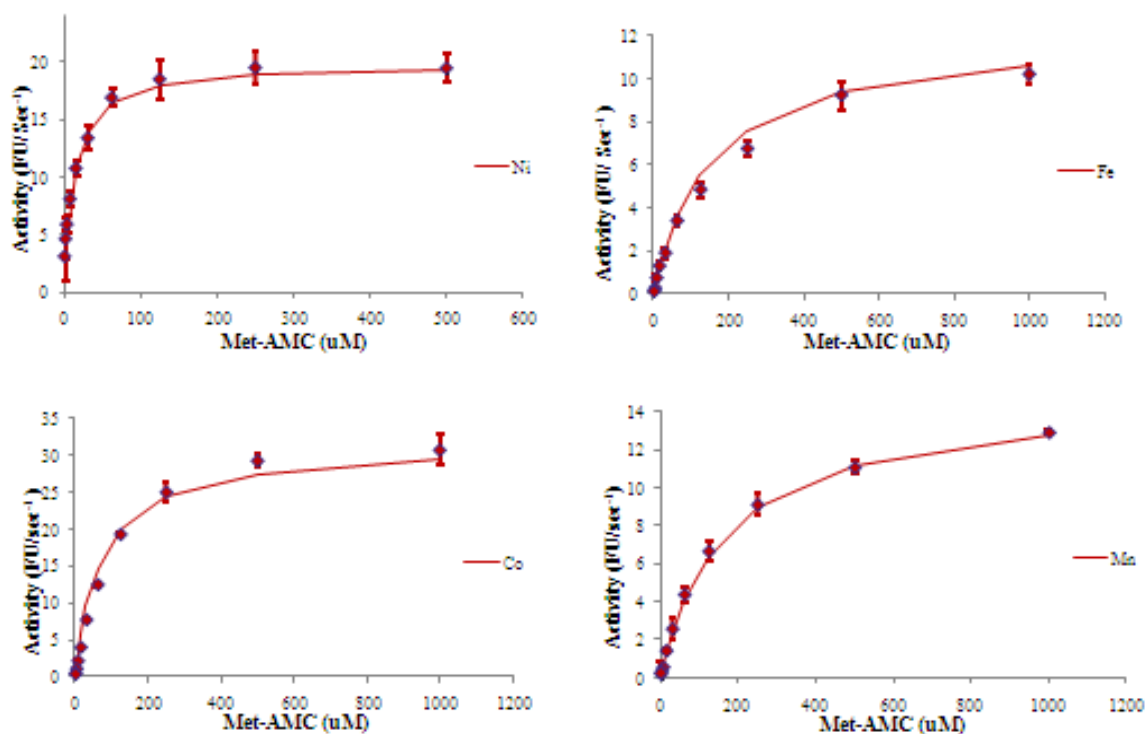


Figure 2-8 Calculation of the K_m of different metalloforms of *MtMetAP* Ia by using no linear regression curve fitting based on Michaelis–Menten equation.

Table 2-4 Kinetic measurement of His*MtMetAP* Ia

His <i>MtMetAP</i> Ia	Fe(II)	Ni(II)	Co(II)	Mn(II)
$K_m, \mu\text{M}$	148.96 ± 9.26	13.13 ± 2.62	70.46 ± 7.52	169.92 ± 10.29
$k_{\text{cat}}, \text{sec}^{-1}$	0.1429 ± 0.0077	0.4779 ± 0.0068	0.3719 ± 0.018	0.062 ± 0.018
$k_{\text{cat}}/K_m, \text{M}^{-1}\text{sec}^{-1}$	959	35634	5277	364

The Ni(II)-substituted His*MtMetAP* Ia showed the highest affinity for substrate, followed by the Co(II)-substituted enzyme. Both Mn(II)-substituted and Fe(II)-substituted His*MtMetAP* Ia gave K_m values that were about 11 ~ 13 fold bigger than the K_m of Ni(II)-substituted His*MtMetAP* Ia.

around nM. Serially diluted substrates of Met-AMC from 2 mM to 0.9 μ M were prepared and His*Mt*MetAP Ia with the optimal metal concentration used to initiate the hydrolysis of Met from Met-AMC. The increase in fluorescence at 460 nm ($\lambda_{\text{Ex}}=360$ nm) was recorded and converted into μ M AMC per min (Figure 2-8) (Table 2-3).

At the optimal activating metal concentrations for each metal (10 μ M FeCl₂, 20 μ M CoCl₂, 200 μ M MnCl₂, or 20 μ M NiCl₂), Michaelis–Menten constants were calculated for substrate hydrolysis. Ni(II)-activated *Mt*MetAP Ia was most efficient among the metalloforms tested in catalyzing the hydrolysis, with the lowest K_m and the fastest k_{cat} , consistent with the metal titration curves (Figure. 2-5). Co(II) was the next, Fe(II) followed and Mn(II) was the least efficient. It is important to note that although this order of activation is similar for *Mt*MetAP Ia and *Mt*MetAP Ic. However *Mt*MetAP Ia is a much more efficient enzyme.

2.3.5 IC₅₀ determination with different metalloform *Mt*MetAP Ia:

Assignment of the physiologically relevant metalloform has been difficult, and a novel approach was developed for the assignment using the metalloform-selective inhibitors that can distinguish different metals at the active site [11, 22]. In our research on characterization of *Ec*MetAP, a set of MetAP inhibitors were tested for the inhibition of different metalloforms [23]. For comparison, the same inhibitors for metalloform-selective inhibition were investigated with *Mt*MetAP Ia (Table 2-4). From previous tests on *Ec*MetAP; compounds 1 and 2 showed specific inhibition on Fe(II)-form enzyme [24], compounds 3 and 4 were Mn(II)-form selective [22], and compounds 5-7 were Co(II)- and Ni(II)-form selective [22-23]. However, when they were tested on different metal-substituted *Mt*MetAP Ia, compounds 1 and 2 showed potent inhibition in all four metalloforms, and their metalloform selectivity was lost (Table 2-5). It was more surprising

Table 2-5. Inhibition of enzymatic activities of purified *Mt*MetAP Ia^a

Cmpd	MtMetAP Ia ^b			
	Fe(II)	Ni(II)	Co(II)	Mn(II)
1	0.19	0.7	0.031	0.11
2	0.07	2.3	0.53	0.1
3	>250	>250	>250	0.25
4	>250	172	20	104
5	>250	>250	>250	>250
6	>250	>250	>250	>250
7	>250	>250	>250	>250
8	>250	>250	205	>250

^a IC₅₀ values are expressed in μM . ^b Purified enzymes were reconstituted by activating the apoenzyme with different divalent cations [Fe(II), 10 μM ; Co(II) and Ni(II), 20 μM ; Mn(II), 200 μM].

that compounds 3-8 showed almost no activity, even though they inhibited *Ec*MetAP1 and *Mt*MetAP Ic with metalloform selectivity as expected. *Mt*MetAP Ia and *Mt*MetAP Ic are highly homologous in sequence, and many active site residues are conserved (Figure. 2-9). The X-ray structure of *Mt*MetAP Ia is not available, and conceivably a homology model can be built based on the structures of *Mt*MetAP Ic [23, 25].

However, it will be difficult to explain the remarkable differences in inhibition of *Mt*MetAP Ia by these inhibitors both in potency and metalloform selectivity until a structure of *Mt*MetAP Ia is solved experimentally. The differences in inhibition foretell significant differences in structure, especially at the active site, between *Mt*MetAP Ia and *Mt*MetAP Ic.

2.3.6 Co-crystallization of *Mt*MetAP Ia with inhibitors

In order to improve His*Mt*MetAP Ia solubility for purification, LB medium with different additives was tested (Figure 2-1, and Table 2-2). The His*Mt*MetAP Ia solubility did not improve by changing the culture medium and the protein was produced in LB and purified with lower yield (2 mg per liter culture). However, enough protein was purified that protein crystallization screens were performed as described in Table 2-5. In the first trial, CrystalScreenTM, CrystalScreen 2TM, IndexTM, SaltRTM were tested with Mn-substituted His*Mt*MetAP Ia. Even though His*Mt*MetAP Ia did not form crystals that were good enough for diffraction, the protein tended to form light precipitation, or needle clusters in the presence of polyethylene glycol (PEG). Staining by Izit Crystal Dye (Hampton Research, Aliso Viejo, CA) suggested these crystals were proteinaceous. Therefore, *Mt*MetAP Ia (5 mg/mL) with inhibitory compounds were used to set up with PEG/ION kitTM and the protein concentration was reduced from 5 mg/mL to 3 mg/mL because precipitation occurred in most wells in the initial trials. The huge ‘crystal’

Table 2-6: Summary of *MtMetAP 1a* initial crystallization screens (×: screen performed)

Protein	Protein Buffer	Additives or other factor	ScreenBuffer					
			Temp (°C)	Crystal Screen™	Crystal Screen2™	SaltRx™	Index™	PEG/Ion Screen™ Self-Optimized Buffers
His<i>MtMetAP1a</i> 5 mg/mL	50 mM MOPS pH 7.5 150 mM NaCl	2 mM MnCl₂ 0.67 uM compound A54	RT	×	×	×	×	
His<i>MtMetAP1a</i> 5 mg/mL	50 mM MOPS pH 7.5 150 mM NaCl	2 mM MnCl₂ 0.67 uM compound A121	RT	×	×	×	×	
His<i>MtMetAP1a</i> 2.7 mg/mL	50 mM MOPS pH 7.5 150 mM NaCl	2 mM MnCl₂ (Ni Cl₂ or CoCl₂) 0.5 uM compound	RT					×
His<i>MtMetAP1a</i> 2 mg/mL	50 mM MOPS pH 7.5 150 mM NaCl	2 mM MnCl₂, or Ni Cl₂ 0.5 uM compound	RT					×
<i>MtMetAP1a</i> 2.5 mg/mL	50 mM MOPS pH 7.5 150 mM NaCl	None	RT					×
<i>MtMetAP1a</i> 2.5 mg/mL	50 mM MOPS pH 7.5 150 mM NaCl	2 mM MnCl₂	RT					×

formed in solution PEG/ION buffer 1 (0.2M sodium fluoride, 20% PEG3350). However, only a few diffraction spots with strong intensity were obtained in the high resolution area when these crystals were exposed to synchrotron radiation, which suggested these crystals were likely salt crystals and the Izit Crystal dye identified them as salt.

Discussion

Of two MetAPs in *M. tuberculosis*, *MtMetAP Ia* was suggested to have higher expression level in *M. tuberculosis* at the log phase [17]. Knock-down experiment also suggested that *MtMetAP Ia* played a more important role than *MtMetAP Ic* in *M. tuberculosis* viability [26]. When the kinetic characterization of *MtMetAP Ia* was carried out, there was particular interest on its metal-selective inhibition and how the enzymes interact with the metal specific inhibitors in the presence of specific divalent metals.

Thus, the *MtMetAP Ia* was cloned, over-expressed and purified as an active enzyme. It showed a much lower solubility than *EcMetAP* and *MtMetAP Ic* when it was first expressed without a His-tag. The untagged protein with lower solubility posed difficulties for purifying a large amount of the proteins, and achieving highly concentrated protein samples for crystallization. To potentially improve solubility and purification, the *mapA* gene was cloned into a pET28a plasmid so that the protein was expressed with a His tag at the N-terminus. In this system, larger portion of the protein was expressed as inclusion bodies with a small amount of soluble protein, which could be more efficiently purified through a nickel affinity column and used for kinetic characterization. The purified protein was treated with 1,10-phenanthroline to

remove metal ions following metal-affinity chromatography. The resulting apoenzyme showed no activity in hydrolyzing the fluorogenic substrate Met-AMC until metals were added.

MtMetAP Ia is shown to be a metallohydrolase and several divalent metals, including Fe (II) (in the presence of two-fold ascorbic acid), Mn(II), Co(II), and Ni(II) were tested for catalytic activity. Both His-tagged and untagged *MtMetAP Ia* were tested for the metal binding affinities for comparison (Table 2-3). Metal activation profiles of His*MtMetAP Ia* and *MtMetAP Ia* were very similar. The binding affinity of different covalent metals, from high to low, was listed as: Fe (II) > Co (II) > Ni (II) > Mn (II). Even though the apparent K_d values of metals for binding to the untagged *MtMetAP Ia* were higher than the apparent K_d values of metals binding to the His-tagged *MtMetAP Ia*, the overall metal activation scenarios were similar.

The determination of kinetic characteristics was carried out with His*MtMetAP Ia* (Table 2-3). Ni(II) was the most efficient metal to activate the enzyme, having the lowest K_m and the highest k_{cat} . Co(II) with a K_m of 70.46 μ M and a K_{cat} of 0.37 sec^{-1} was the next in efficiency, Fe(II) followed, and Mn(II) was the least efficient. Although the order of activation is similar between His*MtMetAP Ia* and *MtMetAP Ic* [24]. His*MtMetAP Ia* is a much more efficient enzyme, and the catalysis efficiency of Fe-substituted *MtMetAP Ia* was 22-fold higher than Fe-substituted *MtMetAP Ic*; 67 fold higher for Ni-substituted enzymes, 20-fold for Co-substituted enzymes and 4 fold for Mn-substituted enzymes, respectively. It was surprising to see Ni(II) as the best activator for *MtMetAP Ia in vitro*. There are a limited number of enzymes utilizing Ni *in vivo*. It will be interesting to know if Ni is used by *MtMetAP Ia* in *M. tuberculosis* cells.

The ability of metal-selective compounds was tested on His*MtMetAP Ia* and IC_{50} values were calculated. To our surprise, only the Fe (II)-selective enzyme showed inhibition. Yet, the

metal-selectivity was although lost as they inhibited all the metalloforms of *MtMetAP Ia*. This raised the question as to why these compounds lost their inhibitions of *MtMetAP Ia*.

To address this question, we attempted to co-crystallize *MtMetAP Ia* with inhibitory compounds to elucidate the interaction between *MtMetAP Ia* and the compounds. However, We failed to crystallize *MtMetAP Ia*. The failure in obtaining crystals could be partly due to the low solubility of *MtMetAP Ia*. Even though the protein solubility of *MtMetAP1* was predicted to be similar to those of *EcMetAP* and *MtMetAP Ic*, this was not the case. The achievable highest concentration for His*MtMetAP Ia* was about 5 mg/ml in the presence of metals. The concentrated protein was easily precipitated. Later, a lower protein concentration (2.7 mg/ml) was employed to set up crystal trays. Less precipitation occurred while most crystal drops remained clear. Attempts to improve the solubility of His*MtMetAP Ia* were unsuccessfully.

The amino acid sequences of *MtMetAP Ia*, *MtMetAP Ic* and *EcMetAP*, were aligned (Figure 2-9). *MtMetAP Ia* shares a 36.4 % identity of amino acid sequence to its homolog *MtMetAP Ic* in *M. tuberculosis* and a 36.9% identity to *EcMetAP*. The conserved amino acid residues in metal binding site in *EcMetAP* were D97, D108, H171, E204 and E235, and D131, D142, H205, E238 and E269 in *MtMetAP Ic*. *MtMetAP Ia* had them all with different numbering, which were D106, D117, H186, E219 and E250 (Figure 2-9). Theoretically, proteins with conserved function consist of conserved residues, therefore, *MtMetAP Ia* would be expected to retain conserved enzymatic characteristics, and the binding mode for the inhibitors should remain similar to those of *EcMetAP* and *MtMetAP Ic*.

The primary differences observed from the amino acid alignment are an extension of the N-terminus and the length of a loop flanked by two α -helices close to the C-terminus (Figure 2-9). However, the differences of the loops were not observed in the virtual structure of *MtMetAP*

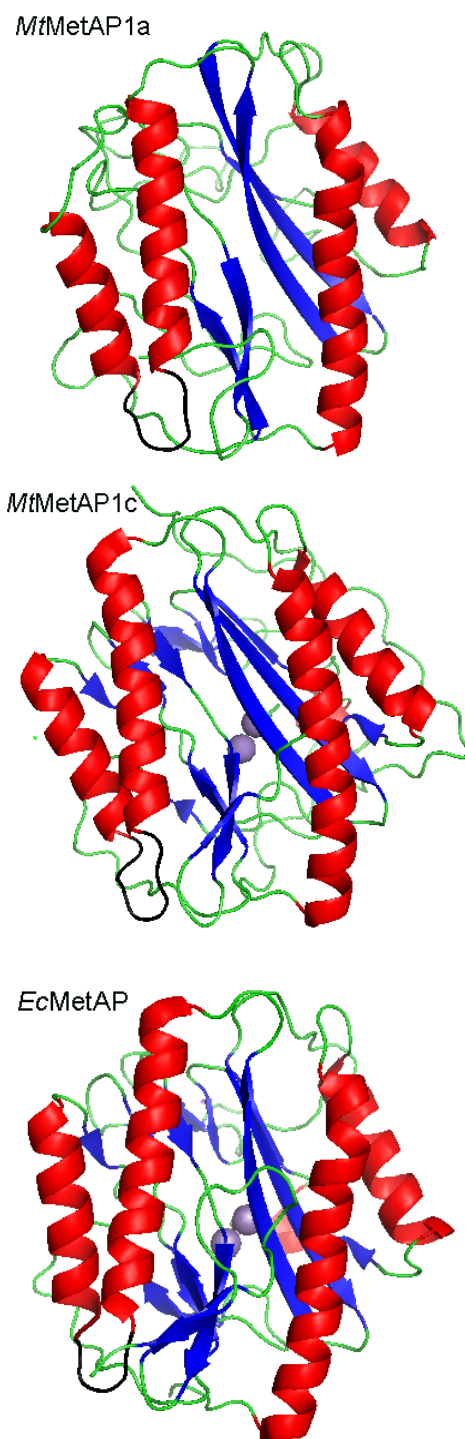


Figure 2-10. Ribbon drawing of the ‘pita-bread’ domain fold existing in *EcMetAP*, *MtMetAP* Ic, and homology model of *MtMetAP* Ia based on *MtMetAP* Ic structure. Protein structure of *MtMetAP* Ia predicted by: 3D-JIGSAW.

Ia, which was generated by molecular modeling (Figure 2-10). The common ‘pita-bread’ domain in the active site of MetAPs was clearly seen in *Mt*MetAP Ia with the pseudo two-fold domain; one fold located in the N-terminus and the other located in the C-terminus domain. Each of them consisted of two α -helices and two anti-parallel β -sheets. The fact the inhibitors failed to access to the active site may be due to the side chains of the amino acids. *Mt*MetAP Ia does not have an N-terminal extension. Neither does *Ec*MetAP1. *Mt*MetAP Ic has a 42-amino acid long loop at the N-terminus, and it is clearly seen in the crystal structure that the loop wraps around the active site and forms sequence-specific contacts with other residues. Its function is proposed to bind MetAPs to the ribosome by a complex between a PxxP (amino acid residue of 14-17 in *Mt*MetAP Ic) motif in MetAPs and an SH3 domain on the ribosome [25]. The presence/absence of this N-terminal extension did not affect the enzyme activity as these compounds were tested in both *Mt*MetAP Ic (chapter 3) and *Ec*MetAP [20, 24], Similar inhibitory activity and metal selectivity were seen in both enzymes. Thus, the absence of N-terminal extension in *Mt*MetAP Ia did not correlate with the loss of the inhibition and metal selectivity. Crystal structure of *Ec*MetAP suggested that the absence of the N-terminal extension did not affect the formation of the active site. Neither should it affect enzyme inhibitions. The loss of inhibition and metal selectivity of these compounds cannot be explained neither by the absence of N-terminal extension nor the different length of the inside loop. Further study is needed to explain the loss of inhibition and metal selectivity of these compounds on *Mt*MetAP Ia.

In this project, about one hundred MetAPs inhibitors were tested with *Mt*MetAP Ia, and it is possible that many potential *Mt*MetAP Ia inhibitors were not included. Screening a compound library with structural diversity would hold the promise of discovering more effective inhibitors for *Mt*MetAP Ia for use as leads for novel antitubercular drugs.

Reference:

1. Gandhi, N.R., et al., *Extensively drug-resistant tuberculosis as a cause of death in patients co-infected with tuberculosis and HIV in a rural area of South Africa*. Lancet, 2006. **368**(9547): p. 1575-80.
2. Organization, W.H., *2009 update TUBERCULOSIS FACTS*. 2010.
3. Giglione, C., A. Boularot, and T. Meinel, *Protein N-terminal methionine excision*. Cell Mol Life Sci, 2004. **61**(12): p. 1455-74.
4. Chang, S.Y., E.C. McGary, and S. Chang, *Methionine aminopeptidase gene of Escherichia coli is essential for cell growth*. J Bacteriol, 1989. **171**(7): p. 4071-2.
5. Chen, X., et al., *Inhibitors of Plasmodium falciparum methionine aminopeptidase 1b possess antimalarial activity*. Proc Natl Acad Sci U S A, 2006. **103**(39): p. 14548-53.
6. Li, X. and Y.H. Chang, *Amino-terminal protein processing in Saccharomyces cerevisiae is an essential function that requires two distinct methionine aminopeptidases*. Proc Natl Acad Sci U S A, 1995. **92**(26): p. 12357-61.
7. Lowther WT, Z.Y., Sampson PB, Honek JF, Matthews BW., *Insights into the mechanism of Escherichia coli methionine aminopeptidase from the structural analysis of reaction products and phosphorus-based transition-state analogues*. Biochemistry, 1999. **38**(45): p. 14810-9.
8. Li, J.Y., et al., *Specificity for inhibitors of metal-substituted methionine aminopeptidase*. Biochem Biophys Res Commun, 2003. **307**(1): p. 172-9.
9. D'Souza V, M. and R.C. Holz, *The methionyl aminopeptidase from Escherichia coli can function as an iron(II) enzyme*. Biochemistry, 1999. **38**(34): p. 11079-85.
10. Lowther, W.T. and B.W. Matthews, *Structure and function of the methionine aminopeptidases*. Biochim Biophys Acta, 2000. **1477**(1-2): p. 157-67.
11. Chai, S.C., W.L. Wang, and Q.Z. Ye, *FE(II) is the native cofactor for Escherichia coli methionine aminopeptidase*. J Biol Chem, 2008. **283**(40): p. 26879-85.
12. Wang, J., et al., *Physiologically relevant metal cofactor for methionine aminopeptidase-2 is manganese*. Biochemistry, 2003. **42**(17): p. 5035-42.
13. Leopoldini, M., N. Russo, and M. Toscano, *Which one among Zn(II), Co(II), Mn(II), and Fe(II) is the most efficient ion for the methionine aminopeptidase catalyzed reaction?* J Am Chem Soc, 2007. **129**(25): p. 7776-84.
14. Schiffmann, R., et al., *Metal ions as cofactors for the binding of inhibitors to methionine aminopeptidase: a critical view of the relevance of in vitro metalloenzyme assays*. Angew Chem Int Ed Engl, 2005. **44**(23): p. 3620-3.
15. Luo, Q.L., et al., *Discovery and structural modification of inhibitors of methionine aminopeptidases from Escherichia coli and Saccharomyces cerevisiae*. J Med Chem, 2003. **46**(13): p. 2631-40.
16. Cole, S.T., et al., *Deciphering the biology of Mycobacterium tuberculosis from the complete genome sequence*. Nature, 1998. **393**(6685): p. 537-44.
17. Zhang, X., et al., *Expression and characterization of two functional methionine aminopeptidases from Mycobacterium tuberculosis H37Rv*. Curr Microbiol, 2009. **59**(5): p. 520-5.
18. Oganessian, N., et al., *Effect of osmotic stress and heat shock in recombinant protein overexpression and crystallization*. Protein Expr Purif, 2007. **52**(2): p. 280-5.

19. Yang, G., et al., *Steady-state kinetic characterization of substrates and metal-ion specificities of the full-length and N-terminally truncated recombinant human methionine aminopeptidases (type 2)*. Biochemistry, 2001. **40**(35): p. 10645-54.
20. Huang, M., et al., *Metal mediated inhibition of methionine aminopeptidase by quinolinyl sulfonamides*. Biochem Biophys Res Commun, 2006. **339**(2): p. 506-13.
21. Meng, L., et al., *Overexpression and Divalent Metal Binding Properties of the Methionyl Aminopeptidase from Pyrococcus furiosus†*. Biochemistry, 2002. **41**: p. 7199-7208.
22. Ye, Q.Z., et al., *Metalloform-selective inhibitors of escherichia coli methionine aminopeptidase and X-ray structure of a Mn(II)-form enzyme complexed with an inhibitor*. J Am Chem Soc, 2004. **126**(43): p. 13940-1.
23. Lu, J.P., S.C. Chai, and Q.Z. Ye, *Catalysis and inhibition of Mycobacterium tuberculosis methionine aminopeptidase*. J Med Chem, 2010. **53**(3): p. 1329-37.
24. Wang, W.L., et al., *Discovery of inhibitors of Escherichia coli methionine aminopeptidase with the Fe(II)-form selectivity and antibacterial activity*. J Med Chem, 2008. **51**(19): p. 6110-20.
25. Addlagatta, A., et al., *Identification of an SH3-binding motif in a new class of methionine aminopeptidases from Mycobacterium tuberculosis suggests a mode of interaction with the ribosome*. Biochemistry, 2005. **44**(19): p. 7166-74.
26. Olaleye, O., et al., *Methionine aminopeptidases from Mycobacterium tuberculosis as novel antimycobacterial targets*. Chem Biol, 2010. **17**(1): p. 86-97.

CHAPTER 3

BIOCHEMICAL CHARACTERIZATION OF METHIONINE AMINOPEPTIDASE 1c IN MYCOBACTERIA TUBERCULOSIS

The work described in this chapter was published in the Journal of Medicinal Chemistry, entitled “Catalysis and inhibition of *Mycobacterium tuberculosis* methionine aminopeptidase”.

3.1 Introduction

Methionine aminopeptidase (MetAP) is a unique metallohydrolase. It removes the N-terminal initiator methionine from nascent polypeptides[1]. This N-terminal modification occurs in majority of the proteins; indicating the important roles of MetAP in protein maturation, stability, function and degradation. The essential function for MetAP has been demonstrated by the fact that deletion of MetAP from the genomes of *E.coli*[2], *Salmonella typhimurium*[3], and *Saccharomyces cerevisiae*[4] is lethal. Therefore, inhibitors against MetAP offer hope for the treatment of microbial and fungal infections.

Tuberculosis (TB) caused by *Mycobacterium tuberculosis* is one of leading cause of mortality worldwide. Approximately one third of the world's population is infected by *M. tuberculosis* and about 1.8 million people die each year [5]. Due to the extreme survival capability of *M. tuberculosis* in the human host, current treatments of TB usually involve three to four antibiotics that are administered at the same time. Additionally, a prolonged period for drug treatment (six to nine months) is required to completely eliminate the causative agent in TB patients. With the presence of multidrug-resistant and extensively drug-resistant forms of TB[6-

7], and the prevalence of TB-HIV co-infection [8], the need for new and improved antibiotics with novel mechanisms of action to fight TB infections has increased

Recently, two MetAP genes (*mapA* and *mapB*) from *M. tuberculosis* H37Rv [9], were cloned, and two corresponding *MtMetAPs* were purified, and characterized. Their mRNA transcripts were also analyzed in log phase and stationary phase bacterial culture [10]. The *MtMetAP Ia* gene (*mapA*) is expressed more in log phase, while *MtMetAP Ic* gene (*mapB*) shows a higher level in stationary phase culture, suggesting that the two MetAPs play their roles in different growth phases of *M. tuberculosis*. Olaleye et al introduced a plasmid pSCW35DsigF with *mapA* or *mapB* into *M. tuberculosis* and constructed MetAP knock-in strains. Over-expressed *MtMetAP Ia* and *MtMetAP Ic* in these knock-in strains of *M. tuberculosis* conferred the resistance to the MetAP inhibitors [11], indicating MetAP in *M. tuberculosis* may be a promising target for the development of antituberculosis agents.

In order to further characterize MetAP in *M. tuberculosis*, particular the metal activation, both *MtMetAP Ia* and *MtMetAP Ic* were cloned, purified and characterized in our laboratory. In this chapter, the characterization of *MtMetAP Ic* is described. The *MtMetAP* complemented the functional of inactive *EcMetAP* in the *E. coli* with amber mutant and enabled *E. coli* to grow in the non-permissive medium. A set of metal-selective inhibitors were tested towards the Fe(II)-form, the Mn(II)-form, or the Co(II)- and Ni(II)-forms of the enzyme, and their metal-selective inhibition on *MtMetAP Ic* were consistent with what observed in *EcMetAP*. These metalloform selective inhibitors were then used to identify which metalloform of *MtMetAP Ic* was physiologically important. Only the Fe (II)-form selective inhibitors inhibited the cellular *MtMetAP Ic* activity and inhibited the *MtMetAP Ic*-complemented cell growth. The data suggested that Fe (II) is the native metal used by *MtMetAP Ic* in an *E. coli* cellular environment.

X-ray structures of *Mt*MetAP Ic in complex with metalloform-selective inhibitors were analyzed and showed different binding modes and different interactions between metal ions and active site residues. Understanding the catalytic mechanism and inhibition of the mycobacterial MetAP is essential to discovering and developing effective MetAP inhibitors as therapeutics.

3.2 Materials and Methods

3.2.1 Cloning of *Mt*MetAP Ic into pGEMEX-1 plas mid.

The DNA encoding *Mt*MetAP Ic (*mapB*, locus_tag Rv2861c) was obtained by PCR using genomic DNA of *M. tuberculosis* H37Rv as the template (a kind gift from Professor Scott G. Franzblau at the University of Illinois at Chicago). The forward primer was 5'-GGA TCA CCA GCT AGC ATG CCT AGT CGT ACC GCG, and the reverse primer was 5'-AGC ACT CGA ATT CTA CAG ACA GGT CAT (the restriction sites were underlined). The resulting PCR product of *Mt*MetAP Ic was digested with *Eco*RI and *Nhe*I (New England Biolabs, Ipswich, MA), and cloned into an *E. coli* plasmid pGEMEX-1 (Promega, Madison, Wisconsin) for overexpression under the control of a T7 promoter. The final recombinant protein *Mt*MetAP Ic has three residues MAS added to its N-terminus and were not removed. The sequence of the desired plasmid of pGEMEX1-*Mt*MetAP Ic was confirmed by DNA sequence analysis, and transformed into *E. coli* BL21(DE3) (Invitrogen, Carlsbad, CA) for protein over-production.

3.2.2 Over-expression and purification of *Mt*MetAP Ic.

E.coli BL21(DE3) harboring the plasmid *Mt*MetAP Ic was grown in a 5 mL of LB medium with 50 ng/mL ampicillin at 37 °C overnight. The culture was then used to inoculate 1 liter of LB containing 50 ng/mL of ampicillin the next day for protein expression. The cells

were grown at 37 °C with shaking at 225 rpm until the OD₆₀₀ reached 0.6 ~ 0.8 before 0.4 mM IPTG was added to initiate protein expression. Thereafter, the induced *E.coli* cells were kept growing at 16 °C for 20 hours. The cells were harvested by centrifugation at 4400 × g for 5 minutes. A resuspension buffer (50 mM Tris-HCl, pH 8.0, 150 mM NaCl, 5 mM EDTA) was used to suspend cell pellets, and the cell suspension was stored at -20 °C.

Frozen cells after thawing were broken by three consecutive passes through a French Press (Thermo Fisher Scientific, Asheville, NC) at 20000 psi. The supernatant was collected from centrifugation at 47,810 × g for 30 minutes and loaded onto a 20 mL Q-Sepharose column pre-equilibrated with buffer A (50 mM Tris-HCl, pH 8.0). The proteins were eluted with a linear gradient of NaCl from 0 to 1 M. The *MtMetAP Ic* appeared in the flow-through fractions. Solid ammonium sulfate was added to the combined fractions in a step-wise manner. The majority of *MtMetAP Ic* was precipitated when ammonium sulfate was 40% saturated. The pellet was resuspended in buffer A, and the mixture was loaded onto a 5-mL HiTrap desalting column (GE Healthcare Life Science, Piscataway, NJ) to remove ammonium sulfate. Chelex-100 resin (BioRad, Hercules, CA) was added to the desalted fractions, and was shaken at 4 °C for 2 hr to remove the metals. The sample was filtered to remove the resin, and loaded onto a desalting column. Buffer B (50 mM Tris-HCl, pH 8.0, 150 mM NaCl, which was pre-treated with Chelex-100 resin) was used to elute the protein.

The *MtMetAP Ic* in the apo-form was verified by hydrolysis of Met-AMC in the presence and absence of divalent metals. No activity was detected before metal was added.

3.2.3 Metal activation of *MtMetAP Ic*.

Several covalent metals (NiCl_2 , CoCl_2 , MnCl_2 , ZnCl_2 or FeCl_2 with twice the concentration of ascorbic acid) were used to test the metal activation of apo-*MtMetAP Ic*. The measurement was carried out in 384-well plates and the total reaction volume was 80 μL . The well contained 50 mM MOPS-NaOH, pH 7.5, 100 μM fluorogenic substrate Met-AMC (Bachem Bioscience, King of Prussia, PA), 0.5 μM apoenzyme and increasing amounts of metal ions. The initial velocity values, which were measured changes in relative fluorescent intensity (Relative Fluorescence Unit), were converted to specific activity values and plotted against increasing concentrations of the metals.

An improved model of the multiple independent binding sites (MIBS) was used to accurately calculate the binding affinity (apparent K_d) when the amount of functional enzyme was taken into consideration [12]. Briefly, the initial rate of hydrolysis was plotted against increasing concentrations of Co(II) at two *MtMetAP Ic* protein concentrations (20 μM and 0.5 μM) and fit with the MIBS model [12] via an iterative process to obtain an accurate protein concentration. For apparent K_d determination of the various divalent metals to *MtMetAP Ic*, the titration curves were generated using the calculated apoenzyme concentration of 0.54 μM in 50 mM MOPS-NaOH, pH 7.5, 200 μM Met-AMC and increasing concentrations of either CoCl_2 , MnCl_2 , NiCl_2 or FeCl_2 . In the case of FeCl_2 , ascorbic acid was added at double the concentration of FeCl_2 . An iterative process was allowed to proceed until apparent K_d and functional enzyme concentration values converged after a few cycles.

3.2.4 Kinetic measurement of different metalloforms of *MtMetAP Ic*.

To obtain the k_{cat} and K_m , reactions were carried out in 80 μL assay mixture with 50 mM MOPS-NaOH, pH 7.5, 0.5 μM *MtMetAP Ic* and divalent metal ions (50 μM FeCl_2 with 100 μM ascorbic acid, 10 μM CoCl_2 , 20 μM MnCl_2 , or 20 μM NiCl_2), and increasing concentrations of

Met-AMC from 0.9 mM to 2mM. The k_{cat} and K_m values of *MtMetAP Ic* were derived from a nonlinear regression fitting of the curve in the plot of the initial rates vs the substrate concentrations, using the Michaelis-Menton equation $V = V_{max}[S]/(K_m + [S])$.

3.2.5 IC₅₀ determination with different metalloform *MtMetAP Ic*.

Serial dilution of the tested compounds was performed by Precision liquid handling system from BioTek (Winooski, VT). For IC₅₀ determination, the hydrolysis of Met-AMC was monitored in the presence of the 3-fold diluted inhibitors, with concentrations varying from 1000 μ M to 0.5 μ M. In addition to the inhibitors, each well contained 50 mM MOPS-NaOH, pH 7.5, 100 μ M Met-AMC, 0.5 μ M *MtMetAP Ic*, and the metal ion that gave the optimal activity of *MtMetAP Ic* (50 μ M FeCl₂ with 100 μ M ascorbic acid, 10 μ M CoCl₂, 20 μ M MnCl₂, or 20 μ M NiCl₂). The IC₅₀ values were calculated from non-linear regression curve fitting of percent inhibitions as a function of inhibitor concentrations.

3.2.6 Complementation of the essential function of *EcMetAP* with *MtMetAP Ic* in *E. coli*.

To evaluate the *MtMetAP Ic* function in the cellular environment, an *E. coli* strain with conditional expression of the endogenous *EcMetAP* under the control of pBAD promoter, was used for complementation testing [13-14]. This *E. coli* strain with an amber mutation is constructed by inserting a n amber stop codon (UAG) in the chromosomal *EcMetAP* gene, and has a plasmid pBAD/sup2 that encodes an amber-mutation-suppressor tRNA under the control on arabinose promoter. Since the *EcMetAP* gene is essential for cell viability, the insertion of this amber mutation in the *EcMetAP* gene causes a premature termination of protein translation thus leading to cell death. However, the lethal effect can be suppressed by expression of the

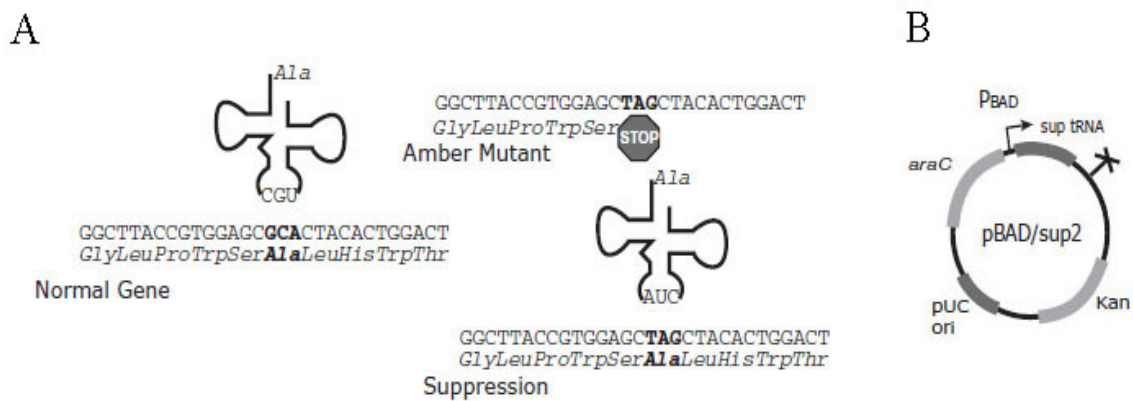


Figure 3-1 Conditional control of growth of *E. coli*. amber mutant.

A) In the normal gene, tRNA attaches an appropriate amino acid into the elongated peptide based on the three-base codon region in mRNA. In the amber mutant, the amber stop codon (TAG) in the gene will result in the termination of protein synthesis. In the amber suppression mutant, the suppressor tRNA, which is encoded by the pBAD plasmid and controlled by arabinose, can recognize the amber stop codon and insert an Ala to the elongation of the peptide. B) The map of pBAD/sup2 plasmid (from reference [13] with modification.)

suppressor tRNA, which has modification in its encoding DNA sequence that allows it to insert an amino acid at the UAG codon. Therefore, the translation continues regardless of the Amber mutation so that *EcMetAP* is fully translated and enable the *E.coli* to survive in the non-permissive medium. By adjusting the amount of glucose or arabinose in the medium, the expression of suppressor tRNA can be tightly controlled (Figure 3-1).

Plasmid pFLAGCTC was used as the vector for complementation tests as the desired gene could be expressed under the control of an IPTG-inducible *tac* promoter. *MtMetAP* Ic gene was taken from plasmid pGEMEX1-*MtMetAP* Ic by digestion of *Nde*I and *Bam*H I, and cloned into pFLAGCTC. Similarly, the *EcMetAP* gene was cloned into the pFLAGCTC plasmid as pFLAGCTC-*EcMetAP*. Both the parent plasmid pFLAGCTC and the plasmid pFLAGCTC-*EcMetAP* were used as controls. These plasmids were all transformed into the *E. coli* amber mutant. The cells were cultured in a special MOPS-NaOH-based liquid medium (Teknova, Hollister, CA) or on agar plates prepared with the medium. The MOPS-based rich defined medium was used in combination with kanamycin, ampicillin, IPTG and L-arabinose, or D-glucose.

3.2.7 Inhibition of cellular *MtMetAP* Ic activity

The above-mentioned pFLAGCTC-*MtMetAP* Ic-transformed *E. coli* cells (*MtMetAP* Ic-complemented cells) were used to establish the cellular *MtMetAP* Ic activity assay. Bacterial cells were allowed to grow to the exponential phase, harvested and washed twice with water. The final cell pellet was resuspended in 10 mM CaCl₂, 100 mM Tris-HCl, pH 7.5 [15] and then an equal volume of glycerol was added. The cell suspension was kept at -80 °C for storage.

For the cellular *MtMetAP* Ic activity assay, the cell suspension was diluted with 10 mM CaCl_2 , and 100 mM Tris-HCl, pH 7.5. The cells, substrate Met-AMC, and inhibitors at 12 serially diluted concentrations were combined in wells of a 384-well plate. The final assay volume was 80 μl with 150 μM Met-AMC, 5 mM CaCl_2 , and 50 mM Tris-HCl, pH 7.5. Increase of the fluorescent product was monitored via fluorescence (λ_{ex} 360 nm, λ_{em} 460 nm) at room temperature every 2 min for 6-8 hr. The IC_{50} values were calculated from the rate of substrate hydrolysis.

3.2.8 Inhibition of *MtMetAP* Ic-complemented *E. coli* cell growth

Inhibition of bacterial growth was carried out using the *MtMetAP* Ic-complemented *E. coli* cells. The experiments were performed in a similar way as previously reported with minor modifications[15]. The assay was carried out on 384-well opaque plates containing 12 serially diluted concentrations for each inhibitor (40 μL per well) with the highest final concentration of 1 mM in the assay. A suspension of bacterial cells was prepared from agar plates containing rich defined media with 0.2% glucose, 50 $\mu\text{g/mL}$ kanamycin and 100 $\mu\text{g/mL}$ ampicillin grown to the exponential phase, which was used to inoculate a second culture batch. This ensured that the survival of the cells was due to *MtMetAP* Ic complementation rather than residual endogenous *EcMetAP*. The suspension was adjusted to 0.5 McFarland optical density [16] and then further diluted by 1000 fold in the same medium containing 100 mM Tris-HCl, pH 7.5, and 225 μM resazurin. Cells were dispensed into the microplate (40 μL per well) by a Multidrop Combi reagent dispenser (Thermo Scientific, Waltham, MA). The conversion from resazurin to resofurin was monitored kinetically by fluorescence at λ_{em} 590 nm with λ_{ex} 530 nm using a SpectraMax Gemini XPS plate reader. Fluorescence kinetic experiments were carried out for 10

hours at 37 °C, with readings taken every 5 min. Signal intensities at time points along the exponential phase of the growth curve corresponding to 50-85% of total intensity of an uninhibited sample were averaged and converted to percent inhibition to calculate IC₅₀ values by non-linear regression curve fitting.

3.2.9 Crystallization and data collection

Crystals of the enzyme-inhibitor complexes were obtained independently by using a hanging-drop vapor-diffusion method at room temperature. The *MtMetAP Ic* crystal was first grown in buffer 3 (0.1M Bis-Tris-HCl pH 5.5, 2.0 M ammonium sulfate) and buffer 4 (0.1M Bis-Tris-HCl pH 6.5, 2.0 M ammonium sulfate) in Index™ kit (Hampton Research, Aliso Viejo, CA). The well solutions were optimized by changing the ammonium sulfate concentration, pH buffer and addition of additives, such as glycerol and PEG400. Each of the inhibitors (100 mM or 50 mM in DMSO) was added to high concentration of metalated enzyme (10 mg/mL, 0.32 mM protein; 2 mM metal) in 50 mM Tris-HCl, pH 8.0, 150 mM NaCl and the molar ratio of inhibitor to *MtMetAP Ic* was 5:1 or 10:1. The enzyme/inhibitor mixture was mixed with the reservoir buffer in a 1:1 ratio. The reservoir buffer was 100 mM Bis-Tris-HCl, pH 5.5, 1.1 M – 1.4 M NH₄SO₄, 5% - 15% glycerol or PEG400. Diffraction data were collected at the Advanced Photon Source, Argonne National Laboratory (beamline 19BM) and processed with HKL3000 [17]. All of the crystals belong to space group *P6₃*. One molecule is in the asymmetric unit.

3.2.10 Structural solution and refinement

The structures were solved by molecular replacement with MolRep [18] in CCP4 [19] with CCP4i interface [20], using the previously published *MtMetAP Ic* structure (PDB code

1YJ3) [21] as the search model. The structure was refined with REFMAC5 [22] with iterative model building using WinCoot [23]. The refinement was monitored with 5% of the reflections set aside for R_{free} factor analysis throughout the whole refinement process. Electron density was clear for all residues except a few residues at the N-terminus, and residues from the second (P2) in the native protein to the end (L285) were modeled. Comparison of structures and generation of structural drawings were carried out by using PyMOL [24]. Statistic parameters in data collection and structural refinement are shown in Table 3-3. Atomic coordinates and structure factors for the three structures were deposited in the Protein Data Bank.

3.2.11 Identification of quaternary structure of *MtMetAP* Ic using size exclusion chromatography

As the crystal structure of *MtMetAP* Ic showed a trimeric form, it is suspect whether it also exhibited as a trimer in solution. Therefore, size exclusion chromatography was employed to identify the quaternary structure of *MtMetAP* Ic in solution. Protein molecular weight standards from Gel Filtration Calibration Kits (GE Healthcare Life Science, Piscataway, NJ) including blue dextran (2000 Kd), aldolase (153 Kd), bovine serum albumin (67 Kd), ovalbumin (43 kD) and ribonuclease (13.7 kD) were dissolved into water to make 10 mg/mL stock solution. In order to make the protein standard, one hundred microliter samples were taken from each stock and mixed to make a 500- μ L protein standard. The protein standard was applied to a size-exclusion column, Superdex 75 10/300 GL, (GE Healthcare Life Science, Piscataway, NJ) and eluted with 50 mM MOPS-NaOH pH 7.5 and 150 mM NaCl at a rate of 0.5 mL/min until all the proteins were eluted from the Superdex 75 10/300 GL column. Two hundred and fifty microliter of purified *MtMetAP* Ic (5 mg/mL) was applied to Superdex column and washed with 50 mM

MOPS-NaOH pH 7.5 and 150 mL NaCl. The elution volume was recorded and compared to that of protein standard to determine the size of *MtMetAP* Ic in solution.

3.3 Results

3.3.1 Expression and purification of *MtMetAP* Ic.

The *MtMetAP* Ic protein was expressed in *E.coli* as a soluble protein and was purified using anion exchange chromatography followed by ammonium sulfate precipitation. The purified *MtMetAP* Ic was ~99% homologous as determined by SDS-PAGE (Figure 3-2) with a yield of 20-30 mg per liter of cells. Three amino acid residues MAS were added to the N-terminus of the protein for cloning purposes. No attempt was made to remove the extra sequence, although the terminal methionine is often processed cotranslationally by MetAP in *E. coli* cells. The apoenzyme showed no activity when tested by the fluorogenic substrate Met-AMC and could be immediately activated by adding divalent metals ions.

3.3.2. Metal binding and activation of *MtMetAP* Ic

A metalloenzyme usually can be activated by several different metal ions because the similar sizes of these metal ions make this isomorphous replacement possible. The *MtMetAP* Ic was tested for activation by divalent metals, including Co(II), Ni(II), Mn(II), Fe(II) and Zn(II) (Figure 3-3). Bell-shaped metal activation curves were observed, similar to these observed previously with *EcMetAP*. The apoform of *MtMetAP* Ic did not show activity in the absence of metal ions or when the metal concentrations were lower. As the metal concentrations increased, the metallated *MtMetAP* Ic could hydrolyze the substrate Met-AMC, as indicated by the increase of fluorescence detected at λ_{em} 460 nm (λ_{ex} 360 nm). High concentrations of a metal often inhibit

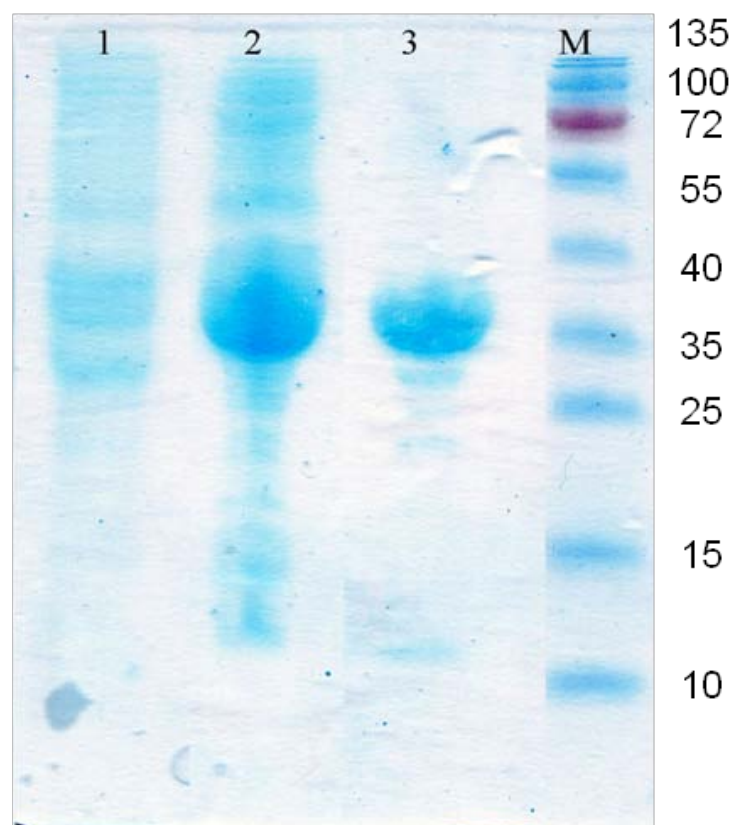


Figure 3-2 : The purification of *MtMetAP Ic*

Lane 1: Cell lysate of BL21 (DE3)-pGEMEX1-*MtMetAP Ic* before IPTG-induction

Lane 2: Cell lysate of BL21 (DE3)-pGEMEX1-*MtMetAP Ic* after IPTG-induction

Lane 3: Purified *MtMetAP Ic*

Lane 4: pre-stained protein ladders from Fermentas

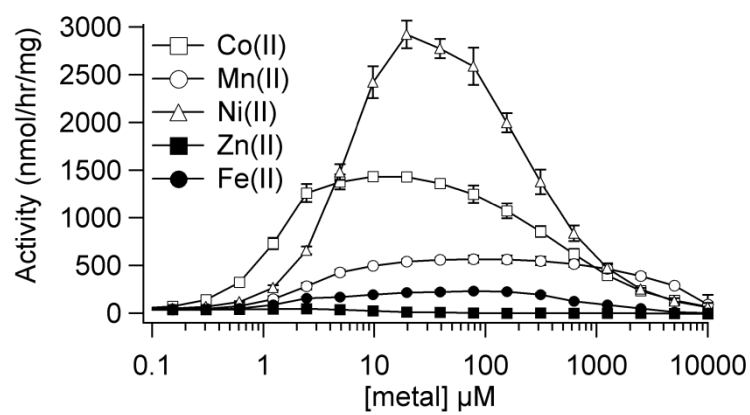


Figure 3-3. Activation of *Mt*MetAP Ic apoenzyme by divalent metals.

MetAP enzymatic activity [25-26], which was observed in all the metals tested on *Mt*MetAP Ic. Co(II) activated *Mt*MetAP Ic effectively, starting at a low concentration less than 1 μ M, consistent with its activation for many MetAPs. Mn(II) and Fe(II) also showed activation, and the starting concentrations were around 1 μ M, while no activation was observed for Zn(II). What is unique and surprising was the observed strong activation of *Mt*MetAP Ic by Ni(II), starting around 1 μ M. This has not been observed in *Ec*MetAP or other MetAPs, and raises the question whether Ni(II) is the native cofactor for *Mt*MetAP Ic. To further understand the metal binding and activation of *Mt*MetAP Ic, a detailed kinetic study was carried out with the activating metal ions. The hydrolysis of Met-AMC can be conveniently monitored by fluorescence from the released aminomethylcoumarin. The affinity (apparent K_d) for each of the activating metals was measured by fitting a model of multiple independent binding sites (MIBS), taking into consideration the amount of functional enzyme [12]. It is apparent that Co(II) bound to *Mt*MetAP Ic the tightest with the lowest apparent K_d values, followed by Fe(II) and Mn(II) (Table 3-1). Ni(II) was shown to have the weakest affinity, which is about 4-fold weaker than Co(II).

3.3.3. Kinetic characterization of purified *Mt*MetAP Ic.

For K_m measurements of an enzyme, it is used that the substrate concentration is higher than the enzyme concentration. In this case, the concentration of *Mt*MetAP Ic was fixed at 0.5 μ M, which was much lower than the concentrations of Met-AMC, ranging from 1 μ M to 2 mM. The increase in fluorescence at λ_{em} 460 nm (λ_{ex} 360 nm) was recorded and converted into μ M product per min at the optimal metal concentrations, Michaelis–Menten constants were calculated (Table 3-2). Interestingly, Ni(II)-activated *Mt*MetAP Ic was the most efficient among

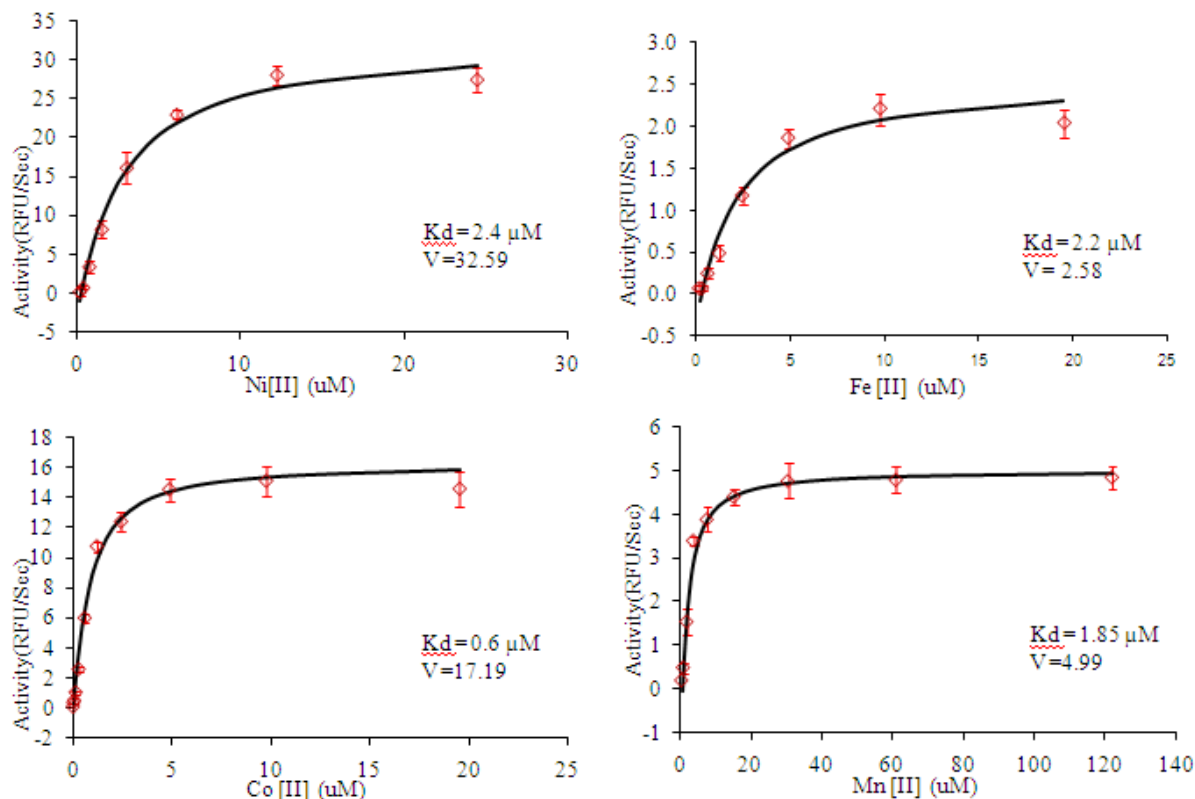


Figure 3-4 Calculation of the apparent K_d of different metalloforms of *MtMetAP Ic* by using a MIBS model [12]

Table 3-1 Activation of *MtMetAP Ic* by different metals ^a

<i>MtMetAP Ic</i>	Fe(II)	Ni(II)	Co(II)	Mn(II)
<i>App K_d</i> , μM	2.2 ± 0.1	2.4 ± 0.2	0.6 ± 0.1	2.1 ± 0.2

^a *App K_d* is apparent K_d , which represents the metal concentration when apoform *MtMetAP Ia* achieves 50% activation. The constants were obtained with 0.5 μM apoenzyme, 100 μM substrate Met-AMC in 50 μM MOPS-NaOH. The *apparent K_d* was obtained from three separate tests and it is represented as the mean and the standard deviation (s.d.) of three experiments.

3.3.4. Functional complementation of *EcMetAP I* in *E.coli* growth by *MtMetAP Ic*

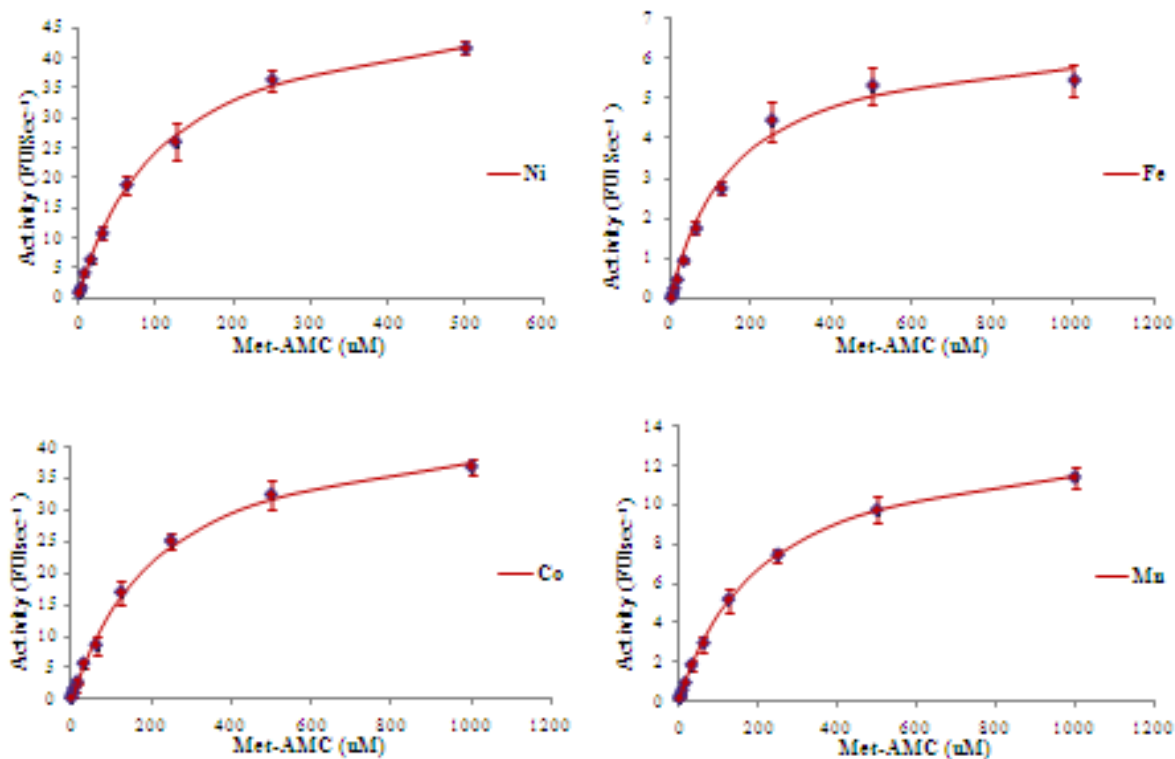


Figure 3-5 Calculation of K_m value of different metalloform of *MtMetAP Ic*

Table 3-2 Kinetic measurement of *MtMetAP Ic*

	Fe(II)	Ni(II)	Co(II)	Mn(II)
K_m , μM	160.7 ± 6.0	96.3 ± 9.8	221.1 ± 13.2	227.3 ± 8.8
k_{cat} , sec^{-1}	0.0039 ± 0.0002	0.029 ± 0.002	0.027 ± 0.0004	0.0082 ± 0.00033
k_{cat}/K_m , $\text{M}^{-1}\text{sec}^{-1}$	24.3	301.1	122.1	36.1

K_m and K_{cat} are the Michaelis-Menten constants and they were obtained with Fe(II) at 50 μM , Ni(II) and Mn(II) at 20 μM , and Co(II) at 10 μM .

the metalloforms tested in catalyzing the hydrolysis of the substrate, with the lowest K_m and the highest k_{cat} , consistent with the metal titration curve (Table 3-2).

A functional MetAP enzyme is essential for *E. coli* growth [2] and the *EcMetAP* gene cannot be deleted. However, an *E. coli* strain with an amber mutation at its chromosomal *EcMetAP* gene and a plasmid with a pBAD-regulated amber suppressor tRNA gene suppresses the lethal effect of the amber mutation and provides a perfect tool to evaluate the function of *MtMetAP* Ic in the *E.coli* environment [14]. When the *E. coli* cells grow in the presence of arabinose, because expression of the tRNA induced, which suppresses the lethal effect of the amber mutation, functional *EcMetAP* is produced. On the other hand, the cells cannot grow in the presence of glucose, because no such tRNA is expressed and the translation of *EcMetAP* is prematurely terminated due to the amber mutation in the *EcMetAP* gene. The hypothesis for this experiment is that function of the chromosomally expressed *EcMetAP* can be complemented with a functional MetAP expressed from a plasmid. In order to test whether *MtMetAP* Ic can function in an *E. coli* cellular environment, the *MtMetAP* Ic gene was inserted into pFLAGCTC and transformed into the *E.coli* amber mutant. The parent plasmid pFLAGCTC without any MetAP gene, and the plasmid pFLAGCTC-*EcMetAP* with *EcMetAP* gene, were used as controls and were transformed into *E.coli* amber mutant as well. On agar plates, cells transformed with parent plasmid pFLAGCTC grew in the presence of arabinose and did not grow in the presence of glucose (Figure. 3-6A). This confirmed that a functional MetAP is required for cell growth. The cells with either pFLAGCTC-*EcMetAP* or pFLAGCTC- *MtMetAP* Ic grew on the agar plate in the absence of arabinose and presence of glucose (Figure 3-6A), which suggests that *EcMetAP* or *MtMetAP* Ic expressed from the plasmids was functional and complemented the function of chromosomally expressed *EcMetAP* to support the growth.

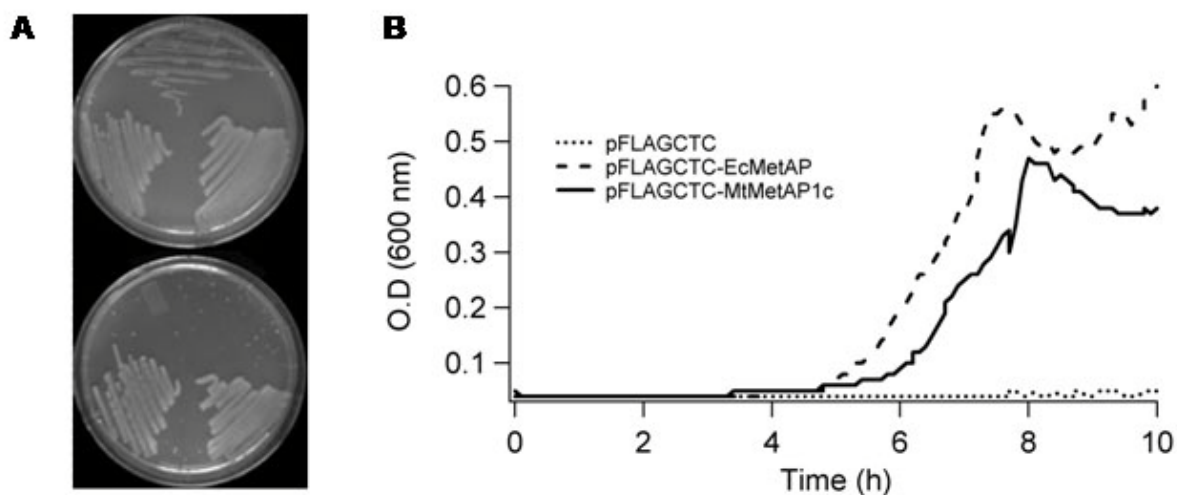


Figure 3-6. Complementation of *EcMetAP I* function by *MtMetAP Ic*.

A. *E. coli* cells carrying an amber mutation in chromosomal *EcMetAP* gene were streaked on agar plates with glucose (bottom plate) or with arabinose (top plate). Each plate displays cells containing pFLAGCTC (top), pFLAGCTC-*MtMetAP Ic* (bottom left) or pFLAGCTC-*EcMetAP* (bottom right). **B.** Growth of the *E. coli* cells in liquid medium supplemented with glucose.

The growth of the transformed *E. coli* strains was also tested in a liquid medium supplemented with glucose and without arabinose. The cells with either pFLAGCTC-*EcMetAP* or pFLAGCTC-*MtMetAP* Ic showed robust growth, while the *E. coli* cells with the parent plasmid pFLAGCTC did not grow under the same conditions (Figure. 3-6B). These results confirm that *MtMetAP* Ic expressed from a plasmid in *E. coli* was a functional enzyme and supported the growth of *E. coli* cells when *EcMetAP* was absent.

3.3.5. Metalloform-selective inhibition of purified *MtMetAP* Ic and the enzyme in an *E. coli* cellular environment

Assignment of the physiologically relevant metalloform has been difficult, and a new approach was developed in our lab for the assignment using metalloform-selective inhibitors that can distinguish different metals at the active site [15, 27]. A set of inhibitors (Table 3-3) with known metalloform-selectivity for *EcMetAP* were used to evaluate inhibition of purified *MtMetAP* Ic enzyme and the same enzyme in an *E. coli* cellular environment, to provide clues for the metal cofactor used by *MtMetAP* Ic in cells. The catechol compounds **1** and **2** inhibited selectively the Fe(II) form of *EcMetAP* [28], while compound **3** and **4** were shown to be highly selective inhibitors for the Mn(II) form [27]. Triazole inhibitors were shown to interact directly with the catalytic metal ions through nitrogen atoms [29], and it was hypothesized that they may inhibit the Co(II) and Ni(II) forms of MetAP because of their chelation through nitrogen atoms [30]. Four such triazole compounds, **5-8**, were selected for this study. All of the eight MetAP inhibitors were first tested with purified *MtMetAP* Ic apoenzyme activated by Co(II), Ni(II), Mn(II) or Fe(II). Indeed, all of these inhibitors showed potent and metalloform-selective inhibition at low micromolar or submicromolar concentrations (Table 3-3). Compounds **1** and **2**

were selective for the Fe(II) form, compounds **3** and **4** were selective for the Mn(II) form, and compounds **5-8** were selective for the Ni(II) and Co(II) forms.

3.3.6. Growth inhibition of *MtMetAP* Ic-complemented *E. coli* cells.

Subsequently, the ability of compounds **1-8** to inhibit the cellular enzymatic activity of *MtMetAP* Ic in permeabilized *E. coli* cells was tested. Inclusion of Ca(II) at 5 mM made these cells permeable to substrates and inhibitors, and Ca(II) had no effect on MetAP activity[15]. Clearly, the highest inhibition of the cellular *MtMetAP* Ic activity was achieved by the two Fe(II)-form selective inhibitors **1** and **2** (Table 3-3), suggesting that *MtMetAP* Ic present in the live *E. coli* cells used Fe(II), not Ni(II) or Co(II), as the cofactor for catalysis.

The excision of N-terminal methionine is an important co-translational process, and a lethal phenotype is observed when the single gene coded for *EcMetAP* was deleted in *E. coli* [2], demonstrating that it is essential for bacterial survival. In our construct, it was observed that the *MtMetAP* Ic complemented the essential function of *EcMetAP* in *E. coli* cells. Therefore, effective inhibition of cellular *MtMetAP* Ic would conceivably inhibit the growth of the *E. coli* cells. Therefore, some of the metalloform-selective inhibitors were also tested on the *E. coli* cells with *MtMetAP* Ic complementation and we observed that only the Fe(II)-form selective inhibitors **1** and **2** arrested bacterial cell growth (Table 3-3). In contrast, inhibitors **3**, **5** and **6** showed no inhibition at the highest concentration (1 mM) tested. Although there are many reasons a compound may not work in whole cells, including lack of cell penetration, the observed inhibition by **1** and **2** is consistent with the conclusion that the functional metalloform of cellular *MtMetAP* Ic exists as the Fe(II)-form in *E.coli*.

Table 3-3. Inhibition of enzymatic activities of purified and cellular *MtMetAP* Ic and inhibition of cell growth of *MtMetAP* Ic-complemented *E. coli* by metalloform-selective inhibitors ^a

Cmpd	Purified Enzyme ^b				Cellular Enzyme ^c	Bacterial Growth ^d
	Fe(II)	Ni(II)	Co(II)	Mn(II)		
1	3.6	104	76	37	20	208
2	1.4	60	38	14	35	89.5
3	>500	>500	>500	14	623	>1000
4	>500	>500	>500	16	N.D. ^e	N.D.
5	>500	1.3	0.74	18	121	>1000
6	>500	2.5	0.69	26	281	>1000
7	>500	0.58	2.0	143	N.D.	N.D.
8	40	0.24	0.26	2.0	N.D.	N.D.

^a IC₅₀ values are expressed in μ M. ^b Purified enzymes were reconstituted by activating the apoenzyme with different divalent cations [Fe(II), 50 μ M; Ni(II) and Mn(II), 20 μ M; Co(II), 10 μ M]. ^c Cellular enzyme was the recombinant *MtMetAP* Ic expressed in *E. coli* cells lacking endogenous *EcMetAP*. ^d Growth of *E. coli* cells with the recombinant *MtMetAP* Ic was monitored. ^e Not determined.

3.3.7 Co-crystallization of *Mt*MetAP Ic with inhibitors

Structural information for mycobacterial MetAPs is lacking, and only two X-ray structures of *Mt*MetAP Ic either as an apoenzyme or in complex with product methionine were reported [21]. With the confirmed inhibition of *Mt*MetAP Ic by the metalloform selective inhibitors, crystallization and structural analysis were utilized to elucidate their binding mode at the active site of *Mt*MetAP Ic. Three structures of such enzyme-inhibitor complexes with **4**, **7**, or **8** were determined independently. All of the structures were folded in the “pita-bread” shape commonly seen in previous MetAP structures [31]. Electron density for two Mn(II) or Ni(II) ions was clearly observed at the dinuclear metal site, and fluorescence spectrum scan was used to confirm the divalent metal ion existed in the crystals based on the excitation energy. All there inhibitors bound in the shallow and mostly hydrophobic active site pocket.

All *Mt*MetAP Ic-inhibitor complex crystals belonged to the space group $P6_3$ with unit cell dimension $a = 106.4 \text{ \AA}$, $b = 106.4 \text{ \AA}$, $c = 50.5 \text{ \AA}$. Data collection statistics are listed in Table 3-4.

The structure was solved with a resolution of 1.4 \AA , and two molecules of inhibitor **4** were fitted to the structure. One of the inhibitor molecules occupied the active site, and the other took a position on the opposite side of the protein molecule, 10.9 \AA away from the active site inhibitor. The structure of *Ec*MetAP in complex with the same inhibitor was solved before (pdb code 1XNZ), and only one inhibitor molecule was identified [32]. When these two structures were overlaid, the active site inhibitor showed the same binding mode with a non-coplanar conformation between its two aromatic rings (Fig. 3-7B). Occupation of **4** at the active site is likely sufficient for MetAP inhibition, because the second molecule of **4** was not observed in the *Ec*MetAP structure, and **4** inhibited both *Mt*MetAP Ic and *Ec*MetAP potently at 16 \mu M and 0.24

Table 3-4 X-ray data collection and refinement statistics

Inhibitor	4	7	8
Inhibitor code	FCD	T03	T07
PDB code	3IU7	3IU8	3IU9
Metal ion	2 Mn(II)	3 Ni(II)	2 Ni(II)
Cell Parameters			
space group	$P6_3$	$P6_3$	$P6_3$
a (Å)	106.4	105.7	106.2
b (Å)	106.4	105.7	106.2
c (Å)	50.4	50.4	50.8
α (deg)	90	90	90
β (deg)	90	90	90
γ (deg)	120	120	120
X-ray Data Collection			
Resolution range (Å) ^a	50-1.40 (1.42-1.40)	50-1.85 (1.88-1.85)	50-1.75 (1.78-1.75)
Collected reflections	642,578	304,665	301,490
Unique reflections	64,180	27,549	32,971
Completeness (%) ^a	99.9 (100)	99.5 (90.5)	99.5 (92.2)
$I/\sigma(I)$ ^a	43.8 (9.4)	23.3 (3.8)	59.8 (15.7)
R_{merge} (%) ^a	4.5 (21.5)	15.6 (71.4)	7.8 (17.5)
Refinement Statistics			
R (%)	17.1	16.5	16.4
R_{free} (%)	19	20	19.5
R.m.s.d. bonds (Å)	0.031	0.028	0.028
R.m.s.d. angles (°)	2.52	1.97	2.31
No. of solvent molecules	249	162	193
$\langle B \rangle$ protein (Å ²)	11	14.4	14.1
$\langle B \rangle$ inhibitor (Å ²)	9.5	21.4	12.5
$\langle B \rangle$ water (Å ²)	18.6	19.2	19.7

^a Values given in parentheses correspond to the outer shell of data.

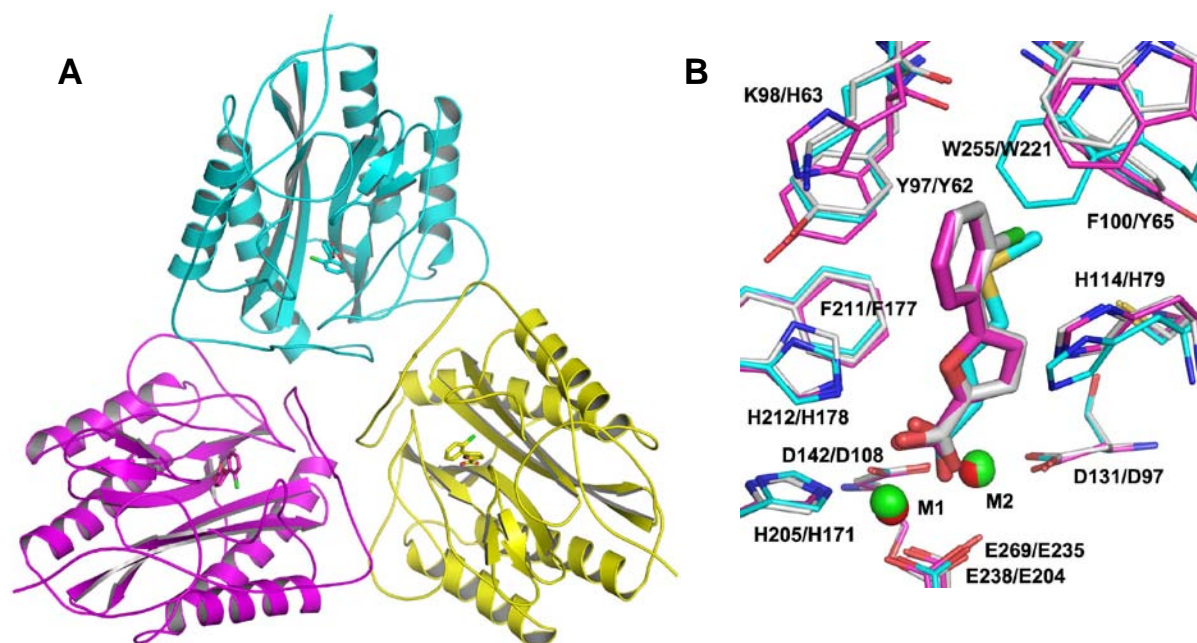


Figure 3-7. Structure of *Mt*MetAP Ic in the Mn(II)-form in complex with the Mn(II)-form selective inhibitor 4. **A.** the trimeric arrangement of *Mt*MetAP Ic in the crystal. Inhibitor 4 at the active site is shown as sticks. The three molecules of *Mt*MetAP Ic were colored cyan, magenta and yellow, respectively. **B.** Overlay of this structure with *Ec*MetAP in complex with the same inhibitor (carbon magenta, pdb 1XNZ) and with the same protein in complex with methionine (carbon cyan, pdb 1YJ3). Only residues (thin sticks) surrounding the ligands (thick sticks) at the active site are shown. Non-carbon atoms are colored: red, oxygen; blue, nitrogen; yellow, sulfur; and green, chlorine. Mn(II) (green) and Co(II) (red) ions are shown as spheres. For residue labeling, the first is for *Mt*MetAP Ic and the second for *Ec*MetAP.

μM [27], respectively. *Ec*MetAP has a longer C-terminus, and the binding of a second **4** is spatially incompatible with residues R251, D253 and D254 in *Ec*MetAP.

The previous *Mt*MetAP Ic structure (pdb code 1 YJ3) is in the Co(II) form, and the ligand used is also different. However, superimposing the two structures by aligning all main chain atoms from residue R4 to the end residue L285 gave a rmsd of 0.301 Å, indicating very similar structures. Due to different ligands, the active site residues showed movements to accommodate the different sizes of the ligands. The most significant movements were H114, which moved by 1.4 Å and is a conserved residue in *Ec*MetAP that plays an important role in catalysis,³⁷ and W255, which moved the most by 2.2 Å.

Triazoles were reported as potent inhibitors of the Co(II)-form of *Staphylococcus aureus* MetAP (IC₅₀, 43.7 nM) [29] and X-ray structures of enzyme-inhibitor complexes were reported. Here we described the inhibition of *Mt*MetAP Ic by similar triazole compounds with high potency at submicromolar concentrations and selectivity for the Co(II) and Ni(II)-form. We crystallized two of the triazole inhibitors (**7** and **8**) with *Mt*MetAP Ic in a unique Ni(II)-form and solved the complexes to 1.85 Å and 1.75 Å resolution, respectively. Although both inhibitors have the same triazole moiety, they bound differently at the active site. While inhibitor **8** bound at the active site as a dimetalated structure (Figure 3-8 B), inhibitor **7** acquired an additional Ni(II) ion to form a trimetalated structure (Figure 3-8A). The extra ion was tetra coordinated with ligation to the conserved H144 mentioned before and to a water molecule and a chlorine ion as the third and fourth coordination points. Trimetalated MetAP enzymes in complex with other types of inhibitors have been observed before [30, 33-34] and their formation requires specific spatial arrangement of coordinating heteroatoms. However, it is interesting to note that inhibitor **7** formed a trimetalated structure, while inhibitor **8** formed a dimetalated structure with small

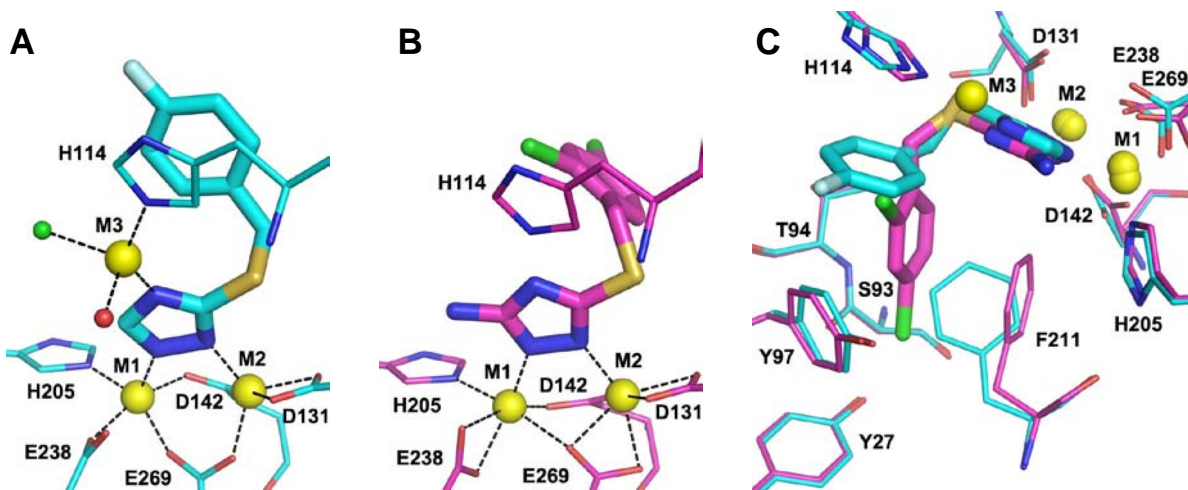


Figure 3-8. Structures of *MtMetAP Ic* in the Ni(II)-form in complex with the Co(II)- and Ni(II)-form selective inhibitors **7 and **8**.** **A.** Trimetalated active site with inhibitor **7** bound. Inhibitor is shown as thick sticks and the protein residues as thin sticks (carbon, cyan; oxygen, red; nitrogen, blue; sulfur, yellow; and fluorine, pale). Ni(II) ions (yellow) are shown as large spheres, and water (red) and chlorine ion (green) are shown as small spheres. Metal coordination is shown as dashed lines. **B.** Dimetalated active site with inhibitor **8** bound. The same color scheme as in A is used, except carbon is colored magenta and chlorine is colored green. **C.** Comparison of the bound conformations of **7** and **8**. For clarity, only selected protein residues are shown.

structural differences. These two structures also differ significantly at the dinuclear metal site. M1 and M2 were both pentacoordinated in the complex with inhibitor **7**, and they became hexacoordinated in the complex with inhibitor **8**. The distances from M1 to the two oxygen atoms of E238 are 2.0 Å and 3.2 Å in the complex with **7**, therefore, E238 provided only one oxygen atom for coordination. In contrast, the distances are 2.1 Å and 2.2 Å in the other complex, and both oxygen atoms coordinated with M1. For M2 coordination, one of the oxygen atoms of E269 shifted from a monodentate mode to M1 in complex with inhibitor **7** to a bridging bidentate mode to both M1 and M2 in complex with inhibitor **8**, providing the additional coordination point for M2.

A unique structural feature of the complex with inhibitor **8** is the bound conformation of the inhibitor. Although both inhibitors **7** and **8** have the core benzylthiotriazole structure, inhibitor **8** adapted a bound conformation, with its benzyl group turning into a pocket formed by rotation of F211 by 90° (Figure 3-8C). This binding pocket identified by this structure has not been seen in any other MetAP structures and provides additional interactions for MetAP inhibitor design.

3.3.8 Identification of the quaternary structure of *Mt*MetAP Ic using size exclusion chromatography

It is interesting that all of the three structures showed $P6_3$ space group in the crystal packing, instead of the common $P2_1$ space group seen in other MetAPs. This symmetry indicates a trimeric arrangement in the crystals (Figure 3-7A), and indeed, the calculation on the PISA server (http://www.ebi.ac.uk/msd-srv/prot_int/pistart.html, Protein Interface Surfaces and

Assemblies service) showed that there are large contact surfaces between the protein molecules, and a trimetric form is energetically favored.

A similar analysis for the previous *MtMetAP Ic* structures (PDB codes 1Y1N and 1YJ3, with $P2_1$ space group) yielded no specific interactions between protein molecules, and a monomeric solution structure was predicted. The previously reported *MtMetAP Ic* has a longer N-terminus with a His-tag present [21], and it is not known whether the extra sequence, although not visible in the X-ray structures, prevented its packing within the crystals as a trimer. The His-tag has identified not locate near the contact surfaces. One question is whether *MtMetAP Ic* is trimeric in solution. We eluted our *MtMetAP Ic* (31 kDa predicted molecular weight) in 50 mM Tris-HCl pH 7.5 with 150 mM NaCl through a Superdex 75 size-exclusion column, with blue dextran (2000 kDa), aldolase (153 kDa), bovine serum albumin (67 kDa), ovalbumin (43 kDa), and ribonuclease (13.7 kDa) as molecular weight standards (Figure 3-9A). *MtMetAP Ic* was eluted between ovalbumin and ribonuclease and its calculated Mw was 33 kDa, suggesting a monomeric state in the solution condition (Figure 3-9C). Disagreement in oligomer states between crystal packing and solution has been noted [35], and it is possible that *MtMetAP Ic* exists in a trimeric form in some crystals, while it is monomeric in solution.

3.4 Discussion

Although the majority of bacteria have only one MetAP gene, two or more MetAP genes have been identified in a small number of bacteria, but most of them have not been characterized enzymatically. Two homologous type 1 MetAP isozymes in *Bacillus subtilis* were isolated and investigated. Although both showed enzymatic activity, only one of them was essential for

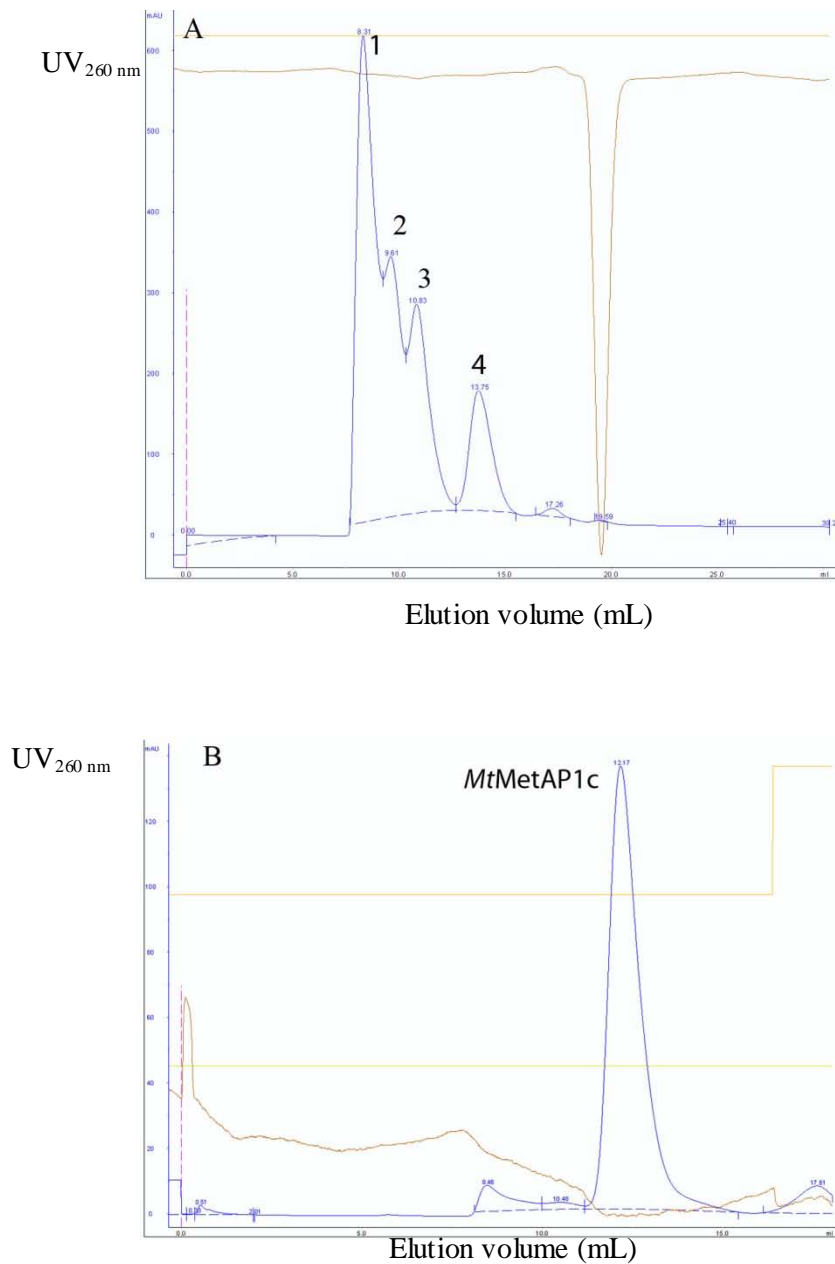


Figure 3-9 Identification of quaternary structure of *MtMetAP1c* using Superdex 75.

- A) The elution curve of protein standard. Peaks were 1) blue dextran and Aldolase; 2) bovine serum albumin, 3) ovalbumin; 4) ribonuclease
- B) The elution curve of *MtMetAP1c*

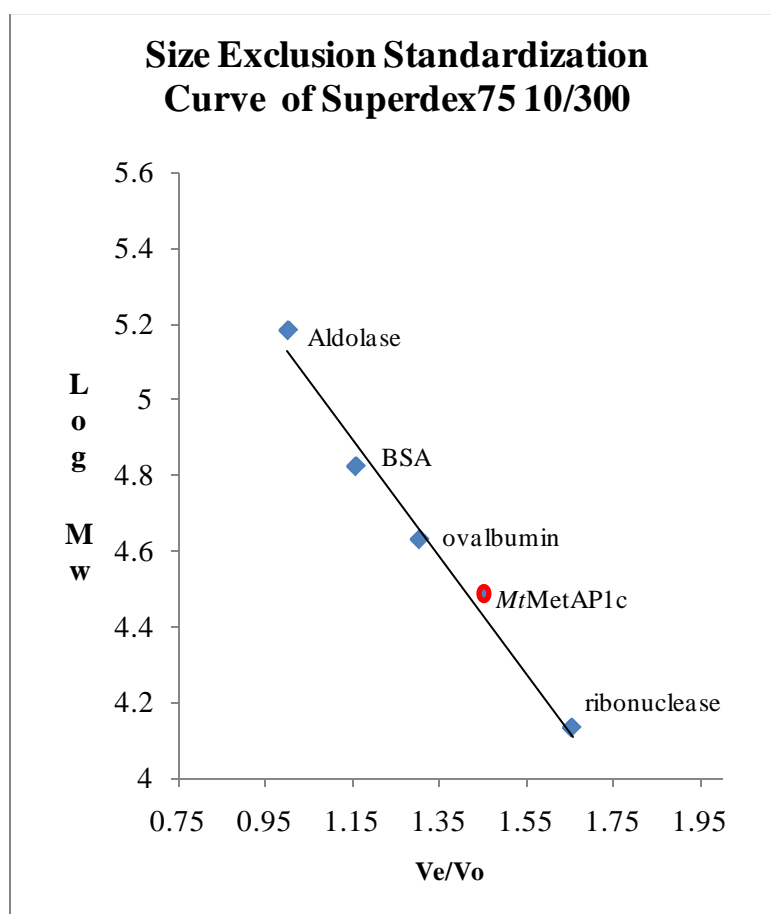


Figure 3-9 Identification of quaternary structure of *MtMetAP1c* using Superdex 75.

C) The standardization curve of Superdex 75 10/300. The eluted *MtMetAP1c* (illustrated as a red dot) was between ribonuclease and ovalbumin, consisting with a molecular weight of 30.9 Kd, which indicated it was a monomer.

growth, and the other was concluded to be non-essential due to low expression [36]. Two MetAP genes were also identified in *Acinetobacter baumannii*, but none of them has been demonstrated as a functional enzyme. The protozoan parasite *Plasmodium falciparum* has four MetAP sequences, and inhibitors discovered and characterized on one of the four showed antimalarial activity [3]. Deletion of the single MetAP gene from *E. coli* [30] or *Salmonella typhimurium* [37] is lethal. For those organisms that have two copies of MetAP enzymes, one type 1 and one type 2, such as *Saccharomyces cerevisiae*, deletion one of MetAP showed a slow growth phenotype, and deletion of both was proved [4].

There are two MetAP enzymes in *M. tuberculosis*, *MtMetAP Ia* and *MtMetAP Ic*. Both belong to type I MetAP, and an alignment of their protein sequences showed 36% identity to each other [38]. Because *MtMetAP Ia* and *MtMetAP Ic* are homologous enzymes, it is likely that the function of one can be complemented by the other, and inhibitors of one will inhibit the other as well. Therefore, both *MtMetAP Ia* and *MtMetAP Ic* are potential drug targets, and inhibition of one or both is likely required to show antimycobacterial activity. The mRNA transcript analysis of these two MetAPs in *M. tuberculosis* showed different mRNA levels in the log phase and the stationary phase [10]. The expression of *MtMetAP Ia* gene (*mapA*) expressed more in the log phase, while the expression of *MtMetAP Ic* gene (*mapB*) showed a higher level in the stationary phase, suggesting that the two MetAPs may perform important functions in different growth phases of *M. tuberculosis* [10]. The special characteristics of the mycobacterial life cycle may require more than one MetAP enzyme to carry out this important cotranslational modification.

We purified *MtMetAP Ic* to homogeneity as an apoenzyme and demonstrated its enzymatic function not only as a purified enzyme but also in live *E. coli* cells. Divalent metals

Co(II), Mn(II), Ni(II), and Fe(II) all showed immediate activation of the purified apoenzyme. Co(II) and Fe(II) had a higher affinity, while Ni(II) bound more weakly but showed the highest catalytic efficiency. Zhang et al [10] described Fe(II) and Ni(II) as inhibitors of *Mt*MetAP Ic activity, partially contradicting our results. However, their enzyme showed high activities before the metal ions were added, indicating that a metalated enzyme was already present. Considering that the enzyme was purified as a His-tagged protein, and no procedure was described for metal removal, their observed inhibitory effect of Fe(II) or Ni(II) was probably due to competition of the metal added with the active site metal already in place. Another possibility is that higher metal concentrations (in addition to the metal already in place) were used in their experiments, as our metal activation profiles (Figure 3-3) showed that a metal can also inhibit MetAP activity at high concentrations. It is interesting to note that a MetAP enzyme was purified from *Mycobacterium smegmatis* mc²155 strain, and its enzymatic activity was enhanced by Mg(II) and Co(II) and inhibited by Fe(II) and Cu(II)[39]. However, the enzyme was purified by following the hydrolysis of a MetAP substrate, and its identity as a mycobacterial MetAP was not confirmed by sequencing.

Many dinuclear metallohydrolases [40] play key roles in physiological and pathological processes and often are targets for therapeutics. For instance, MetAP in protein cotranslational modification, dicer in RNA interference [41], HIV reverse transcriptase in AIDS [42], and protein phosphatase-1 in cell cycle regulation [43]. Assignment of their physiologically relevant metalloform is often difficult and confusing, but it is critically important for the discovery and development of inhibitors that are effective against cellular enzymes. Initially from high-throughput screening, we discovered several classes of unique MetAP inhibitors that can distinguish different metal ions at the enzyme active site [27-28]. These metalloform-selective

inhibitors are valuable research tools for the assignment, and here we presented an example of their application to clarification of the native metalloform of *MtMetAP Ic* in an *E. coli* cellular environment. With confirmed inhibitory potency and selectivity on the metalloforms of the purified *MtMetAP Ic*, we characterized these inhibitors for inhibition of MetAP activity from the recombinant *MtMetAP Ic* in live *E. coli* cells. Only the Fe(II)-form selective inhibitors inhibited the cellular *MtMetAP Ic* activity and inhibited the growth of *MtMetAP Ic*-complemented *E. coli* cells, leading to the conclusion that *MtMetAP Ic* is in the Fe(II)-form in an *E. coli* cellular environment. It is intriguing why *MtMetAP Ic* utilizes Fe(II) for catalysis when Ni(II) offers higher catalytic efficiency. One possible explanation is that the higher binding affinity and easier availability of Fe(II) results in its preferential use. It was demonstrated that *E. coli* peptide deformylase utilized Fe(II) as the native metal cofactor, but the *Borrelia burgdorferi* used Zn(II) after heterologous expression in *E. coli* [44]. Therefore, expression of *MtMetAP Ic* in *E. coli* probably does not swap the intracellular type of metal utilized by *MtMetAP Ic* in *M. tuberculosis*. Nevertheless, the native metalloform of *MtMetAP Ic* in *M. tuberculosis* remains to be confirmed. Our approach of using *MtMetAP Ic* in *E. coli* cells is an attractive alternative to the direct manipulation of pathogenic organisms for drug discovery in that the conventional approach would not be readily accessible due to the dangers they pose.

The first group of small molecule inhibitors for a mycobacterial MetAP enzyme was presented and elucidated their binding characteristics at the enzyme active site. They showed not only potency but also selectivity for different metalloforms and were initial lead compounds for the development of inhibitors of mycobacterial MetAPs as novel anti-TB drugs. Although metalloform selectivity may not be required for effective inhibition of cellular MetAPs, selective inhibition of different metalloforms may be advantageous. Fe(II) is likely the metal used by

MetAPs in bacteria such as *E. coli* and *Bacillus* [15]. On the contrary, human type 2 MetAP uses Mn(II) as its physiologically relevant metal cofactor [45] . It is unknown which metal the human type 1 MetAP uses for its catalysis, but it is possibly not Fe(II) because free Fe(II) concentration in mammalian cells is low and sequestering iron is a defense mechanism against bacterial infection [46-47]. Metalloform-selectivity may provide a viable strategy for selective inhibition of bacterial MetAP enzymes.

References:

1. Bradshaw, R.A., W.W. Brickey, and K.W. Walker, *N-terminal processing: the methionine aminopeptidase and N alpha-acetyl transferase families*. Trends Biochem Sci, 1998. **23**(7): p. 263-7.
2. Chang, S.Y., E.C. McGary, and S. Chang, *Methionine aminopeptidase gene of Escherichia coli is essential for cell growth*. J Bacteriol, 1989. **171**(7): p. 4071-2.
3. Chen, X., et al., *Inhibitors of Plasmodium falciparum methionine aminopeptidase 1b possess antimalarial activity*. Proc Natl Acad Sci U S A, 2006. **103**(39): p. 14548-53.
4. Li, X. and Y.H. Chang, *Amino-terminal protein processing in Saccharomyces cerevisiae is an essential function that requires two distinct methionine aminopeptidases*. Proc Natl Acad Sci U S A, 1995. **92**(26): p. 12357-61.
5. Organization, W.H., *2009 update TUBERCULOSIS FACTS*. 2010.
6. Fauci, A.S., *Multidrug-resistant and extensively drug-resistant tuberculosis: the National Institute of Allergy and Infectious Diseases Research agenda and recommendations for priority research*. The Journal of Infectious Disease 2008. **197**: p. 1493-8.
7. Gandhi, N.R., et al., *Extensively drug-resistant tuberculosis as a cause of death in patients co-infected with tuberculosis and HIV in a rural area of South Africa*. Lancet, 2006. **368**(9547): p. 1575-80.
8. Corbett, E.L., et al., *The growing burden of tuberculosis: global trends and interactions with the HIV epidemic*. Arch Intern Med, 2003. **163**(9): p. 1009-21.
9. Cole, S.T., et al., *Deciphering the biology of Mycobacterium tuberculosis from the complete genome sequence*. Nature, 1998. **393**(6685): p. 537-44.
10. Zhang, X., et al., *Expression and characterization of two functional methionine aminopeptidases from Mycobacterium tuberculosis H37Rv*. Curr Microbiol, 2009. **59**(5): p. 520-5.
11. Olaleye, O., et al., *Methionine aminopeptidases from Mycobacterium tuberculosis as novel antimycobacterial targets*. Chem Biol, 2010. **17**(1): p. 86-97.
12. Chai, S.C., J.P. Lu, and Q.Z. Ye, *Determination of binding affinity of metal cofactor to the active site of methionine aminopeptidase based on quantitation of functional enzyme*. Anal Biochem, 2009. **395**(2): p. 263-4.
13. Herring, C.D. and F.R. Blattner, *Conditional lethal amber mutations in essential Escherichia coli genes*. J Bacteriol, 2004. **186**(9): p. 2673-81.
14. Herring, C.D., *Introduction of conditional lethal amber mutations in Escherichia coli*. Methods Mol Biol, 2008. **416**: p. 323-34.
15. Chai, S.C., W.L. Wang, and Q.Z. Ye, *FE(II) Is the Native Cofactor for Escherichia coli Methionine Aminopeptidase*. J Biol Chem, 2008. **283**(40): p. 26879-85.
16. Standards, N.C.f.C.L., *Methods for dilution antimicrobial susceptibility tests for bacteria that grow aerobically, Approved standard 2000*, National Committee for Clinical Laboratory Standards: Wayne, PA.
17. Minor, W., et al., *HKL-3000: the integration of data reduction and structure solution--from diffraction images to an initial model in minutes*. Acta Crystallogr D Biol Crystallogr, 2006. **62**(Pt 8): p. 859-66.
18. Vagin, A. and A. Teplyakov, *Molecular replacement with MOLREP*. Acta Crystallogr D Biol Crystallogr, 2010. **66**(Pt 1): p. 22-5.

19. Collaborative Computational Project, N., *The CCP4 suite: programs for protein crystallography*. Acta Crystallogr D Biol Crystallogr, 1994. **50**(Pt 5): p. 760-3.
20. Potterton, E., et al., *A graphical user interface to the CCP4 program suite*. Acta Crystallogr D Biol Crystallogr, 2003. **59**(Pt 7): p. 1131-7.
21. Addlagatta, A., et al., *Identification of an SH3-binding motif in a new class of methionine aminopeptidases from Mycobacterium tuberculosis suggests a mode of interaction with the ribosome*. Biochemistry, 2005. **44**(19): p. 7166-74.
22. Murshudov, G.N., A.A. Vagin, and E.J. Dodson, *Refinement of macromolecular structures by the maximum-likelihood method*. Acta Crystallogr D Biol Crystallogr, 1997. **53**(Pt 3): p. 240-55.
23. Emsley, P. and K. Cowtan, *Coot: model-building tools for molecular graphics*. Acta Crystallogr D Biol Crystallogr, 2004. **60**(Pt 12 Pt 1): p. 2126-32.
24. DeLano, W.L. *The PyMOL Molecular Graphics System*. 2000.
25. Li, J.Y., et al., *Specificity for inhibitors of metal-substituted methionine aminopeptidase*. Biochem Biophys Res Commun, 2003. **307**(1): p. 172-9.
26. Meng, L., et al., *Overexpression and Divalent Metal Binding Properties of the Methionyl Aminopeptidase from Pyrococcus furiosus†*. Biochemistry, 2002. **41**: p. 7199-7208.
27. Ye, Q.Z., et al., *Metalloform-selective inhibitors of escherichia coli methionine aminopeptidase and X-ray structure of a Mn(II)-form enzyme complexed with an inhibitor*. J Am Chem Soc, 2004. **126**(43): p. 13940-1.
28. Wang, W.L., et al., *Discovery of inhibitors of Escherichia coli methionine aminopeptidase with the Fe(II)-form selectivity and antibacterial activity*. J Med Chem, 2008. **51**(19): p. 6110-20.
29. Oefner, C., et al., *The 1.15 Å crystal structure of the Staphylococcus aureus methionyl-aminopeptidase and complexes with triazole based inhibitors*. J Mol Biol, 2003. **332**(1): p. 13-21.
30. Xie, S.X., et al., *Structural analysis of metalloform-selective inhibition of methionine aminopeptidase*. Acta Crystallogr D Biol Crystallogr, 2006. **62**(Pt 4): p. 425-32.
31. Lowther, W.T. and B.W. Matthews, *Structure and function of the methionine aminopeptidases*. Biochim Biophys Acta, 2000. **1477**(1-2): p. 157-67.
32. Roderick, S.L. and B.W. Matthews, *Structure of the cobalt-dependent methionine aminopeptidase from Escherichia coli: a new type of proteolytic enzyme*. Biochemistry, 1993. **32**(15): p. 3907-12.
33. Huang, M., et al., *Metal mediated inhibition of methionine aminopeptidase by quinolinyl sulfonamides*. Biochem Biophys Res Commun, 2006. **339**(2): p. 506-13.
34. Douangamath, A., et al., *Crystal structures of Staphylococcus aureus methionine aminopeptidase complexed with keto heterocycle and aminoketone inhibitors reveal the formation of a tetrahedral intermediate*. J Med Chem, 2004. **47**(6): p. 1325-8.
35. Krissinel, E., *Crystal contacts as nature's docking solutions*. J Comput Chem, 2010. **31**(1): p. 133-43.
36. You, C., et al., *The two authentic methionine aminopeptidase genes are differentially expressed in Bacillus subtilis*. BMC Microbiol, 2005. **5**: p. 57.
37. Miller, C.G., et al., *pepM is an essential gene in Salmonella typhimurium*. J Bacteriol, 1989. **171**(9): p. 5215-7.

38. Needleman, S.B. and C.D. Wunsch, *A general method applicable to the search for similarities in the amino acid sequence of two proteins*. J Mol Biol, 1970. **48**(3): p. 443-53.
39. Narayanan, S.S., et al., *Purification and biochemical characterization of methionine aminopeptidase (MetAP) from Mycobacterium smegmatis mc2155*. Appl Biochem Biotechnol, 2008. **151**(2-3): p. 512-21.
40. Wilcox, D.E., *Binuclear Metallohydrolases*. Chem Rev, 1996. **96**(7): p. 2435-2458.
41. Macrae, I.J., et al., *Structural basis for double-stranded RNA processing by Dicer*. Science, 2006. **311**(5758): p. 195-8.
42. Davies, J.F., 2nd, et al., *Crystal structure of the ribonuclease H domain of HIV-1 reverse transcriptase*. Science, 1991. **252**(5002): p. 88-95.
43. Maynes, J.T., et al., *Crystal structure of the tumor-promoter okadaic acid bound to protein phosphatase-1*. J Biol Chem, 2001. **276**(47): p. 44078-82.
44. Nguyen, K.T., et al., *Zinc is the metal cofactor of Borrelia burgdorferi peptide deformylase*. Arch Biochem Biophys, 2007. **468**(2): p. 217-25.
45. Wang, J., et al., *Physiologically relevant metal cofactor for methionine aminopeptidase-2 is manganese*. Biochemistry, 2003. **42**(17): p. 5035-42.
46. Wooldridge, K.G. and P.H. Williams, *Iron uptake mechanisms of pathogenic bacteria*. FEMS Microbiol Rev, 1993. **12**(4): p. 325-48.
47. Payne, S.M., *Iron acquisition in microbial pathogenesis*. Trends Microbiol, 1993. **1**(2): p. 66-9.

CHAPTER 4

CONCLUSIONS AND FUTURE PLANS

In this project, two methionine aminopeptidase (MetAP) enzymes from *Mycobacterium tuberculosis* were purified and characterized. Both MetAPs were active and could be activated by Ni(II), Co(II), Mn (II) and Fe(II). The plasmid-expressed *MtMetAP Ic* rescued an *EcMetAP* amber mutant in *E.coli*, which was otherwise lethal [1] [2]. A set of compounds with specific inhibitory activities against different metal-substituted MetAP were identified and tested in a cellular assay. Only Fe(II)-selective inhibitors show inhibition in this cellular *MtMetAP Ic* assay and the growth of *E. coli*, indicating that Fe(II) was most likely the metal used by *MtMetAP Ic* when it is expressed in *E.coli*. Both *MtMetAPs* were co-crystallized with inhibitors. Only crystal structures of different metalloforms *MtMetAP Ic* in complex with inhibitors were solved. The structural information of *MtMetAP Ic* with inhibitors has provided awareness for development of anti-TB agents.

A number of questions regarding to the physiological functions of MetAP enzyme remain unsolved and further investigation is needed to address them. Compounds that inhibit *MtMetAP Ia* activity are still of great interest and needed for: 1) Testing their inhibition on different metalated *MtMetAP Ia*; 2) Testing their inhibitory activity on cellular growth; 3) Illuminating the interaction between the active sites of *MtMetAP Ia* and the inhibitory compounds; and 4) Identifying the role of *MtMetAP Ia* in *M. tuberculosis* pathogenesis.

MtMetAP Ia and *MtMetAP Ic* share approximately 36.9% sequence identity. In addition, a homology model of *MtMetAP Ia* has an active site consisting of amino acid residues of Glu,

His, and Asp, which is similar to that of *MtMetAP Ic* [3]. *MtMetAP Ia*, however, showed different enzymatic characteristic from *MtMetAP Ic* in our study. The metal binding affinities to *MtMetAP Ia*, from the highest to lowest, are showed as following; Fe(II) > Co(II) > Ni(II) > Mn(II). In contrast, in *MtMetAP Ic*, the affinities are Co(II) > Mn(II) ≥ Fe(II) > Ni(II).

While both *MtMetAP* can hydrolyze the fluorogenic substrate Met-AMC, *MtMetAP Ia* is a more efficient enzyme than *MtMetAP Ic* as indicated by the larger K_{cat}/K_m value (Table 4-1). In testing inhibition, most MetAP inhibitors of *EcMetAP Ia*, *HsMetAP Ia* and *MtMetAP Ic* did not inhibit *MtMetAP Ia*. The only exceptions were the Fe(II)-selective inhibitors. However, these Fe(II)-selective inhibitors lose their metal specificity for *MtMetAP Ia*. These *in vitro* kinetic differences between *MtMetAP Ia* and *MtMetAP Ic* may contribute to their different functions as observed in the *E. coli* growth complementary experiment.

In the experiment, the *E. coli* with an amber mutation in the *map* gene could be rescued from death by the plasmid-expressed *MtMetAP Ic*, which complementated of the function of the mutated *EcMetAP*. However, *MtMetAP Ia* gave an inconsistent result. *MtMetAP Ia* could suppress the lethal effect of amber mutation in *E.coli* but it gave a much weaker complementation when compared with *EcMetAP* and *MtMetAP Ic* and it was not reproducible. Figure 4-1 shows the culture plates comparing relative growth of cells harboring plasmids of pFLAG-*MtMetAP Ia*, pFLAG-*MtMetAP Ic*, pFLAG-*EcMetAP* and pFLAG. In the plates, cells with *MtMetAP Ia* grew much slower than the others. Even after several days, the colonies were smaller than the other cells. It would be of significance to clarify the function of *MtMetAP Ia* in the pathogenesis of TB.

Table 4-1 ^a comparison of Kinetic measurement of His *MtMetA* Ia and *MtMetAP* Ic

<i>MtMetAP</i> Ia	Fe(II)	Ni(II)	Co(II)	Mn(II)
k_{cat} , sec ⁻¹	0.1429 ±0.0077	0.4779± 0.0068	0.3719± 0.018	0.062± 0.018
k_{cat}/K_m , M ⁻¹ sec ⁻¹	959	35634	5277	364

<i>MtMetAP</i> Ic	Fe(II)	Ni(II)	Co(II)	Mn(II)
k_{cat} , sec ⁻¹	0.0039 ± 0.0002	0.029 ± 0.002	0.027 ± 0.0004	0.0082 ± 0.00033
k_{cat}/K_m , M ⁻¹ sec ⁻¹	24.3	301.1	122.1	36.1

^a Data taken from Table 2-4 in Chapter 2 and Table 3-1 in Chapter 3.

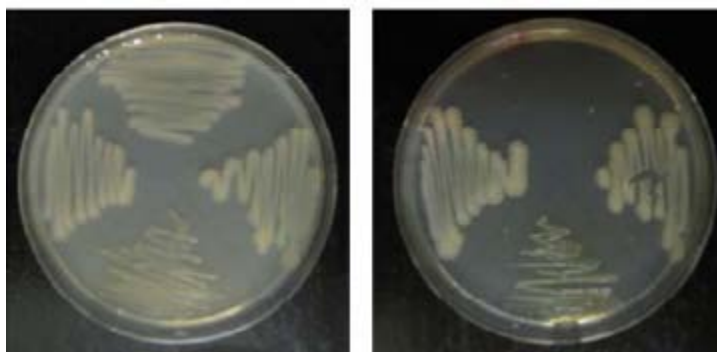


Figure 4-1. Complementation of *EcMetAP* function by *MtMetAP*1a.

A. *E. coli* cells carrying an amber mutation in the chromosomal *EcMetAP* gene were streaked on agar plates with arabinose (the left plate) or glucose (the right plate). Each plate displays cells containing pFLAGCTC (top), pFLAGCTC-*MtMetAP*1a (bottom), pFLAGCTC-*EcMetAP* (left) and pFLAGCTC-*MtMetAP*1c (right).

Differences between *MtMetAP Ia* and *MtMetAP Ic* have also been reported in other studies. Zhang *et al.* investigated the mRNA expression levels of *MtMetAP Ia* and *MtMetAP Ic* in the 14-day-old and the 60-day-old cultures of *M. tuberculosis* H37Rv [4]. The *mapA* gene showed a two-fold decrease in the 60-day-old culture compared with the 14-day-old culture; the *mapB* gene showed a 1.5-fold higher expression in the 60-day-old culture than in the 14-day-old culture. The various transcription levels of the *map* gene indicate the important functions that *MtMetAP Ia* and *MtMetAP Ic* perform in different growth stages. Olaley et al made a *M. tuberculosis* strains with knocked-down copies of the *mapA* or *mapB* genes by introducing a plasmid containing either the anti-*mapA* gene or the anti-*mapB* gene [5]. Inhibitors from a high-throughput screening of *MtMetAP Ic* were tested in these knock-down *M. tuberculosis* strains and compared to a control, in which neither the *mapA* nor *mapB* genes were down-regulated. The *M. tuberculosis* with the knock-down of *MtMetAP Ia* showed decreased cell viability to 76%. The knock-down of *MtMetAP Ic* only caused a marginal effect on cell viability. The result suggested that *MtMetAP Ia* is likely the essential enzyme in cell viability and the observed inhibition on *M. tuberculosis* growth caused by the inhibitors is through the function of *MtMetAP Ia*, not *MtMetAP Ic*. All of these results indicate the essential role that *MtMetAP Ia* plays in pathogenesis of *M. tuberculosis*.

The inhibitors that selectively suppress the *MtMetAP Ia* enzyme in *M. tuberculosis* would be a helpful tool to achieve our goal of elucidating the role of *MtMetAP Ia* in tuberculosis pathogenesis. So far, there are no such compounds reported. The inhibitors used in the study of Olaley *et al.* were from a high-throughput screening against Co-metalated *MtMetAP Ic*. They have not identified their inhibitory activities on *MtMetAP Ia* even though the knock-down experiment indicated the possible inhibition of *MtMetAP Ia*. The reason may be the relatively

low yield of *MtMetAP Ia* and thus the difficulty in obtaining sufficient amount of *MtMetAP Ia* [4] [5]. Another reason maybe the lack of the knowledge about the function of *MtMetAP Ia* in *M. tuberculosis* when these two studies were carried out. In conclusion, identifying the inhibitors that specifically target *MtMetAP Ia*, or/and *MtMetAP Ic*, would facilitate our understanding of the rules of MetAP in *M. tuberculosis* pathogenesis in addition to identifying new pathway for development of anti-TB agents.

References

1. Herring, C.D., *Introduction of conditional lethal amber mutations in Escherichia coli*. Methods Mol Biol, 2008. **416**: p. 323-34.
2. Lu, J.P., S.C. Chai, and Q.Z. Ye, *Catalysis and inhibition of Mycobacterium tuberculosis methionine aminopeptidase*. J Med Chem, 2010. **53**(3): p. 1329-37.
3. Addlagatta, A., et al., *Identification of an SH3-binding motif in a new class of methionine aminopeptidases from Mycobacterium tuberculosis suggests a mode of interaction with the ribosome*. Biochemistry, 2005. **44**(19): p. 7166-74.
4. Zhang, X., et al., *Expression and characterization of two functional methionine aminopeptidases from Mycobacterium tuberculosis H37Rv*. Curr Microbiol, 2009. **59**(5): p. 520-5.
5. Olaleye, O., et al., *Methionine aminopeptidases from Mycobacterium tuberculosis as novel antimycobacterial targets*. Chem Biol, 2010. **17**(1): p. 86-97.